


12-2017

# INTEGRATIVE CANCER IMMUNOGENOMIC ANALYSIS OF SERIAL MELANOMA BIOPSIES REVEALS CORRELATES OF RESPONSE AND RESISTANCE TO SEQUENTIAL CTLA-4 AND PD-1 BLOCKADE TREATMENT

Whijae Roh

Follow this and additional works at: [http://digitalcommons.library.tmc.edu/utgsbs\\_dissertations](http://digitalcommons.library.tmc.edu/utgsbs_dissertations)

 Part of the [Bioinformatics Commons](#), [Computational Biology Commons](#), [Genomics Commons](#), [Medical Immunology Commons](#), and the [Skin and Connective Tissue Diseases Commons](#)

---

## Recommended Citation

Roh, Whijae, "INTEGRATIVE CANCER IMMUNOGENOMIC ANALYSIS OF SERIAL MELANOMA BIOPSIES REVEALS CORRELATES OF RESPONSE AND RESISTANCE TO SEQUENTIAL CTLA-4 AND PD-1 BLOCKADE TREATMENT" (2017). *UT GSBS Dissertations and Theses (Open Access)*. 813.  
[http://digitalcommons.library.tmc.edu/utgsbs\\_dissertations/813](http://digitalcommons.library.tmc.edu/utgsbs_dissertations/813)

This Dissertation (PhD) is brought to you for free and open access by the Graduate School of Biomedical Sciences at DigitalCommons@TMC. It has been accepted for inclusion in UT GSBS Dissertations and Theses (Open Access) by an authorized administrator of DigitalCommons@TMC. For more information, please contact [laurel.sanders@library.tmc.edu](mailto:laurel.sanders@library.tmc.edu).

**INTEGRATIVE CANCER IMMUNOGENOMIC ANALYSIS OF SERIAL  
MELANOMA BIOPSIES REVEALS CORRELATES OF RESPONSE AND  
RESISTANCE TO SEQUENTIAL CTLA-4 AND PD-1 BLOCKADE  
TREATMENT**

**by**

**Whijae Roh, MS**

APPROVED:

-----  
P. Andrew Futreal, Ph.D.  
Advisory Professor

-----  
James P. Allison, Ph.D.

-----  
Giulio Draetta, M.D., Ph.D.

-----  
Patrick Hwu, M.D.

-----  
Greg Lizee, Ph.D.

-----  
Nicholas Navin, Ph.D.

-----  
Paul A. Scheet, Ph.D.

APPROVED:

-----  
Dean, The University of Texas  
MD Anderson Cancer Center UTHealth Graduate School of Biomedical  
Sciences

**INTEGRATIVE CANCER IMMUNOGENOMIC ANALYSIS OF SERIAL  
MELANOMA BIOPSIES REVEALS CORRELATES OF RESPONSE AND  
RESISTANCE TO SEQUENTIAL CTLA-4 AND PD-1 BLOCKADE  
TREATMENT**

A

DISSERTATION

Presented to the Faculty of

The University of Texas

MD Anderson Cancer Center UTHealth

Graduate School of Biomedical Sciences

in Partial Fulfillment

of the Requirements

for the Degree of

DOCTOR OF PHILOSOPHY

by

Whijae Roh, MS

Houston, Texas

December 2017

To my parents, Gab Kyun Roh and Joung Soon Bae,  
my beloved wife, Cindy Park, and my son, Daniel Hajoan Roh,  
for their love and support...



## **Acknowledgments**

First and foremost, I would like to thank the Creator for providing me with the opportunity to grow as a scientist studying one of the most intricate systems of His creations, the cell, with the hope of finding a better way to combat cancer by harnessing the human immune system.

I would like to express my deepest gratitude to my advisor, Dr. Andrew Futreal, for being my role model of a scholar and a mentor. Despite his busy schedules, he has spent tremendous amount of time for discussing my thesis project. During all these meetings, I have learned a lot of his incredible insights in cancer genomics and the ability to find important biomedical problems. He also allowed me to have enough freedom to lead my thesis project so that I can learn how to work independently. At the same time, he provided me with all the resources for my thesis project including collaboration opportunities with great scientists from whom I could learn how to work interdependently. Above all, his ceaseless intellectual curiosity and passion about solving unknown mysteries of critical biomedical problems taught me the core characteristics of a great scholar. I also appreciate his deep commitment to academic integrity and courageous act of taking a full responsibility in leading a project as a senior scientist. I am grateful to him for showing me an excellent example of a scholar and a mentor.

I also would like to express my gratitude to my committee members. I would like to thank Dr. James Allison for serving as my CPRIT graduate scholar mentor as well as a committee member providing me with critical insights in cancer

immunology and immunotherapy and helpful advice for my future career. I thank Dr. Giulio Draetta for his helpful comments from a functional validation perspective, which was helpful for me to think about the next step of this project. I thank Dr. Patrick Hwu for kindly providing me with training opportunities in cancer immunology by inviting me to the weekly Melanoma Medical Oncology department meetings and allowing me to shadow a clinician as well. I thank Dr. Greg Lizee for his helpful comments and suggestions about my project from a cancer immunology perspective. I thank Dr. Nicholas Navin for taking me as a rotation student in his lab where I could learn single cell sequencing data analysis. I am also grateful for his helpful comments during committee meetings and writing many recommendation letters for my scholarship applications. I thank Dr. Paul Scheet for his computational and statistical advice for the project and his kind advice for my future career.

I am also very grateful to Dr. Michelle Barton, the Dean of The University of Texas MD Anderson Cancer Center UTHealth Graduate School of Biomedical Sciences, for allowing me to rotate in her lab and to learn cancer epigenetics. She has been a wonderful supporter for my graduate study from the beginning to this moment. I sincerely appreciate her constant support for my study with many recommendation letters, her appreciation of the role of computational biologists in biomedical research, and her incredible commitment to our graduate school.

I would also like to thank Dr. Jennifer Wargo and her lab members, especially Dr. Pei-Ling Chen for providing me with their clinical perspectives during close collaboration for this project. I thank Dr. Hannah Beird for her helpful

comments and critical feedbacks on many research proposals and presentations during my Ph.D. training. I thank Dr. Jianhua Zhang for always being available for bioinformatics discussions. I also thank his bioinformatics team for providing a bioinformatics pipeline for the project. I thank Dr. Wei-Shen Chen for having intellectually stimulating discussions for each other's projects. I thank all other Futreal lab members for their kind help with my thesis project and healthy discussion during lab meetings.

Finally, I would like to thank my parents, Gab Kyun Roh and Joung Soon Bae, and my younger brother, Heesung Roh, for supporting me with their love and care. They have always supported my career choices and encouraged me to overcome difficult moments. I also would like to thank my wife, Cindy Park, for constantly supporting me with her love and wisdom during the ups and downs of my Ph.D. journey. Last but not least, I would like to thank my son, Daniel Hajoan Roh, for supporting my Ph.D. study with his welcoming big smiles whenever I went home after work.

**INTEGRATIVE CANCER IMMUNOGENOMIC ANALYSIS OF SERIAL  
MELANOMA BIOPSIES REVEALS CORRELATES OF RESPONSE AND  
RESISTANCE TO SEQUENTIAL CTLA-4 AND PD-1 BLOCKADE  
TREATMENT**

**Whijae Roh, M.S.**

**Advisory Professor: P. Andrew Futreal, Ph.D.**

Melanoma is the most malignant form of skin cancer. The five-year survival rate for metastatic melanoma is 19.9%. Although targeted therapy of BRAF and MEK inhibitors were developed for melanoma, resistance to therapy is inevitable. Immune checkpoint blockade, which reverses the suppression of the immune system, on the other hand, has shown a durable response in 20-30% of patients with metastatic melanoma. However, more predictive and robust biomarkers of response to this therapy are still needed, and resistance mechanisms remain incompletely understood. To address this, we examined a cohort of metastatic melanoma patients treated with sequential checkpoint blockade against cytotoxic T lymphocyte antigen-4 (CTLA-4) followed by programmed death receptor-1 (PD-1) by immunogenomic profile analyses from serial tumor biopsies.

From immune profiling (12 marker immunohistochemistry and NanoString Gene Expression Profiling), we found that adaptive immune signatures in tumor biopsies obtained from early on-treatment time points are predictive of response to immune checkpoint blockade. We also demonstrated differential mechanistic

signatures of tumor microenvironment induced by CTLA-4 and PD-1 blockade. Importantly, VEGFA was identified as a potential target of combination therapy with PD-1 blockade.

From genomic profiling (whole exome sequencing and T cell receptor sequencing), we demonstrated that a higher TCR clonality in pre-treatment biopsy was predictive of response to PD-1 but not CTLA-4 blockade. We also observed increased TCR clonality after CTLA-4 blockade treatment in patients responding to the following PD-1 blockade treatment. Analysis of copy number alterations (CNAs) identified a higher burden of copy number loss in nonresponders to CTLA-4 and PD-1 blockade and found that it was associated with decreased expression of genes in immune-related pathways. The effect of mutational load and burden of copy number loss on response was nonredundant, suggesting the potential utility of these as a combinatorial biomarker to optimize patient care with checkpoint blockade therapy.

In summary, our integrative cancer immunogenomic analysis shows that genomic and immune profiling of longitudinal tumor biopsies can identify novel biomarkers and resistance mechanisms of immune checkpoint blockade.

## Table of Contents

<b>Approval</b> .....	<b>i</b>
<b>Title</b> .....	<b>ii</b>
<b>Dedication</b> .....	<b>iii</b>
<b>Acknowledgements</b> .....	<b>iv</b>
<b>Abstract</b> .....	<b>vii</b>
<b>Table of Contents</b> .....	<b>ix</b>
<b>Lists of Illustrations</b> .....	<b>xii</b>
<b>List of Tables</b> .....	<b>xv</b>
<b>CHAPTER ONE - INTRODUCTION</b> .....	<b>1</b>
1.1 Melanoma .....	2
1.2 Cancer immunology and immune checkpoint blockade (ICB) .....	3
1.2.1 Cancer Immunology.....	3
1.2.2 Immune checkpoint blockade (ICB).....	5
1.3 Cancer immunogenomics .....	6
1.3.1 Next-generation sequencing (NGS).....	6
1.3.2 Characterization of immune infiltrates.....	7
1.3.3 In Silico prediction of neoantigens .....	7
1.3.4 T cell receptor (TCR) profiling.....	8
1.4 Biomarkers and resistance mechanisms of immune checkpoint blockade (ICB) ...	9
1.4.1 Known biomarkers and resistance mechanisms of ICB.....	9
1.4.2 Potential biomarkers and resistance mechanisms of ICB.....	11
1.4.3 Integrative and longitudinal approach for discovery of biomarkers and resistance mechanisms of ICB .....	12
1.5 Hypothesis, specific aims and rationale.....	12
<b>CHAPTER TWO - MATERIALS AND METHODS</b> .....	<b>15</b>
2.1 Patient Cohort and Tumor Samples.....	16
2.1.1 Study design .....	16
2.1.2 Patient cohort and tumor samples .....	16

2.2. Immune Profiling .....	17
2.2.1 Immune profiling by IHC .....	17
2.2.2 Immunofluorescence.....	20
2.2.3 NanoString Gene Expression Analysis .....	20
2.2.4 Statistical Analysis .....	22
2.2.4.1 Immune Profiling by IHC .....	22
2.2.4.2 NanoString Data Preprocessing .....	22
2.2.4.3 Differential Gene Expression Analysis.....	23
2.2.4.4 Assessment of Time-by-Response Interaction .....	23
2.3. Genomic Profiling.....	24
2.3.1 Sample processing .....	24
2.3.2 Whole exome sequencing.....	25
2.3.3 Mutation calling and intratumor heterogeneity analysis .....	26
2.3.4 Neoantigen prediction .....	27
2.3.5 Copy number alteration analysis.....	27
2.3.6 TCR sequencing and clonality analysis .....	28
2.3.7 NanoString gene expression profiling .....	29
2.3.8 Independent (Van Allen) cohort analysis .....	30
2.3.9 Statistical analysis.....	31
<b>CHAPTER THREE - IMMUNE PROFILING .....</b>	<b>32</b>
3.1 Introductions and Rationale .....	34
3.2 Results .....	37
3.2.1 Patient Cohort, Checkpoint Blockade Treatment, and Longitudinal Tumor Biopsies .....	37
3.2.2 Immune Profiling in Early On-Treatment Biopsies Is Predictive of Response to CTLA4 Blockade in a Unique Cohort of Patients Treated with Sequential CTLA4 and PD- 1 Blockade .....	45
3.2.3 Immune Profiling in Early On-Treatment Biopsies Is Highly Predictive of Response to PD-1 Blockade.....	52
3.2.4 Gene Expression Profiling in Longitudinal Tumor Biopsies Is Predictive of Response in Patients Treated with Sequential CTLA4 and PD-1 Blockade .....	65
3.3 Discussion .....	77
<b>CHAPTER FOUR - GENOMIC PROFILING .....</b>	<b>81</b>

4.1 Introductions and Rationale .....	82
4.2 Results .....	84
4.2.1 T cell clonality predicts response to PD-1 blockade but not CTLA-4 blockade	84
4.2.2 High copy number loss burden is associated with poor response to immune checkpoint blockade .....	102
4.2.3 An independent patient cohort shows copy number loss as a putative resistance mechanism .....	113
4.2.4 Integrated analysis reveals putative mechanisms through which CNAs may influence response to therapy.....	125
4.2.5 Mutational load and burden of copy number loss may allow better patient stratification for response than either correlate alone .....	133
4.3 Discussion .....	138
<b>CHAPTER FIVE - DISCUSSION, CONCLUSIONS AND FUTURE DIRECTIONS.....</b>	<b>141</b>
5.1 Discussion and Conclusions .....	142
5.2 Future Directions.....	147
<b>References.....</b>	<b>150</b>
<b>VITA.....</b>	<b>177</b>



## List of Illustrations

### Chapter 3. IMMUNE PROFILING

Figure 1. A cohort of patients treated with sequential CTLA4 and PD-1 blockade .....	39
Figure 2. Immune profiling of pre-treatment, on-treatment and progression CTLA-4 blockade samples by immunohistochemistry .....	46
Figure 3. Representative IHC images of CD8, CD4, and PD-L1 in responders and nonresponders at the pre- and on-treatment time point.....	48
Figure 4. Myeloid cell profiling of pre-treatment, on-treatment and progression CTLA-4 blockade samples by immunohistochemistry .....	50
Figure 5. Increased contact between CD8 T cells and CD68 myeloid cells in non-responding patients to anti-CTLA-4 and anti-PD-1 therapy at pre-treatment CTLA-4 blockade, pre-treatment PD-1 blockade, and on-treatment PD-1 blockade time points .	51
Figure 6. Immune profiling of pre-treatment, on-treatment and progression PD-1 blockade samples by immunohistochemistry .....	53
Figure 7. Representative immunohistochemistry images of selected markers at pretreatment and early on-treatment time points .....	56
Figure 8. Longitudinal increase in CD8, PD-1, and PD-L1 expression in responders to anti-PD-1 therapy .....	57
Figure 9. Relative increase in CD8 T cell infiltrate at tumor center in responders to anti-PD-1 on treatment.....	59
Figure 10. Significant increase in immune infiltrate between responders and non-responders to PD-1 blockade in absence of prior anti-CTLA-4 therapy .....	63
Figure 11. Immune profiling of myeloid cells atpre-treatment and on-treatment PD-1 blockade time points by immunohistochemistry.....	64

Figure 12. Gene expression profiling in longitudinal tumor biopsies is predictive of response in a unique cohort of patients treated with sequential CTLA4 and PD-1 blockade.....	67
Figure 13. Heatmap of 54 NanoString samples.....	69
Figure 14. Gene-specific NanoString concordance with immune profiling by IHC in pre-treatment, on-treatment and progression CTLA-4 blockade samples .....	70
Figure 15. Gene-specific NanoString concordance with immune profiling by IHC in pre-treatment, on-treatment and progression PD-1 blockade samples.....	72
Figure 16. Prior CTLA-4 blockade is not required for PD-1 early on-treatment profile ...	75
<b>Chapter 4. GENOMIC PROFILING</b>	
Figure 17. Patient cohort diagram and genomic landscape of serial tumor biopsies.....	86
Figure 18. Workflow diagram of multidimensional profiling analysis.....	89
Figure 19. Distribution of sequencing coverage and tumor purities across samples.....	90
Figure 20. Mutational load, neoantigen load, and clinical response .....	93
Figure 21. Intratumor heterogeneity and clinical response .....	94
Figure 22. TCR clonality and clinical response.....	97
Figure 23. The effects of previous CTLA-4 blockade exposure on the baseline TCR clonality of pre-PD-1 blockade samples.....	98
Figure 24. The correlation between TCR clonality and immune scores .....	101
Figure 25. Burden of copy number alterations in responders versus non-responders .	104
Figure 26. Burden of copy number alterations in responders versus double non-responders .....	106
Figure 27. Copy number profiles of responders and double non-responders.....	107
Figure 28. Correlation between burden of copy number loss and mutational load.....	109
Figure 29. Recurrent copy number loss in double non-responders .....	111

Figure 30. Burden of copy number alterations in each clinical response group from an independent cohort .....	116
Figure 31. Correlation between burden of copy number loss and mutational load in the Van Allen cohort.....	117
Figure 32. Segment Gain or Loss (SGOL) scores in three patient subgroups from the Van Allen cohort.....	118
Figure 33. Burden of recurrent CNAs in patients in Van Allen cohort.....	120
Figure 34. Correlation between burden of copy number loss and immune scores.....	126
Figure 35. Gene set enrichment analysis of differentially expressed genes between tumors with high burden of copy number loss and those with low burden of copy number loss.....	130
Figure 36. Up and down-regulated pathways in patients with high versus low copy number loss in the Van Allen cohort .....	131
Figure 37. Patient stratification based on mutational load and burden of copy number loss in the Van Allen cohort .....	135
Figure 38. Clinical response rate in patient subgroups stratified by mutational load and burden of copy number loss.....	136

## List of Tables

### Chapter 3. IMMUNE PROFILING

Table 1. Cohort level clinical summary .....	41
Table 2. Patient level clinical characteristics.....	42
Table 3. Immune profiling by IHC sample log .....	43
Table 4. Immune profiling by NanoString 54 sample log .....	44

### Chapter 4. GENOMIC PROFILING

Table 5. Sample information, tumor purity, mutational load, neoantigen load, number of clones per tumor, and burden of copy number alterations.....	88
Table 6. Summary measure of the data across clinical subgroups .....	91
Table 7. TCR clonality.....	96
Table 8. Immune scores (NanoString) in our cohort.....	100
Table 9. Recurrent copy number alterations in double non-responders with burden of copy number loss > 2000.....	112
Table 10. Burden of copy number alterations in the Van Allen cohort.....	115
Table 11. Relative contribution of copy number loss burden by chromosome 10 in CTLA-4 blockade resistance .....	122
Table 12. Relative contribution of copy number loss burden outside chromosome 10 in CTLA-4 blockade resistance.....	123
Table 13. Relative contribution of PTEN loss in CTLA-4 blockade resistance .....	124
Table 14. Immune scores (RNA-seq) in the Van Allen cohort .....	128
Table 15. Additive effect of high mutational load and low burden of copy number loss on response to CTLA-4 blockade .....	137

## **CHAPTER ONE – INTRODUCTION**

## Chapter 1 INTRODUCTION

### 1.1 Melanoma

Melanoma is a malignancy of melanocytes, the melanin-producing cells of neuroectodermal origin (1). Melanocytes can be found throughout the body including the skin, iris, and rectum, and melanocytes at different sites can develop into phenotypically diverse malignancies. The cutaneous form of melanoma is common in the Western world and contributes 75% of deaths from skin cancer (2). The major risk factor for cutaneous melanoma is UV exposure. Therefore, a typical UV exposure signature, C-to-T transition, is frequently observed in the mutational signatures of cutaneous melanoma. Due to mutagenic effect of UV radiation, cutaneous melanoma has a high mutation rate of 16.8 mutations/Mb (3).

Sequencing studies of melanoma have identified melanoma driver genes involved in mitogen-activated protein kinase (MAPK) and other signaling pathways (4-6). The most common genetic alterations occur in *BRAF* and *NRAS*, which leads to MAPK pathway hyperactivation (7, 8). Amplification of *AKT3* by copy number increases and loss of *PTEN* by deletion are also recurrent genetic alterations (9, 10). The recent The Cancer Genome Atlas (TCGA) study of cutaneous melanoma further identified four subtypes based on genomic classification: mutant *BRAF*, mutant *RAS*, mutant *NF1*, and Triple-WT (wild-type) (11).

The identification of genetic alterations in melanoma led to development of targeted therapies. The first targeted therapy for melanoma was a *BRAF*

inhibitor. In phase III clinical trial of vemurafenib (a *BRAF* inhibitor) in *BRAF* V600E-mutant melanoma patients, an overall response rate was 48% with a survival advantage compared to chemotherapy of dacarbazine (12). Dabrafenib (another *BRAF* inhibitor) showed similar clinical benefit (13). Vemurafenib and dabrafenib were approved by the U.S. Food and Drug Administration (FDA) for treatment of advanced *BRAF*-mutant melanoma patients. However, the response to targeted therapy was transient with median progression-free survival of 5 to 7 months due to intrinsic and acquired resistance mechanisms (12-14). The first-line *BRAF*/MEK combination therapy showed an overall response rate of 67%, which is significant improvement in response rates compared to *BRAF* monotherapy, but the median progression-free survival was only 9.3 months (15). Although there has been considerable amount of efforts to overcome drug resistance for targeted therapies in melanoma, durability of clinical response is still limited.

## **1.2 Cancer immunology and immune checkpoint blockade (ICB)**

### **1.2.1 Cancer Immunology**

Cancer is a genetic disease. Tumor cells support their growth by mutations activating oncogenes or suppressing tumor suppressor genes. However, factors extrinsic to cancer cells, such as the immune system, can also affect their fate as they evolve over their lifetime under the selective pressure from tumor microenvironment. For instance, cancer cells can be recognized as 'foreign' by the immune system due to the mutated peptides presented by cancer cells on

their cell surface. Therefore, the tumor is visible to the immune system and the immune system can act as a critical selective pressure in tumor microenvironment.

The interaction between cancer and the immune system can be explained by the 'cancer-immunity cycle' (16). In the first step, peptides containing mutated amino acid residues (neoantigens) produced by mutations in cancer cells are released and captured by dendritic cells (DCs). Then, DCs present these antigens on MHC I and MHC II molecules to T cells. This leads to the priming and activation in effector T cells with antigen specificity. Next, the activated effector T cells traffic to and infiltrate into tumor sites, resulting in recognition of cancer cells through interaction between TCR and MHC-bound antigen on the surface of cancer cells. Finally, the activated effector T cells can kill their target cancer cell. Death of cancer cells releases additional tumor-associated antigens providing fuel for the next round of cancer-Immunity cycle.

However, the cancer-immunity cycle is not always continuous. The flow of cancer-immunity cycle is tightly controlled by balance between positive regulators and negative regulators. Positive regulators can be tumor intrinsic (cytokine secretion, genetic composition) or extrinsic (gut microbiota composition and infection status, exposure to sunlight). Checkpoint molecules are examples of negative regulators in the cancer-immunity cycle. The equilibrium between positive and negative regulators is termed 'cancer-immune set point' (17). The threshold of cancer-immunity set point should be surpassed for the immune system to eliminate target cancer cells.



According to the cancer immunoediting theory (18), cytotoxic antigen-specific T cells can recognize and eliminate subclinical tumors, but at some point the tumor remains *in situ* in a state of equilibrium. Then, most tumors can escape from equilibrium and become clinically visible. Therefore, effective immunotherapy should aim to lower the threshold of cancer-immune set point by activating positive regulators of cancer-immunity cycle or by suppressing negative regulators of cancer-immunity cycle.

### **1.2.2 Immune Checkpoint Blockade (ICB)**

The diversity, specificity, and memory of the immune cells that target tumor cells expressing tumor-associated-antigens and neoantigens (non-self peptides resulting from exonic missense mutations) are unique features that are harnessed in immunotherapy strategies (19). Melanoma is particularly responsive to immunotherapy due to the high infiltration of immune cells into tumors and potentially, the greater number of neoantigens that are presented due to its high mutation burden (3). However, the natural balance between cancer and immune cells is tolerance (the failure to mount an immune response) and thus cancer cells can evade immune surveillance (20). The tolerance mechanisms can be immunosuppressive cytokines and chemokines, regulatory immune cells, and immune checkpoint pathways suppressing immune activation. Among several ways to reverse tolerance are the immune checkpoint blockades (ICB) (CTLA-4 blockade, PD-1 blockade), antibodies blocking the negative signals of T cell activation. ICB is recognized as breakthrough cancer

immunotherapy. The first FDA-approved agent ICB was ipilimumab, an antibody against CTLA-4, which showed long-term survival for 20% of melanoma patients (21). More recently, PD-1 blockade (nivolumab and pembrolizumab) has been approved with response rates between 28% and 40% (22, 23).

### **1.3 Cancer immunogenomics**

#### **1.3.1 Next-generation sequencing (NGS)**

Next-generation sequencing (NGS) technologies have changed the landscape of cancer research and clinical care by enabling identification of alterations at the base-pair resolution in cancer patients. From NGS technologies, multiple variants (single nucleotide variants, small insertions and deletions, copy number variants, structural variants and gene fusions), gene expression, and DNA methylation can be profiled in a genome-wide scale from a same sample. Therefore, multidimensional profiling of genome, transcriptome, and epigenome from individual patients becomes feasible. A genomic directed approach of tailoring cancer therapy to individual patients (precision oncology) is currently being implemented in many centers. The application of NGS technologies (whole exome sequencing, RNA-seq, and bisulfite sequencing for DNA methylation) and computational pipelines can build major databases for cancer immunogenomics (24). For example, in addition to the multidimensional profiling data generated from our study, we could download and analyze the publicly available genomic data (whole exome sequencing and RNA-seq) from

an independent cohort of melanoma patients treated with CTLA-4 blockade, termed *Van Allen* cohort in our study (25).

### **1.3.2 Characterization of immune infiltrates**

The composition of tumor-infiltrating lymphocytes (TILs) can affect tumor progression (26). Therefore, cellular characterization of TILs can provide a framework for discovery of prognostic and predictive markers. A large number of bioinformatics tools have been developed to quantify the cellular composition of TILs from transcriptome data. One approach is gene set enrichment analysis (GSEA) which can evaluate ranked gene list for enrichment of certain pathways and cellular processes (27). Immunological signatures (ImmuneSigDB) can be used with GSEA to characterize cellular composition of TILs from transcriptome data. Another approach is deconvolution method which uses cell type-specific expression signature matrix to infer cellular composition of TILs. Several algorithms (DeconRNASeq, CIBERSORT, and TIMER) were developed for this purpose (28-30).

### **1.3.3 *In silico* prediction of neoantigens**

Neoantigens are somatic mutations in the cancer genome that can be presented and recognized by the immune system as foreign. From NGS data, we can profile predicted neoantigens *in silico* by three steps: identification of predicted mutated peptides, HLA typing, and prediction of binding affinity between neoantigens and MHC molecules. First, somatic mutations are called

from somatic variant callers. Then, the DNA sequences spanning somatic point mutations are virtually translated into the mutated “peptides” with amino acid sequence length ranging between 8 and 11 (31). Next, HLA typing can be performed from NGS data by several computational methods including Polysolver (32) and Optitype (33). Finally, binding affinity between virtually translated mutated peptides and patient-specific HLA molecules can be predicted by neural network algorithms trained on data from the Immune Epitope Database (IEDB) (34). Mutated peptides with predicted binding affinity below IC50 value of 500nM are generally considered as predicted neoantigens (31).

#### **1.3.4 T cell receptor (TCR) profiling**

T lymphocytes of the adaptive immune system can recognize foreign molecules through antigen binding receptors. The diversity of immune repertoire can be obtained by V(D)J recombination, which is the somatic recombination of gene segments in the variable (V), diversity (D), and joining (J) loci. Further diversification occurs by the addition or removal of random nucleotides at the junction sites and by combination of  $\alpha$  and  $\beta$  subunits. Antigen-specificity is largely determined by the complementary-determining regions 3 $\beta$  (CDR3 $\beta$ ), which is the junctional site of V(D)J recombination, because this region accounts for the most variability in T cell repertoire. T cells with the same CDR3 $\beta$  are considered as the same clone.

TCR sequencing is a targeted repertoire sequencing of the TCR locus. MiXCR algorithm (35) can extract CDR3 $\beta$  sequences from TCR sequencing data

and profile the type and frequency of T cell clones in a person's T cell repertoire. TRUST algorithm (36) can also detect TCR hyper-variable region sequences from RNA-seq data. Once all the T cell clones are profiled, diversity of T cell repertoire and clonal expansion of T cell clones can be characterized.

## **1.4 Biomarkers and resistance mechanisms of immune checkpoint blockade (ICB)**

### **1.4.1 Known biomarkers and resistance mechanisms of ICB**

Response rates to immune checkpoint blockade (ICB) can be modest but are often durable (21-23). Therefore, there are ongoing efforts to identify biomarkers that predict patient response to ICB. First, it is important to understand how tumor cell intrinsic factors and extrinsic factors of tumor immunogenicity contribute to resistance to ICB (37). Tumor cell intrinsic factors include the mechanisms involved with tumor antigens and interaction with T cells. Absence of antigenic proteins due to low mutational load, lack of viral antigens, or lack of cancer-testis antigens is one of the tumor cell intrinsic factors (25, 38-41). Absence of antigen presentation due to alterations in antigen presentation pathways can also contribute to resistance (40). Other tumor-intrinsic mechanisms include genetic T cell exclusion (42-44) and loss of interferon-gamma signaling pathways (45-47). Tumor cell extrinsic factors include absence of T cells due to lack of T cells with tumor antigen-specific TCRs (48), expression of inhibitory immune checkpoints such as VISTA, LAG-3, and TIM-3 (49, 50),

presence of immunosuppressive cells such as tumor-associated macrophages and regulatory T cells (51, 52), and gut microbiota composition (53).

Biomarker discovery can be aided by mechanistic insights from resistance mechanisms. Tumor cell intrinsic factors are closely related with genetic biomarkers and tumor cell extrinsic factors are closely related with immunological biomarkers. For example, high mutational load and neoantigen load (tumor cell intrinsic factors) were associated with response to ICB (25, 38-41), and high CD8+ T cell density at the invasive tumor margin and high TCR clonality (tumor cell extrinsic factors) were correlated with response to PD-1 blockade TCR clonality (48).

Additionally, resistance mechanisms can provide insights into new biomarker discovery. For example, the resistance mechanism by absence of antigenic proteins due to low mutational load suggested that the tumor types with defects in DNA mismatch repair complex (MMR) might show higher response to ICB due to their higher mutational load. These tumor types can be detected with microsatellite instability (MSI) or with the absence of a single MMR protein by immunohistochemistry. Notably, MMR-deficient tumors have 10- to 100-fold higher mutational load than MMR-proficient tumors. Since MMR deficiency confers high mutational load in tumors, it was hypothesized that MSI phenotype would be associated with increased antitumor immunity. As predicted, MSI colon cancers showed high infiltration of T cells relative to microsatellite stable (MSS) colon cancers (54), and the clinical response of colorectal cancer patients treated with PD-1 blockade was higher in patients with MSI phenotype than those with

MSS phenotype (55). In line with these results, FDA recently approved PD-1 blockade treatment for cancer patients with microsatellite instability-high (MSI-H) or mismatch repair deficient (dMMR). The example of FDA approval of MSI-H and dMMR as a biomarker for PD-1 blockade treatment shows that understanding of resistance mechanisms can help discovery of novel biomarkers.

#### **1.4.2 Potential biomarkers and resistance mechanisms of ICB**

There is an active ongoing effort for discovering novel genetic and immunological biomarkers predictive of clinical benefit to ICB. Intratumor heterogeneity (ITH) is generally associated with drug resistance and worse prognosis (56-58) and several studies have investigated the implication of ITH in cancer immunotherapy. One study reported that ITH is associated with expression of immunomodulators and enrichment of immune cell subtypes in colorectal cancer (59). Another study showed that a high burden of clonal neoantigens was correlated with better prognosis, increased immune cell infiltration into tumors, and a durable response to immunotherapy (60). Therefore, I hypothesized that ITH might also confer resistance to immune checkpoint blockade in melanoma. In addition to ITH, I further investigated somatic HLA mutations because recent pan-cancer study showed the evidence of recurrent somatic HLA mutations as immune escape mechanism (32). I also extensively investigated copy number alterations because previous studies mostly focused on only somatic point mutations and mutational load.

### **1.4.3 Integrative and longitudinal approach for discovery of biomarkers and resistance mechanisms of ICB**

Previous studies have focused on identifying genetic biomarkers and immunological biomarkers independently. Therefore, there is lack of information about mechanistic link between genetic and immunological biomarkers. In this study, we generated patient-matched genomic (whole exome sequencing, TCR sequencing) and immune (12 marker immunohistochemistry, NanoString Gene Expression Profiling) profiling data. Therefore, our patient-matched genomic and immune profiling data provided novel insight into the interaction between cancer and the immune system.

Our study was also unique in that longitudinal tumor biopsies (pre-, on-, and post-treatment) were analyzed for discovery of biomarkers and resistance mechanisms of ICB. By comparing on-/post-treatment samples with pre-treatment samples, we could investigate dynamic change in mechanistic signatures and adaptive resistance signatures after treatment.

### **1.5 Hypothesis, specific aims and rationale**

My **hypothesis** is that integrative and longitudinal analysis of genomic and immune profiling data can provide predictive signatures and mechanistic signatures for response and resistance of sequential immune checkpoint blockade treatment (CTLA-4 blockade followed by PD-1 blockade). The primary objective of this study is to discover genetic and immunological biomarkers for



immune checkpoint blockade response and elucidate resistance mechanisms to find potential strategies to overcome them and increase response rate to immune checkpoint blockades.

### **Specific Aims**

I tested the hypothesis by the following specific aims:

**Aim 1) Determine the immunological biomarkers and resistance mechanisms of immune checkpoint blockade**

**Aim 2) Determine the genetic biomarkers and resistance mechanisms of immune checkpoint blockade**

**Aim 3) Investigate the molecular interplay between the immune system and cancer under immune checkpoint blockade**

**Rationale:** Blockade of T cell coinhibitory molecules such as CTLA-4 and PD-1, can activate T cell antitumor response. Although the immune checkpoint blockades (CTLA-4 blockade and PD-1 blockade) have shown durable response in metastatic melanoma, response rate is modest. Therefore, there is a pressing need to find stable biomarkers predictive of response to immune checkpoint blockades and to understand underlying resistance mechanisms. We collected longitudinal (pre-/on-/post-treatment) tumor biopsies from a cohort of metastatic melanoma patients treated with sequential immune checkpoint blockade and performed multidimensional genomic and immune profiling of this cohort. We aim to discover stable biomarkers and resistance mechanisms by identifying the predictive signatures from pre-treatment biopsies and the mechanistic signatures

that change during treatment from longitudinal biopsies. Multidimensional approach of genomic and immune profiling can allow discovery of novel combinatorial biomarkers, mechanistic insights into the interaction between tumors and the immune system, and understanding of how their interaction leads to differential response to immune checkpoint blockade.

## **CHAPTER TWO – MATERIALS AND METHODS**

## **Chapter 2 MATERIALS AND METHODS**

### **2.1 Patient Cohort and Tumor Samples**

#### **2.1.1 Study design**

Serial tumor biopsies were collected from patients with metastatic melanoma treated with CTLA-4 blockade and/or PD-1 blockade through the Expanded Access Program for MK-3475 at the UT MD Anderson Cancer Center. From serial tumor biopsies, we generated multidimensional profiling data (whole exome sequencing data, TCR sequencing data, and NanoString gene expression profiling). These data were analyzed to identify genomic and immune correlates of treatment response and resistance mechanisms of immune checkpoint blockade.

#### **2.1.2 Patient cohort and tumor samples**

A cohort of 56 patients with metastatic melanoma were included in this study. These patients were treated at the UT MD Anderson Cancer Center between October 2011 and March 2015 and had tumor samples collected with appropriate written informed consent and analyzed (IRB LAB00-063; LAB03-0320; 2012-0846; PA13-0291; PA12-0305). All tumor measurements were performed by a physician formally trained in tumor metrics, specifically RECIST 1.1 (61) as it applies to the cohort. All metrics used computerized axial tomography scan imaging of measurable lesions (5 lesions total and 2 per organ max.) that met measurability based on strict RECIST 1.1 criteria (i.e > 10mm long axis per target lesion or > 15mm short axis for target lymph nodes). The sum of

these respective diameters were compared to the sum at baseline. Per RECIST 1.1 criteria a lymph node < 10mm short axis was considered non-pathologic. As such patients were first defined at those having either a (1) complete response (disappearance of ALL target lesions, reduction in any pathological lymph nodes (whether target or not) in short axis to <10 mm, and the appearance of NO new lesions), (2) partial response (at least a 30% decrease in the sum of diameters of target lesions, no PD in non-target lesions and the appearance of NO new lesions), (3) progressive disease (at least a 20% increase in the sum of diameters of target lesions, taking as reference the smallest sum or baseline, with a minimum absolute increase of 5mm, and/or the development of any new lesions), or (4) stable disease [neither sufficient decrease to designate complete response (CR)/partial response (PR) nor increase to qualify as progressive disease (again using as a reference the smallest sum of appropriate diameters)]. All image responses were vetted with  $\geq 2$  serial images over a  $\geq 6$  month interval between baseline and assignment of response. RECIST 1.1 quantification of response was then used to assign patient designation as responder (i.e. CR, PR, or stable disease (SD)  $\geq 6$  months) or non-responder (progressive disease (PD) or SD < 6 months duration). All specimens were excisional biopsies or resection specimens.

## **2.2 Immune Profiling**

### **2.2.1 Immune profiling by IHC**

Tumor samples (n=88) were formalin-fixed and paraffin-embedded, including pretreatment anti-CTLA4 (n=36; 5 responders and 31 nonresponders), on-treatment anti-CTLA4 (n=5; 2 responders and 3 nonresponders), progression anti-CTLA4 (n=22), pretreatment anti-PD-1 (n=24; 7 responders and 17 nonresponders), on-treatment anti-PD-1 (doses 2–3; n=11; 5 responders and 6 nonresponders), and progression anti-PD-1 (n=12) biopsies. To examine the effect of CTLA4 blockade on pretreatment and on-treatment PD-1 blockade biopsies, additional immune profiling analysis by IHC was performed on a separate cohort of patients treated with PD-1 blockade who were CTLA4 blockade-naïve (n = 13), including pretreatment anti-PD-1 (n=9; 7 responders and 2 nonresponders) and on-treatment anti-PD-1 (n=4; 2 responders and 2 nonresponders) biopsies. From each tissue block, a hematoxylin and eosin-stained slide was examined to evaluate tumor cellularity. IHC was performed using an automated stainer (Leica Bond Max, Leica Biosystems), and the primary antibodies used included CD3 (DAKO, A0452, 1:100), CD4 (Leica Biosystems, NCL368, 1:80), CD8 (Thermo Scientific MA5-13473, 1:25), CD20 (DAKO, L26, 1:1,400), CD45RO (Leica Biosystems, PA0146, ready to use), CD57 (BD Biosciences, 347390, 1:40), CD68 (DAKO, MO876, 1:450), FOXP3 (BioLegend, 320102, 1:50), Granzyme B (Leica Microsystems, PA0291, ready to use), LAG3 (LifeSpan Bioscience, 17B4, 1:100), PD-1 (Epitomics, ab137132, 1:250), PD-L1 (Cell Signaling Technology, 13684, 1:100), CD14 (Abcam, Ab133503, 1:100), CD33 (Leica Microsystems, LCD33-L-CE, 1:100), CD163 (Leica Biosystems, NCL- L-CD163, 1:500), and CD206 (Abcam, Ab64693,

1:2,000). All slides were stained using previously optimized conditions with appropriate positive and negative controls. The IHC reaction was detected using the Leica Bond Polymer Refine detection kit (Leica Biosystems) and diaminobenzidine (DAB) was used as chromogen. Counterstaining was done using hematoxylin. IHC and hematoxylin and eosin–stained slides were converted into high-resolution digital images using an Aperio slide scanner (Aperio AT Turbo, Leica Biosystems). The digital images were then analyzed using the Aperio Image Toolbox analysis software (Leica Biosystems), Aperio image analysis algorithms nuclear and cytoplasmic v9. From each e-slide, 5 × 1 mm<sup>2</sup> areas within the tumor region (except for small biopsy samples) were chosen by a pathologist for digital analysis. IHC staining for CD3, CD4, CD8, CD20, CD45RO, CD57, CD68, FOXP3, Granzyme B, LAG3, PD-1, CD14, CD33, CD163, and CD206 was evaluated as density of cells, defined as the number of positive cells per mm<sup>2</sup>. PD-L1 expression was evaluated in tumor cells using H-score, which includes the percentage of positive cells showing membrane staining pattern (0–100) multiplied by the intensity of the staining (0 to 3+), with a total score ranging from 0 to 300. The final score for each marker was expressed as the average score of the areas analyzed within the tumor region (tumor center). In addition, of the initial cohort of 88 samples scored, 41 samples showing discernible tumor margins were evaluated for CD8 density at both tumor margin and center. The final scores for each marker from each patient were then transferred to a database for statistical analysis.

### **2.2.2 Immunofluorescence**

For a subset of formalin-fixed and paraffin-embedded samples (n=19), immunofluorescence staining was performed for CD8 (Thermo Scientific, MA5-13473) and CD68 (DAKO, MO876) to investigate potential myeloid–T cell interactions, including pretreatment anti-CTLA4 (n=5; 2 responders and 3 nonresponders), on-treatment anti-CTLA4 (n=2; 1 responder and 1 nonresponder), pretreatment anti-PD-1 (n=6; 3 responders and 3 nonresponders), and on-treatment anti-PD-1 (doses 2–3; n=6; 3 responders and 3 nonresponders) biopsies. This was done following the Opal protocol staining method with CD8 in Alexa488 (1:50) and CD68 in Alexa594 (1:100). For quantification, each individual DAPI-, CD8-, and CD68-stained section was utilized to establish the spectral library of fluorophores required for multispectral analysis. Slides were scanned using the Vectra slide scanner (PerkinElmer) under fluorescent conditions. For each marker, the mean fluorescent intensity per case was then determined as a base point from which positive calls could be established. Finally, an average of five random areas on each slide were analyzed for contact quantification (ratio of number of CD68 cells in contact with CD8 divided by number of CD68 cells) blindly by a pathologist at 20× magnification.

### **2.2.3 NanoString Gene Expression Analysis**

A subset of tumor samples (n=54) with adequate tissue following immune profiling were selected for NanoString analysis using a custom-designed 795-gene codeset (The gene list can be found from Supplementary Table S5 in Chen,



Pei-Ling, et al. "Analysis of immune signatures in longitudinal tumor samples yields insight into biomarkers of response and mechanisms of resistance to immune checkpoint blockade." *Cancer discovery* 6.8 (2016): 827-837.). This gene codeset includes the genes involved in immune response (Chemokines, Cytokines, Cell Functions, B-Cell Functions, Antigen Processing, Regulation, Cytotoxicity, NK Cell Functions, Transporter Functions, Pathogen Defense, Leukocyte Functions, T-Cell Functions, Adhesion, Complement, Senescence, Interleukins, Macrophage Functions, TLR, Microglial Functions, and TNF Superfamily) and cancer pathways (Notch, Wnt, HedgeHog, Chromatin Modification, Transcriptional Regulation, TGF-B, MAPK, STAT, PI3K, RAS, Cell Cycle, and Apoptosis). All tumor samples were prepared from formalin-fixed and paraffin-embedded tissue blocks, including pretreatment anti-CTLA4 (n=16; 5 responders and 11 nonresponders), on-treatment anti-CTLA4 (n=5; 3 responders and 2 nonresponders), progression anti-CTLA4 (n=15), pretreatment anti-PD-1 (n=16; 7 responders and 9 nonresponders), on-treatment anti-PD-1 (doses 2–3; n=10; 5 responders and 5 nonresponders), and progression anti-PD-1 (n=7) biopsies (Supplementary Tables S1D and S5). Hematoxylin and eosin–stained sections were prepared to evaluate tumor cellularity. Total RNA was extracted from each sample individually using the RNeasy Mini Kit (QIAGEN). For each NanoString assay, 1 µg of total tissue RNA was isolated, mixed with a NanoString code set mix, and incubated at 65°C overnight (16–18 hours). The reaction mixes were loaded on the NanoString nCounter Prep Station for binding and washing, and the resulting cartridge was transferred to the NanoString

nCounter digital analyzer for scanning and data collection. A total of 600 fields were captured per sample to generate the raw digital counts for each sample. To examine the effect of prior CTLA4 blockade on anti-PD-1 pretreatment and on-treatment tissue samples, a separate gene expression profiling analysis was performed using a custom-designed, 795-probe codeset on 28 samples. Compared with the initial code set, the  $\beta$ 2-microglobulin probe was deleted and the Melanoma Inhibitory Activity (MIA) probe was added. The same preprocessing, normalization, and statistical analysis of NanoString nCounter data were applied to these 28 anti-PD-1 samples, which included 7 pretreatment samples (4 responders, 3 nonresponders) and 8 on-treatment samples with prior CTLA4 blockade (3 responders, 5 nonresponders), as well as 8 pretreatment samples (6 responders, 2 nonresponders) and 5 on-treatment samples (2 responders, 3 nonresponders) that were CTLA4 blockade-naïve.

## **2.2.4 Statistical Analysis**

### **2.2.4.1 Immune Profiling by IHC**

Analyses were performed using GraphPad Prism software. All tests were two-sided, parametric *t* tests. *P* values of <0.05 were considered statistically significant.

### **2.2.4.2 NanoString Data Preprocessing**

Raw count data were preprocessed using NanoStringNorm R package NanoStringNorm (62). Specifically, geometric mean-based scaling normalization

was performed to account for technical assay variation, followed by background adjustment and RNA content normalization via annotated housekeeping genes. The most stable set of housekeeping genes (ABCF1, GUSB, TBP, and TUBB) was selected by the geNorm algorithm (63). Log<sub>2</sub>-transformed data were used for downstream analyses.

#### **2.2.4.3 Differential Gene Expression Analysis**

Fold change of each gene was calculated as the ratio of average gene expression intensity of the responder group to that of the nonresponder group. A two-sample *t* test was used to compare gene expression intensities between the responder group and the nonresponder group. To account for multiple testing, False Discovery Rate (FDR) (64), defined as the probability of being true under null hypothesis when rejected, was used. The beta-uniform mixture model (65) was used to obtain FDR. A gene was claimed to be differentially expressed if it showed a fold change of  $> 2$  (increased in responders) or  $\leq -1/2$  (increased in nonresponders) and  $FDR \leq 0.05$ . Volcano plots were used to visualize log<sub>2</sub> fold change on the *x*-axis and *P* values on the *y*-axis. Each gene was color-coded based on its fold change and FDR. This analysis was performed at individual time points (pre–anti-CTLA4, on–anti-CTLA4, pre–anti-PD-1, and on–anti-PD-1 treatment).

#### **2.2.4.4 Assessment of Time-by-Response Interaction**

A linear mixed effects model, implemented using R package lme4, was used to evaluate interactions between “Time (pretreatment, on-treatment)” and “Response (responders, nonresponders)” on gene expression intensity (66). In this model, the covariates of time, response, and time-by-response interactions were included as the fixed effects and a patient-specific random intercept was assumed to follow a mean 0 normal distribution. Again, an FDR threshold of 0.05 was used to select genes with significant interaction between time and response. Genes with positive interaction coefficients showed upregulated expression in responders or downregulated expression in nonresponders after a treatment, whereas genes with negative interaction coefficients showed downregulated expression in responders or upregulated expression in nonresponders after a treatment. Volcano plots were used to visualize the interaction coefficients on the *x*-axis and *P* values on the *y*-axis. Each gene was color-coded based on its interaction coefficients and FDR.

## **2.3 Genomic Profiling**

### **2.3.1 Sample processing**

After fixation and mounting, 5 to 10 slices of 5  $\mu$ m thickness were obtained from formalin-fixed, paraffin-embedded (FFPE) tumor blocks. Tumor-enriched tissue was macrodissected, and Xylene (EMD Millipore) was used for deparaffinization, followed by two ethanol washes. Reagents from the Qiagen QIAamp DNA FFPE Tissue Kit (#56404) were used in conjunction with an overnight incubation at 55°C to complete tissue lysis. Next, samples were

incubated at 90°C for one hour to reverse formaldehyde modification of nucleic acids. After isolation by QIAamp MinElute column, variable amounts of buffer ATE were added to each column to elute the DNA. Germline DNA was obtained from peripheral blood mononuclear cells (PBMCs).

### **2.3.2 Whole exome sequencing**

The initial genomic DNA input into the shearing step was 250 ng in 55 µL of low Tris-EDTA buffer. Forked Illumina paired-end adapters with random 8 base pair indexes were used for adapter ligation. All reagents used for end repair, A-base addition, adapter ligation, and library enrichment PCR were from the KAPA Hyper Prep Kit (#KK8504). Unligated adapter and/or adapter-dimer molecules were removed from the libraries before cluster generation using SPRI bead cleanup. The elution volume after post-ligation cleanup was 25 µL. Library construction was performed following manufacturer's instructions. Sample concentrations were measured after library construction using the Agilent Bioanalyzer. Each hybridization reaction contained 650-750 ng of the prepared library in a volume of 3.4 µL. Samples were lyophilized and reconstituted to bring the final concentration to 221 ng/µL. After reconstitution, the Agilent SureSelect-XT Target Enrichment (#5190-8646) protocol was followed, according to manufacturer guidelines. The libraries were then normalized to equal concentrations using an Eppendorf Mastercycler EP Gradient instrument and pooled to equimolar amounts on the Agilent Bravo B platform. Library pools were quantified using the KAPA Library Quantification Kit (#KK4824). Based on qPCR

quantification, libraries were then brought to 2 nM and denatured using 0.2N NaOH. After denaturation, libraries were diluted to 14-20 pM using Illumina hybridization buffer. Next, cluster amplification was performed on denatured templates according to manufacturer's guidelines (Illumina), HiSeq v3 cluster chemistry and flow cells, as well as Illumina's Multiplexing Sequencing Primer Kit. The pools were then added to flow cells using the cBot System and sequenced using the HiSeq 2000/2500 v3 Sequencing-by-Synthesis method, then analyzed using RTA v.1.13 or later. Each pool of whole exome libraries was subjected to paired 76 bp runs. An 8-base index-sequencing read was used to meet coverage and to demultiplex the pooled samples. Mean coverage for exome data was 177X in tumors and 91X in germline. Mean sequencing coverage and tumor purities were similar across groups, with the exception of on-treatment biopsies given the presence of lower tumor content and enriched immune infiltrates. Therefore, whole exome sequencing data from on-treatment samples were excluded from downstream analysis.

### **2.3.3 Mutation calling and intratumor heterogeneity analysis**

Exome sequencing data was processed using SaturnV, the NGS data processing and analysis pipeline developed and maintained by the Bioinformatics group of the Institute for Applied Cancer Science and Department of Genomic Medicine at UT MD Anderson Cancer Center. BCL files (raw output of Illumina HiSeq) were processed using Illumina CASAVA (Consensus Assessment of Sequence and Variation) software (v1.8.2) for demultiplexing/conversion to

FASTQ format. The FASTQ files were then aligned to the hg19 human genome build using BWA (v0.7.5) (67). The aligned BAM files were subjected to mark duplication, realignment, and recalibration using the Picard tool and GATK software tools (68-70). The BAM files were then used for downstream analysis. MuTect (v1.1.4) (71) was applied to identify somatic point mutations, and Pindel (v0.2.4) (72) was applied to identify small insertions and deletions. Somatic mutations in HLA genes were called by POLYSOLVER (v1.0) (32). EXPANDS (v1.6.1) (73) and SciClone (v1.0.7) (74) were applied with only LOH-free regions to estimate the number of clones per tumor.

#### **2.3.4 Neoantigen prediction**

HLA class I neo-epitopes were predicted for each patient as previously described (75). In short, patient HLA-A, -B, and -C variants were identified using ATHLATES (v2014\_04\_26) (76). Next, all possible 9- to 11-mer peptides flanking a nonsynonymous exonic mutation were generated computationally, and binding affinity was predicted based on patient HLA and compared to that of the wild-type peptide counterpart using NetMHCpan (v2.8) algorithm (77). Mutated peptides with predicted IC50 < 500 nM were considered as predicted neoantigens. TCGA melanoma (78) gene expression data were used to further filter out predicted neoantigens with mean gene expression values below 5 (mean RSEM < 5).

#### **2.3.5 Copy number alteration analysis**

Sequenza (v2.1.2) (79) was applied to obtain copy number segments of

$\log_2$  copy ratios (tumor/normal) for each tumor sample. R package 'CNTools' (v1.24.0) (80) was used to identify copy number gain ( $\log_2$  copy ratios  $> \log_2 1.5$ ) or loss ( $\log_2$  copy ratios  $< -\log_2 1.5$ ) at the gene level. The burden of copy number gain or loss was then calculated as the total number of genes with copy number gain or loss per sample. For recurrent copy number alteration analysis, R package 'cghMCR' (v1.26.0) (81) was applied to  $\log_2$  copy ratios (tumor/normal) obtained from 'exomecn' (in-house copy number caller). Segment Gain or Loss (SGOL) scores of copy number segments or genes were calculated as sum of  $\log_2$  copy ratios of each copy number segment or gene across all samples within a group of interest. Copy number segments with both copy number gain and copy number loss present within a group were excluded. We identified genomic regions of recurrent copy number alterations (MCRs: minimum common regions) using cghMCR function with the following parameters: gapAllowed=500, alteredLow= $-\log_2(1.5)$ , alteredHigh= $\log_2(1.5)$ , recurrence=60, spanLimit=2e+07, thresholdType="value" (recurrent copy number loss was defined as copy number loss observed in more than 60% of samples in a group of interest). Tumor suppressor genes annotated in recurrent copy number loss plots were obtained as cancer genes present in both the Catalogue of Somatic Mutations in Cancer (COSMIC) (v77) (82) and TSGene databases (83). Two samples were excluded from analysis due to unusable copy number profiles (45E and 20E).

### **2.3.6 TCR sequencing and clonality analysis**



T cell receptor sequencing of the CDR3 variable region of the beta chain was performed by ImmunoSeq hsTCRB Kit as described previously (Adaptive Biotechnologies) (84, 85). In brief, DNA was extracted from FFPE tumor tissues, and CDR3 regions were amplified prior to sequencing by MiSeq 150X (Illumina). Data were then transferred to Adaptive Technologies for deconvolution of CDR3 beta sequences. For each sample, Shannon entropy and TCR clonality were calculated using the ImmunoSeq Analyzer (86).

### **2.3.7 NanoString gene expression profiling**

NanoString was performed using a custom codeset of 795 genes as previously described (87). In brief, RNA was extracted using the RNeasy Mini Kit (QIAGEN) from FFPE blocks, after initial confirmation of tumor presence and content by two pathologists by H&E. For gene expression studies, 1 µg of RNA was used per sample. Hybridization was performed for 16-18 hours at 65°C, and samples were loaded onto the nCounter Prep Station for binding and washing prior to scanning and capture of 600 fields using the nCounter. Preprocessing of NanoString data was performed as previously described (87). Immune scores were calculated as geometric mean of gene expression of cytolytic markers (*GZMA*, *GZMB*, *PRF1*, *GNLY*), HLA molecules (*HLA-A*, *HLA-B*, *HLA-C*, *HLA-E*, *HLA-F*, *HLA-G*, *HLA-H*, *HLA-DMA*, *HLA-DMB*, *HLA-DOA*, *HLA-DOB*, *HLA-DPA1*, *HLA-DPB1*, *HLA-DQA1*, *HLA-DQA2*, *HLA-DQB1*, *HLA-DRA*, *HLA-DRB1*), IFN-γ pathway genes (*IFNG*, *IFNGR1*, *IFNGR2*, *IRF1*, *STAT1*, *PSMB9*), chemokines

(*CCR5*, *CCL3*, *CCL4*, *CCL5*, *CXCL9*, *CXCL10*, *CXCL11*), and adhesion molecules (*ICAM1*, *ICAM2*, *ICAM3*, *ICAM4*, *ICAM5*, *VCAM1*).

### **2.3.8 Independent (Van Allen) cohort analysis**

Mutational load was obtained from nonsynonymous mutational load in an earlier study (25). WES data (SAM files) from 110 melanoma patients and RNA-seq data from 42 patients (FASTQ files) were downloaded through the dbGaP (accession number phs000452.v2.p1). Copy number alterations were identified from the same computational pipeline as described above. For the Van Allen cohort, recurrent copy number loss was defined as copy number loss observed in more than 40% of samples in a group of interest. Twelve samples were excluded from analysis due to unusable copy number profiles (Pat06, Pat73, Pat78, Pat81, Pat92, Pat106, Pat121, Pat132, Pat165, Pat166, Pat171, and Pat175). In the minimal or no clinical benefit group, samples with low burden of copy number loss (<100) were excluded from recurrent copy number alteration analysis. The relatively low cutoff of 100 was chosen to capture the majority of recurrent events. For RNA-seq analysis, all the RNA-seq samples were first aligned to the human reference genome (hg19, GRCh37.75) with Bowtie2 (v2.2.5). RSEM (v1.2.12) was used to quantify transcript expression at the gene level in FPKM. Immune scores for the independent cohort were calculated by ESTIMATE (88). eBayes-moderated *t*-test was performed to compare the high burden of copy number loss (n=10) and low burden of copy number loss groups (n=10). Rank metric was then calculated as the sign of log<sub>2</sub> fold changes multiplied by inverse

of  $P$  values. Gene set enrichment analysis (GSEA) (89) was performed on the rank metric-sorted list of genes.

### **2.3.9 Statistical analysis**

Statistical analyses were performed using R 3.2.2. Statistical tests included two-sided Fisher's exact tests and two-sided Mann-Whitney tests.

## **CHAPTER THREE – IMMUNE PROFILING**

### **Chapter 3 IMMUNE PROFILING**

Content of this chapter is based on:

(\*Authors contributed equally)

From Pei-Ling Chen\*, Whijae Roh\*, Alexandre Reuben, Zachary A. Cooper, Christine N. Spencer, Peter A. Prieto, John P. Miller, Roland L. Bassett, Vancheswaran Gopalakrishnan, Khalida Wani, Mariana Petaccia De Macedo, Jacob L. Austin-Breneman, Hong Jiang, Qing Chang, Sangeetha M. Reddy, Wei-Shen Chen, Michael T. Tetzlaff, Russell J. Broaddus, Michael A. Davies, Jeffrey E. Gershenwald, Lauren Haydu, Alexander J. Lazar, Sapna P. Patel, Patrick Hwu, Wen-Jen Hwu, Adi Diab, Isabella C. Glitza, Scott E. Woodman, Luis M. Vence, Ignacio I. Wistuba, Rodabe N. Amaria, Lawrence N. Kwong, Victor Prieto, R. Eric Davis, Wencai Ma, Willem W. Overwijk, Arlene H. Sharpe, Jianhua Hu, P. Andrew Futreal, Jorge Blando, Padmanee Sharma, James P. Allison, Lynda Chin and Jennifer A. Wargo, "Analysis of immune signatures in longitudinal tumor samples yields insight into biomarkers of response and mechanisms of resistance to immune checkpoint blockade." *Cancer Discovery* 6, no. 8 (2016): 827-837.

Copyright permissions are not required, since AACR journal policy states

“Authors of articles published in AACR journals are permitted to use their article or parts of their article in the following ways without requesting permission from the AACR. All such uses must include appropriate attribution to the original AACR publication. Authors may do the following as applicable:

1. Reproduce parts of their article, including figures and tables, in books, reviews, or subsequent research articles they write;
2. Use parts of their article in presentations, including figures downloaded into PowerPoint, which can be done directly from the journal's website;
3. Post the accepted version of their article (after revisions resulting from peer review, but before editing and formatting) on their institutional website, if this is required by their institution. The version on the institutional repository must contain a link to the final, published version of the article on the AACR journal website so that any subsequent corrections to the published record will continue to be available to the broadest readership. The posted version may be released publicly (made open to anyone) 12 months after its publication in the journal;
4. Submit a copy of the article to a doctoral candidate's university in support of a doctoral thesis or dissertation.”

### **3.1 Introductions and Rationale**

Major advances have been made in the treatment of metastatic melanoma through the use of immune checkpoint blockade, with the FDA approval of numerous therapeutic regimens within the past several years (21, 90-94) and many more being studied in clinical trials (95, 96). Treatment with immune checkpoint inhibitor monotherapy [such as monoclonal anti- bodies targeting cytotoxic T-lymphocyte–associated antigen-4 (CTLA4) and programmed death-1 (PD-1)] is associated with response rates of 8% to 44%, and many of these responses are durable (i.e., >2 years). However, the majority of patients do not

respond to these regimens as monotherapy, and some patients develop significant toxicity (90, 97-99), particularly when these regimens are combined (92). Given these complexities, a critical need exists to identify biomarkers that accurately predict which patients will benefit from this form of therapy.

Although several genomic and immune predictors of response have been reported based on analysis of pretreatment tumor biopsies, these biomarkers are not very robust, and there is significant overlap between responders and nonresponders to therapy for the markers tested (39, 41, 48, 100). Genomic and RNA-based studies exploring predictors of outcome to immune checkpoint blockade in melanoma suggest that tumor-specific mutational load and neoantigen signature as well as cytolytic activity are significantly associated with clinical benefit and increased overall survival (25, 39, 101). IHC-based studies also support the notion that CD8+, CD4+, PD-1+, and programmed death-ligand 1-positive (PD-L1+) cell densities in pretreatment biopsies can predict response to therapy (48, 100). However, cumulative evidence from these studies suggests that these biomarkers are not perfectly predictive (39, 48), and better biomarkers are clearly needed to optimize therapeutic decisions.

In addition to identifying predictors of response to immune checkpoint blockade, there is growing interest in understanding the mechanistic differences between different forms of immune checkpoint blockade. Transcriptome and pathway analysis using purified human T cells and monocytes from patients on either CTLA4 or PD-1 blockade demonstrates distinct gene expression profile and immunologic effects between these forms of therapy (102, 103). Whereas

CTLA4 blockade induces a proliferative signature in memory T cells, PD-1 blockade leads to changes in genes implicated in cytotoxicity and natural killer cell function (103). This notion is further supported by animal models that demonstrate differential effects of CTLA4 and PD-1 blockade therapies on the transcriptional profiles of tumor-infiltrating CD8<sup>+</sup> T cells, with increased NFAT–JAK–STAT signaling, cell proliferation/cell cycle, and activation of effector T-cell pathways seen in CTLA4 blockade versus changes in IL2 signaling, response to type I IFN, and metabolic pathways seen in PD-1 blockade (102).

Along with this, there is a critical need to identify mechanisms of therapeutic resistance to immune checkpoint inhibitors that are potentially actionable. Groups have begun to study this (50, 101), and there is evidence that somatic mutations in antigen processing and presentation as well as upregulation of genes involved in cell adhesion, angiogenesis, and extracellular matrix remodeling may contribute to immune escape in cancer (104). In addition, molecular analyses of human melanoma samples and animal models also suggest that tumor-intrinsic oncogenic signals related to the WNT/ $\beta$ -catenin signaling pathway may mediate cancer immune evasion and resistance to immunotherapy, including CTLA4- and PD-1–based therapy (105).

In this study, we sought to address each of these areas of critical need by studying a unique cohort of patients with metastatic melanoma who were initially treated with CTLA4 blockade and were then treated with PD-1 blockade at time of progression. A deep immune analysis of longitudinal tumor samples was performed, yielding insights into biomarkers of response, mechanistic differences



between each of these forms of therapy, and means of therapeutic resistance to immune checkpoint blockade.

## **3.2 Results**

### **3.2.1 Patient Cohort, Checkpoint Blockade Treatment, and Longitudinal Tumor Biopsies**

To explore differential changes in the tumor microenvironment in distinct forms of immune checkpoint blockade, we assembled a unique cohort of 53 patients with metastatic melanoma who were initially treated with CTLA4 blockade and were then treated with PD-1 blockade if they did not respond or progressed on therapy. The scheme of treatment and longitudinal tumor sampling is shown in [Figure 1](#). Biopsies were obtained (when available) prior to initiation of CTLA4 blockade, on-treatment, and after restaging in patients who did not respond to or who progressed on therapy. Clinical responders were defined by radiographic evidence of absent disease, stable disease, or decreased tumor volume for >6 months. Nonresponders were defined by tumor growth on serial CT scans after the initiation of treatment or any clinical benefit lasting  $\leq 6$  months (minimal benefit). Nonresponders to CTLA4 blockade were then treated with PD-1 blockade therapy, and additional biopsies were obtained early during the course of therapy and late on-treatment in nonresponders (or progressors) on PD-1 blockade ([Figure 1](#)). Among the patients treated with CTLA4 blockade, 13% achieved clinical benefit, whereas 87% did not, consistent with published response rates (21, 99). [Table 1 and 2](#) shows the clinical and

demographic characteristics of the patients in this cohort. Available biopsies were subsequently processed for downstream immune profiling by IHC and gene expression studies ([Table 3 and 4](#)).

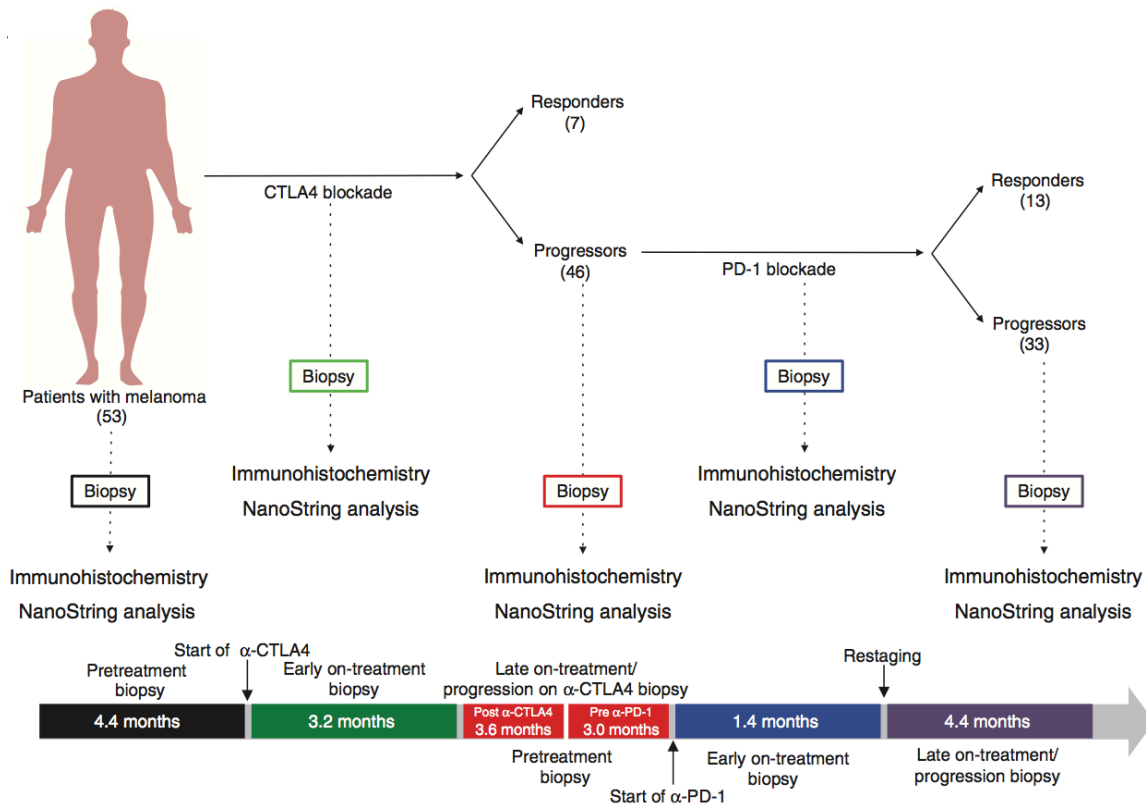


**Figure 1. A cohort of patients treated with sequential CTLA4 and PD-1 blockade.**

Patients with metastatic melanoma were initially treated with CTLA4 blockade (n = 53) and nonresponders to CTLA4 blockade were then treated with PD-1 blockade (n = 46; Expanded Access Program for MK-3475 at the MD Anderson Cancer Center). Of these 46 patients, 13 responded to PD-1 blockade, whereas 33 progressed. Tumor biopsy samples were collected at multiple time points during their treatment when feasible, including pretreatment, on-treatment, and progression anti-CTLA4 biopsies, and pretreatment, on-treatment (doses 2–3), and progression anti-PD-1 biopsies, for downstream immune profiling by IHC and gene expression studies. The median elapsed time between tumor biopsies and treatment is shown for each time point. The profile and kinetics of immune cell infiltrates in the tumor microenvironment were compared between responders and nonresponders to CTLA4 blockade. Tumor samples available for immune profiling by IHC included pretreatment anti-CTLA4 [n = 36; 5 responders (R)

and 31 nonresponders (NR)], on-treatment anti-CTLA4 (n = 5; 2 responders and 3 nonresponders) and progression anti-CTLA4 biopsies (n = 22).

	Anti-CTLA-4 Responders (n=7)	Anti-PD-1 Responders (n=15)	Anti-PD-1 Progressors (n=33)	All Patients* (n=56)
<b>Age at start of first immunotherapy</b>				
Mean	61	57	56	57
Range	47-82	27-86	28-84	27-86
<b>Sex- no. of patients (%)</b>				
Female	5 (71)	4 (27)	10 (30)	19 (34)
Male	2 (29)	11 (73)	23 (70)	37 (66)
<b>Disease Origin- no. of patients (%)</b>				
Acral	1 (14)	2 (13)	4 (12)	7 (12)
Cutaneous	5 (71)	9 (60)	24 (73)	39 (70)
Mucousal	0 (0)	1 (6)	0 (0)	1 (2)
Unknown Primary	1 (14)	3 (20)	5 (15)	9 (16)
<b>Mutational Status- no. of patients (%)</b>				
BRAF	4 (50)	4 (22)	2 (7)	10 (22)
NRAS	1 (12)	5 (28)	10 (34)	16 (29)
CKIT	0	1 (5)	4 (14)	5 (9)
TP53	2 (25)	2 (11)	5 (26)	9 (16)
<b>Lactate dehydrogenase level at start of therapy — no. of patients (%)</b>				
Normal (<618 IU/L)	2 (29)	11 (74)	1 (3)	15 (27)
Above Normal (≥618 IU/L)	4 (57)	2 (13)	25 (76)	31 (55)
Not Available	1 (14)	2 (13)	7 (21)	10 (18)
<b>Previous Therapies -no.*</b>				
Mean	1	2	4	2
Range	0-4	0-7	0-9	0-9
<b>Duration between aCTLA-4 and aPD1--wk</b>				
Mean	NA	21.6	36.7	NA
Range	NA	0-86	0-165	NA
<b>RECIST Response Classification</b>				
Progression of Disease	2 (29)	3 (20)	33 (100)	38 (68)
Stable Disease	0 (0)	3 (20)	0 (0)	3 (5)
Partial Response	5 (71)	7 (47)	0 (0)	12 (21)
Complete Response	0 (0)	2 (13)	0 (0)	2 (4)

\* includes 1 additional patient (Patient 17) who progressed on anti-CTLA-4 and did not receive anti-PD-1

**Table 1. Cohort level clinical summary**

Patient ID	Group (1=IR,2=INR,3=PDR,4=PDNR)	Sex	Age	anti-CTLA-4 Response	anti-PD-1 Response	anti-CTLA-4			anti-PD-1		
						Treated (Y/N)	RECIST (CR, PR, SD, PD)	# of prior or concurrent therapies	Treated (Y/N)	RECIST (CR, PR, SD, PD)	# of prior or concurrent therapies
1	4	F	48	nonresponse	nonresponse	Y	PD	1	Y	PD	3
2	4	M	50	nonresponse	nonresponse	Y	PD	2	Y	PD	3
3	4	F	60	nonresponse	nonresponse	Y	PD	3	Y	PD	4
4	4	M	72	nonresponse	nonresponse	Y	PD	4	Y	PD	8
5	1	F	47	response	NA	Y	PR	3	N	NA	NA
6	3	M	48	nonresponse	response	Y	PD	1	Y	PD*	2
7	3	M	64	nonresponse	response	Y	PD	1	Y	PR	2
8	3	M	54	nonresponse	response	Y	PD	1	Y	CR	2
9	3	M	58	nonresponse	response	Y	PD	2	Y	SD	4
10	1	F	54	response	NA	Y	PR	0	N	NA	NA
11	4	M	82	nonresponse	nonresponse	Y	PD	3	Y	PD	5
12	1	M	70	response	NA	Y	PD*	2	N	NA	NA
13	4	M	52	nonresponse	nonresponse	Y	PD	0	Y	PD	2
14	3	F	66	nonresponse	response	Y	PD	1	Y	PR	2
15	3	F	43	NA	response	N	NA	NA	Y	PD*	0
16	4	M	34	nonresponse	nonresponse	Y	PD	0	Y	PD	2
17	2	F	58	nonresponse	NA	Y	PD	0	N	NA	NA
18	4	F	66	nonresponse	nonresponse	Y	PD	2	Y	PD	3
19	4	M	55	nonresponse	nonresponse	Y	PD	3	Y	PD	8
20	4	M	59	nonresponse	nonresponse	Y	PD	1	Y	PD	2
21	4	M	63	nonresponse	nonresponse	Y	PD	0	Y	PD	1
22	1	F	50	response	NA	Y	PR	0	N	NA	NA
23	4	M	40	nonresponse	nonresponse	Y	PD	0	Y	PD	1
24	3	M	50	nonresponse	response	Y	PD	0	Y	SD	2
25	4	F	46	nonresponse	nonresponse	Y	PD	4	Y	PD	6
26	4	F	60	nonresponse	nonresponse	Y	PD	1	Y	PD	7
27	1	F	56	response	NA	Y	PR	0	N	NA	NA
28	4	M	55	nonresponse	nonresponse	Y	PD	2	Y	PD	4
29	4	M	34	nonresponse	nonresponse	Y	PD	7	Y	PD	9
30	4	M	66	nonresponse	nonresponse	Y	PD	1	Y	PD	2
31	1	F	71	response	NA	Y	PD*	4	N	NA	NA
32	4	F	84	nonresponse	nonresponse	Y	PD	0	Y	PD	1
33	4	F	61	nonresponse	nonresponse	Y	PD	0	Y	PD	2
34	3	M	69	nonresponse	response	Y	PD	1	Y	PR	2
35	3	F	49	nonresponse	response	Y	PD	0	Y	CR	1
36	4	M	56	nonresponse	nonresponse	Y	PD	1	Y	PD	4
37	1	M	82	response	NA	Y	PR	1	N	NA	NA
38	4	F	53	nonresponse	nonresponse	Y	PD	0	Y	PD	2
39	4	M	55	nonresponse	nonresponse	Y	PD	1	Y	PD	4
40	4	M	53	nonresponse	nonresponse	Y	PD	1	Y	PD	5
41	4	M	68	nonresponse	nonresponse	Y	PD	3	Y	PD	6
42	4	F	48	nonresponse	nonresponse	Y	PD	2	Y	PD	6
43	4	M	61	nonresponse	nonresponse	Y	PD	2	Y	PD	2
44	4	F	62	nonresponse	nonresponse	Y	PD	0	Y	PD	1
45	4	M	59	nonresponse	nonresponse	Y	PD	0	Y	PD	5
46	3	F	27	nonresponse	response	Y	PD	3	Y	PR	4
47	3	M	72	nonresponse	response	Y	PD	2	Y	PR	3
48	4	M	68	nonresponse	nonresponse	Y	PD	2	Y	PD	3
49	4	M	46	nonresponse	nonresponse	Y	PD	1	Y	PD	4
50	4	M	68	nonresponse	nonresponse	Y	PD	0	Y	PD	4
51	3	M	37	nonresponse	response	Y	PD	1	Y	PD*	2
52	3	M	65	nonresponse	response	Y	PD	5	Y	SD	7
53	4	M	54	nonresponse	nonresponse	Y	PD	5	Y	PD	6
54	4	M	28	nonresponse	nonresponse	Y	PD	2	Y	PD	3
55	3	M	86	NA	response	N	NA	NA	Y	PR	0
56	3	M	69	nonresponse	response	Y	PD	1	Y	PR	2

**Table 2. Patient level clinical characteristics**

Patient ID	anti-CTLA-4			anti-PD-1		
	Pre	On	Pro	Pre	On	Pro
1						
2						
3						
4						
5						
6						
7						
8						
10						
12						
13						
14						
•15						
16						
17						
18						
19						
20						
21						
22						
23						
24						
25						
26						
27						
28						
29						
30						
31						
32						
33						
34						
35						
38						
39						
40						
41						
42						
43						
44						
45						
47						
49						
50						
51						
52						
53						
54						
•55						
•56						
•58						
•59						
•60						
•61						
•63						
•64						
•65						
•67						
•68						

	No sample profiled
	Sample profiled
	Not applicable

•= CTLA-4 blockade naïve patients

**Table 3. Immune profiling by IHC sample log**

Patient ID	anti-CTLA-4			anti-PD-1		
	Pre	On	Pro	Pre	On	Pro
1						
2						
3						
4						
5						
6						
7						
8						
9						
10						
•15						
16						
18						
19						
22						
23						
24						
25						
26						
27						
31						
37						
40						
42						
43						
45						
47						
49						
50						
52						
54						

	No sample profiled
	Sample profiled
	Not available

•= CTLA-4 blockade naïve patients

**Table 4. Immune profiling by NanoString 54 sample log**



### **3.2.2 Immune Profiling in Early On-Treatment Biopsies Is Predictive of Response to CTLA4 Blockade in a Unique Cohort of Patients Treated with Sequential CTLA4 and PD-1 Blockade**

The profile and kinetics of immune cell infiltrates in the tumor microenvironment were first investigated via a 12-marker IHC panel. At the pretreatment time point, there was no difference in any of the measured markers between responders versus nonresponders to CTLA4 blockade (Figure 2), consistent with previous reports (106). However, analysis of early on-treatment tumor biopsies identified a significantly higher density of CD8+ T cells in responders versus nonresponders to CTLA4 blockade (Figure 2;  $P < 0.05$ ). IHC for other immune and immunomodulatory markers at the on-treatment time point on CTLA4 blockade showed no significant differences in responders versus nonresponders, though a trend toward higher PD-L1 expression was observed in responders (Figure 2). Representative IHC images for CD8, CD4, and PD-L1 expression in responders and nonresponders to CTLA4 blockade are shown for each time point in Figure 3.

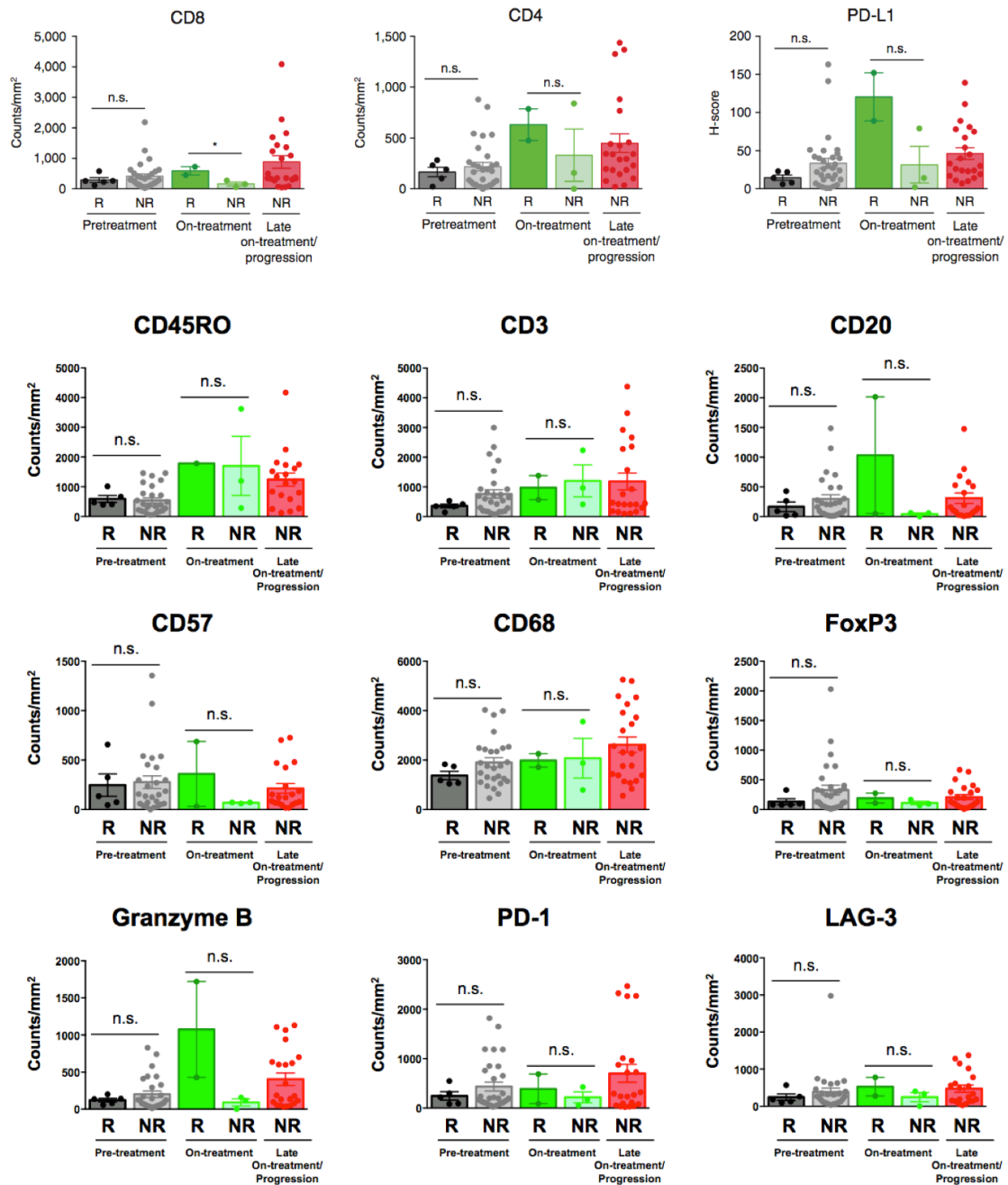


**Figure 2. Immune profiling of pre-treatment, on-treatment and progression CTLA-4 blockade samples by immunohistochemistry.** Immune profiling was performed via a 12-marker immunohistochemistry panel. CD8, CD4, PD-L1 (H-score), CD45RO, CD3, CD20, CD57, CD68, FoxP3, Granzyme B, PD-1, and LAG-3 were assessed for density by quantitative IHC. Error bars represent standard error mean. n.s.= not significant

(The experiment and analysis were done by Dr. Pei-Ling Chen. This figure was used with permission from Dr. Pei-Ling Chen.)

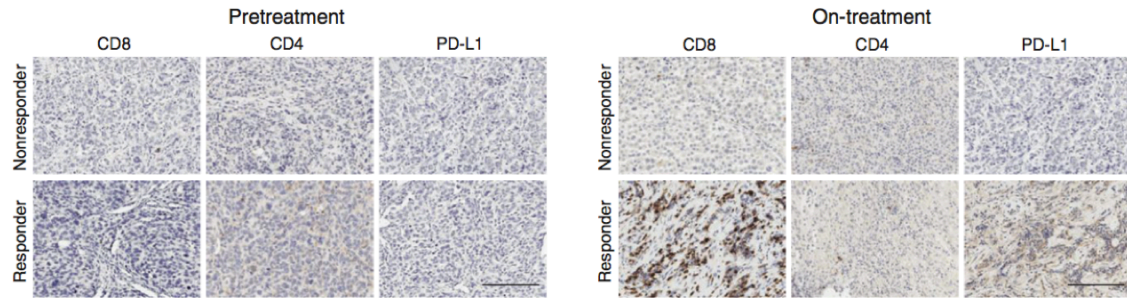


**Figure 3. Representative IHC images of CD8, CD4, and PD-L1 in responders and nonresponders at the pre- and on-treatment time point.** Representative images at pretreatment and early on-treatment time points are shown in responders versus nonresponders to CTLA4 blockade (20× magnification). Error bars, SEM. \*,  $P \leq 0.05$ ; n.s., not significant. Scale bars, 200  $\mu\text{m}$ .

(The experiment and analysis were done by Dr. Pei-Ling Chen. This figure was used with permission from Dr. Pei-Ling Chen.)

In addition, to better understand the contribution of myeloid–T cell interactions to therapeutic response, we also stained sections with additional myeloid markers (CD14, CD33, CD163, and CD206). Though we saw no clear quantitative differences in any of the myeloid subsets in responders versus nonresponders to CTLA4 blockade (Figure 4), we observed a slightly higher proximity of CD68+ myeloid cells to CD8+ T cells in nonresponders at the pretreatment time point (Figure 5A and 5B;  $P = 0.08$ ); however, this did not reach statistical significance in this small cohort.

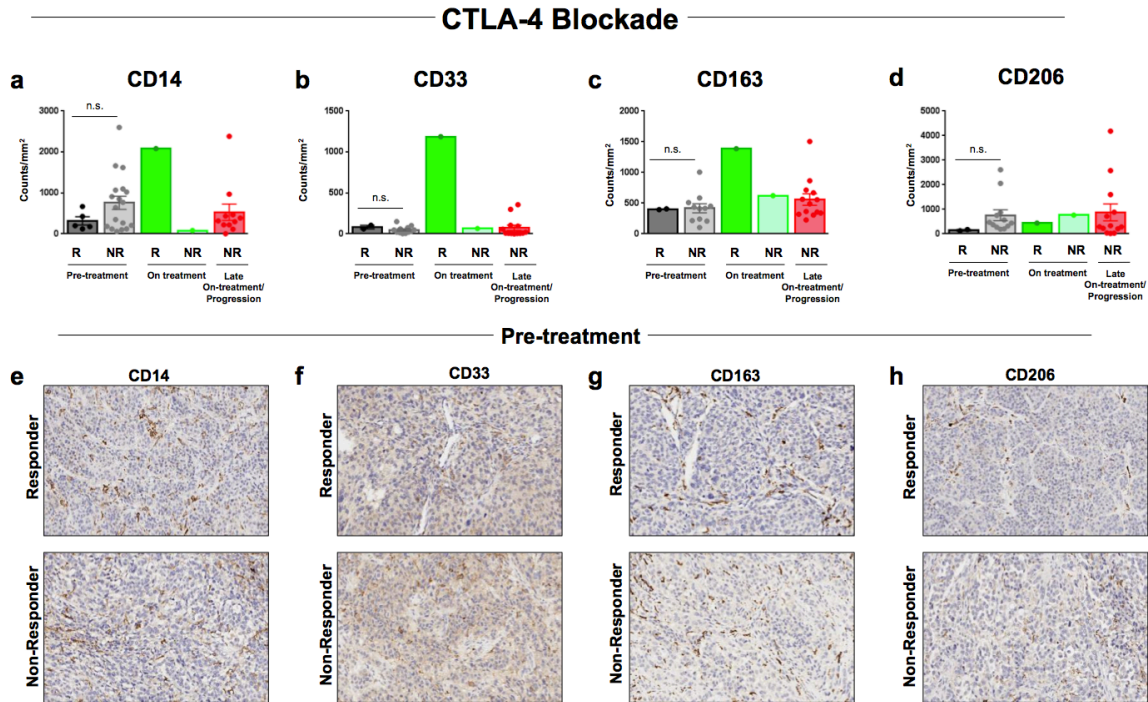
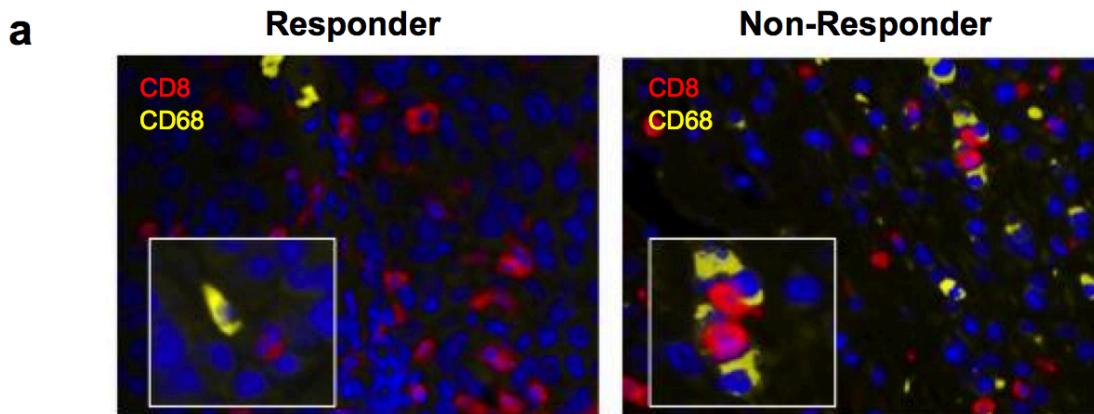


**Figure 4. Myeloid cell profiling of pre-treatment, on-treatment and progression CTLA-4 blockade samples by immunohistochemistry.** Immune profiling was performed via a 4-marker immunohistochemistry panel. CD14 (a), CD33 (b), CD163 (c), and CD206 (d) were assessed for density by quantitative IHC. Shown in (e)-(h) are representative IHC images in responders and non-responders at the pre-treatment timepoint. Error bars represent standard error mean. n.s.= not significant. Statistical analysis was not possible between responders and non-responders at on-treatment time point as only one sample was available per group. (The experiment and analysis were done by Dr. Pei-Ling Chen. This figure was used with permission from Dr. Pei-Ling Chen.)



**b**

Treatment Timepoint	% Contact Between CD8 and CD68 Cells		
	Responders (n)	Non-Responders (n)	p-value
<b>CTLA-4 Blockade</b>			
Pre-treatment	<10% (2)	30-40% (3)	0.08
On treatment	10-20% (1)	30-40% (1)	N/A
<b>PD-1 Blockade</b>			
Pre-treatment	10-20% (3)	50-60% (3)	0.0495
On treatment	<10% (3)	30-40% (3)	0.0495

**Figure 5. Increased contact between CD8 T cells and CD68 myeloid cells in non-responding patients to anti-CTLA-4 and anti-PD-1 therapy at pre-treatment CTLA-4 blockade, pre-treatment PD-1 blockade, and on-treatment PD-1 blockade time points. (a)** Immunofluorescence staining showing nuclei by DAPI (blue), CD8 (red) and CD68 (yellow) cells in a responder and non-responder. **(b)** Semi-quantitative pathological assessment of percentage of CD8 and CD68 cells in contact in responders and non-responders pre-treatment and on treatment with anti-CTLA-4 and anti-PD-1 therapy.

(The experiment and analysis were done by Dr. Pei-Ling Chen. This figure was used with permission from Dr. Pei-Ling Chen.)

### **3.2.3 Immune Profiling in Early On-Treatment Biopsies Is Highly Predictive of Response to PD-1 Blockade**

We next used our 12-marker IHC panel to interrogate the profiles and kinetics of immune cell subsets in tumor samples from patients on anti-PD-1 therapy. Forty-six patients were included who were initially treated with CTLA4 blockade, as well as 11 additional patients who had not received prior CTLA4 blockade to control for possible prior CTLA4 blockade exposure effects. In these studies, we observed a modest but statistically significant difference in the density of CD8+, CD3+, and CD45RO+ T cells in pretreatment samples of responders compared with nonresponders (Figure 6;  $P = 0.03, 0.03, 0.02$ , respectively), though the values between these two groups were largely overlapping, consistent with prior published data (106). There was also a trend toward higher pretreatment expression of CD4 and PD-1 in responders versus nonresponders, though these did not reach statistical significance (Figure 6;  $P = 0.06, P = 0.08$ , respectively).



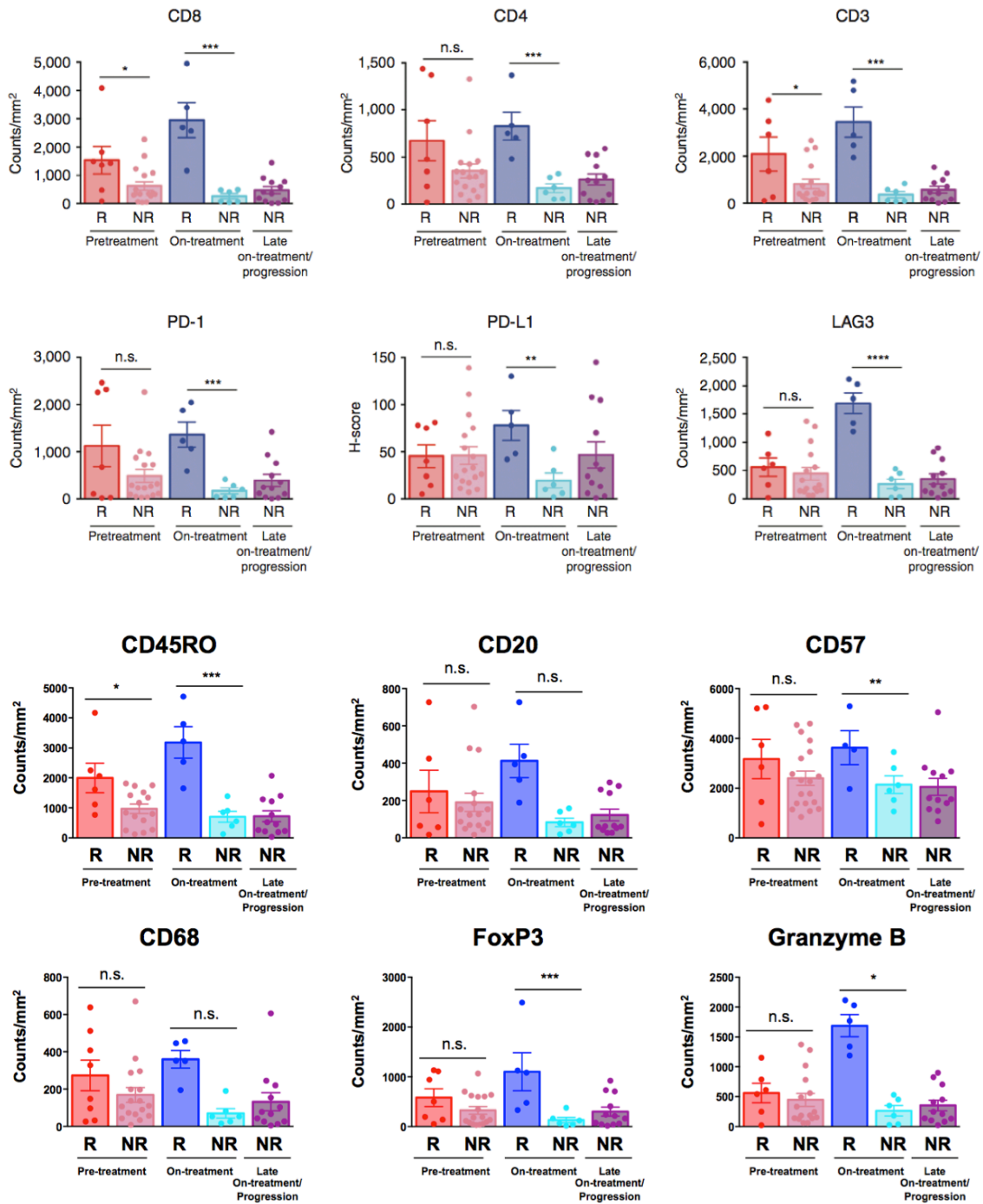


**Figure 6. Immune profiling of pre-treatment, on-treatment and progression PD-1 blockade samples by immunohistochemistry.** Longitudinal tumor biopsies were performed (at pretreatment, early on-treatment, and late on-treatment/progression time points) in patients undergoing treatment with PD-1 blockade (n = 47). The profile and

kinetics of immune cell infiltrates in the tumor microenvironment were compared between responders (R) and nonresponders (NR) to PD-1 blockade. Tumor samples available for immune profiling by IHC included pretreatment anti-PD-1 (n = 24; 7 responders and 17 nonresponders), on-treatment anti-PD-1 (doses 2–3; n = 11; 5 responders and 6 nonresponders), and progression anti-PD-1 (n = 12) biopsies. CD8, CD4, CD3, PD-1, PD-L1 (H-score), LAG3, CD45RO, CD20, CD57, CD68, FoxP3, and Granzyme B density are shown in responders versus nonresponders. (The experiment and analysis were done by Dr. Pei-Ling Chen. This figure was used with permission from Dr. Pei-Ling Chen.)

In contrast, there was a profound and highly statistically significant difference in the expression of markers for T-cell subsets—CD8 ( $P = 0.001$ ), CD4 ( $P = 0.001$ ), and CD3 ( $P < 0.001$ )— and immunomodulatory molecules PD-1 ( $P < 0.001$ ), PD-L1 ( $P = 0.007$ ), and LAG3 ( $P < 0.0001$ ) in responders versus non-responders to therapy in early on-treatment tumor samples, with little to no overlap between groups (Figure 6). Of note, a significantly higher level of expression of FOXP3 ( $P < 0.001$ ) and granzyme B ( $P = 0.02$ ) was observed in responders compared with nonresponders to therapy, likely relating to an enhanced activation status of infiltrating T cells in responding patients (Figure 6). Importantly, these changes were observed in responders as early as 2 to 3 doses following initiation of PD-1–based therapy. Representative IHC images for these markers are shown in Figure 7. Specific analysis performed on longitudinal samples also demonstrated an increase in CD8, PD-1, and PD-L1 in responders compared with nonresponders to PD-1–based therapy (Figure 8).

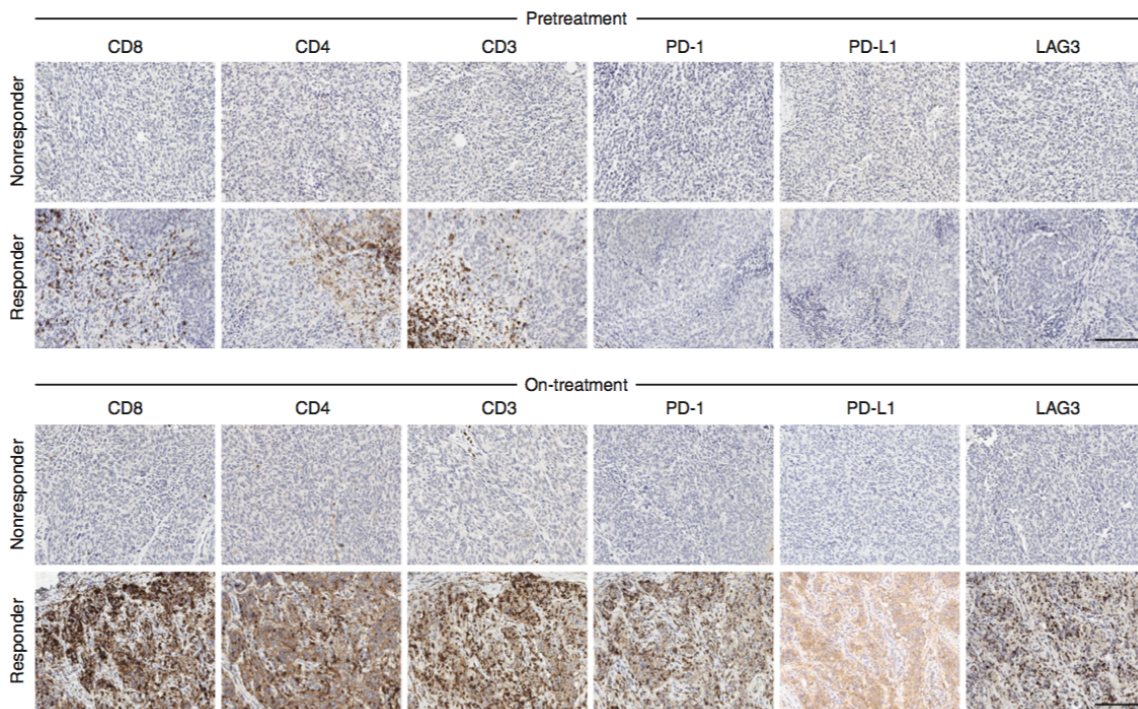


**Figure 7. Representative immunohistochemistry images of selected markers at pretreatment and early on-treatment time points.** Representative images at pretreatment and early on-treatment time points are shown in responders versus nonresponders to PD-1 blockade (20× magnification). Error bars, SEM. \*,  $P \leq 0.05$ ; \*\*,  $P \leq 0.01$ ; \*\*\*,  $P \leq 0.001$ ; \*\*\*\*,  $P \leq 0.0001$ ; n.s., not significant. Scale bars, 200  $\mu\text{m}$ . (The experiment was done by Dr. Pei-Ling Chen. This figure was used with permission from Dr. Pei-Ling Chen.)

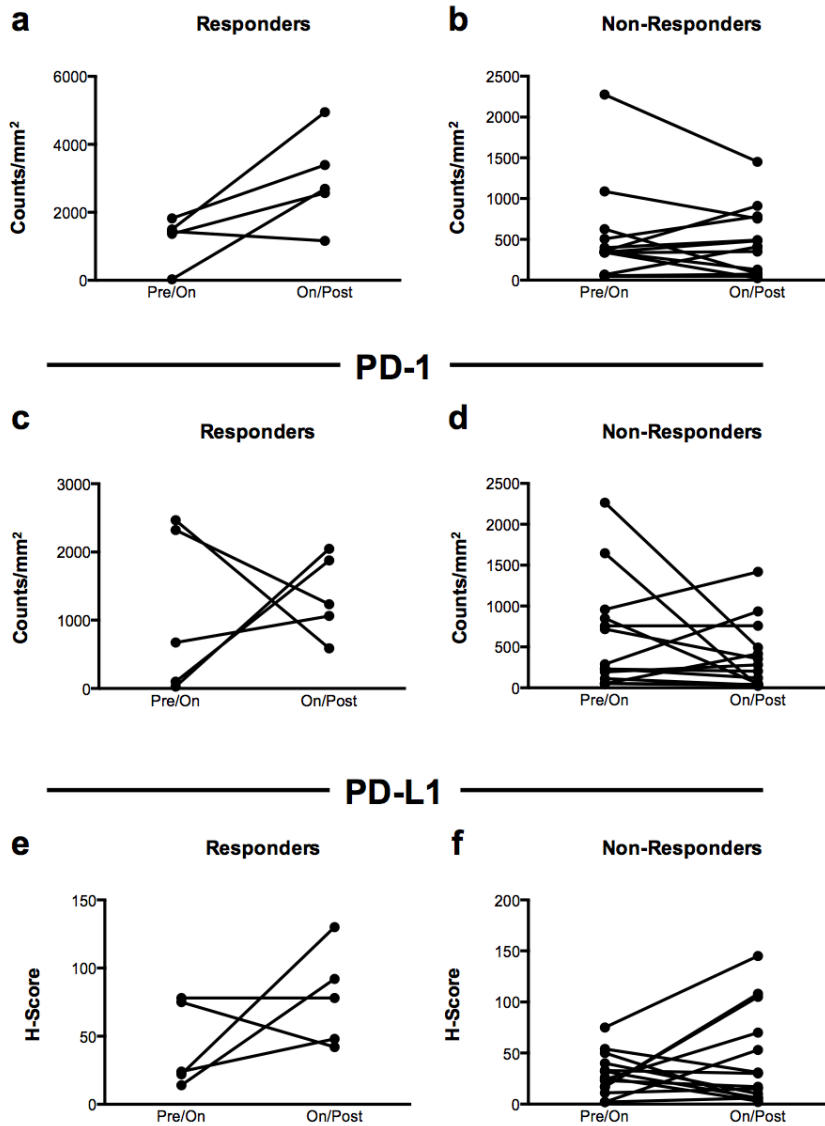


**Figure 8. Longitudinal increase in CD8, PD-1, and PD-L1 expression in responders to anti-PD-1 therapy.** Five paired responder (a, c, e) and 14 paired non-responder (b, d, f) samples were evaluated for changes in CD8 (a-b) and PD-1 (c-d) counts/mm<sup>2</sup> and PD-L1 (e-f) H-Score at pre/on-treatment and on/post-treatment time points by immunohistochemistry. Lines link paired samples.

(The analysis was done by Dr. Pei-Ling Chen. This figure was used with permission from Dr. Pei-Ling Chen.)

In light of previous studies demonstrating the importance of the invasive tumor margin in predicting responses to PD-1 blockade (48), we quantified CD8+ T-cell density at the tumor margin in 41 samples with discernible tumor margins. In these studies, we did not observe significant differences in CD8+ T cells at the tumor margin between responders and non-responders to PD-1–based therapy at all time points examined, though sample size was admittedly limited. However, when we compared the ratio of CD8+ T cells at tumor center versus the margin in early on-treatment biopsies, we observed significantly higher ratios of CD8+ T cells at the tumor center versus the margin within responders compared with nonresponders (Figure 9A–9H), suggesting possible infiltrate from margin to center of the tumor in the context of therapy.

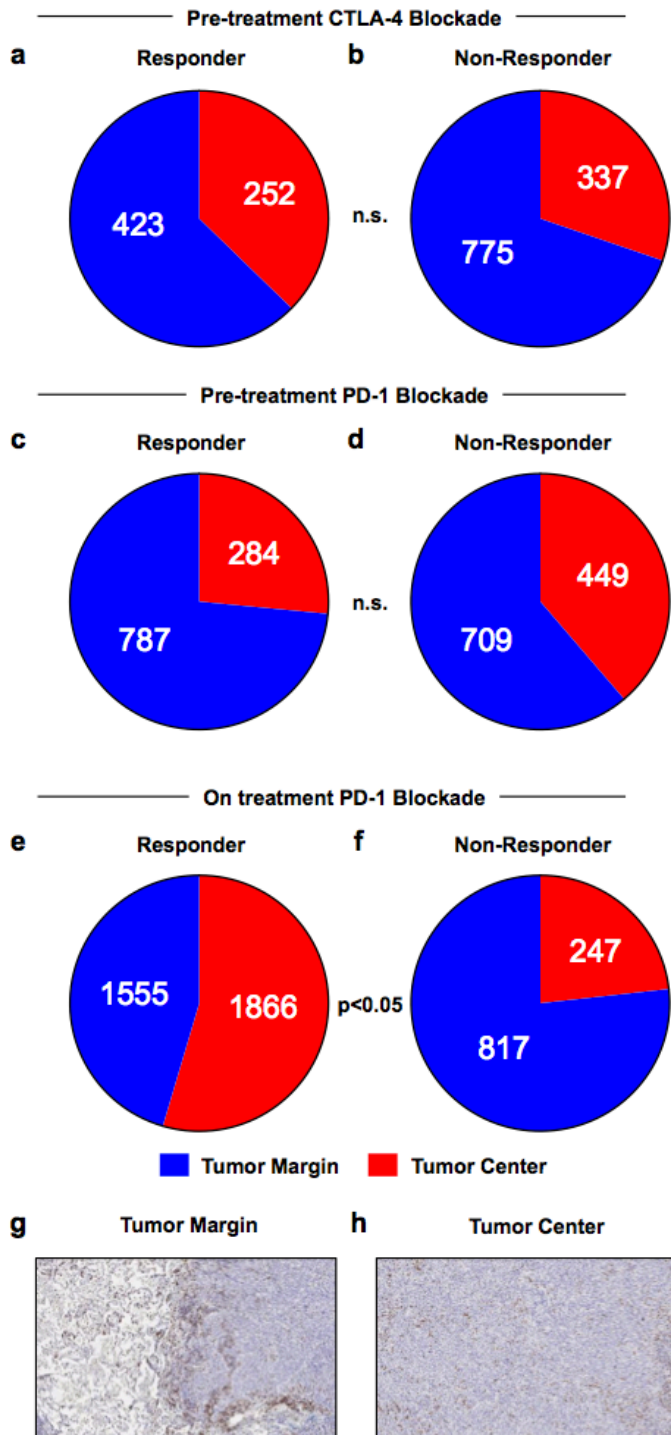


**Figure 9. Relative increase in CD8 T cell infiltrate at tumor center in responders to anti-PD-1 on treatment.** Pie charts depicting the CD8 counts/mm<sup>2</sup> at pre-treatment anti-CTLA-4 (a-b), pre-treatment anti-PD-1 (c, d), and on treatment anti-PD-1 (e, f) time

points in responders and non-responders at tumor margin (**g**) and center (**h**). Numbers represent average counts per treatment time point. Blue = Tumor margin, Red = Tumor center. Pre-treatment anti-CTLA-4: Responders (n=3), Non-responders (n=15); Pre-treatment anti-PD-1: Responders (n=2), Non-responders (n=8); On treatment anti-PD-1: Responders (n=2), Non-responders (n=2).

(The experiment and analysis were done by Dr. Pei-Ling Chen. This figure was used with permission from Dr. Pei-Ling Chen.)



To augment these studies, we performed immune profiling in the separate cohort of patients who received PD-1 blockade in the absence of prior CTLA4 exposure, and observed no significant differences in our prior observations when these patients were included in the analysis (Figure 10A–10H). As observed previously with CTLA4 blockade, we saw no clear quantitative difference in any of the myeloid subsets in responders and nonresponders to PD-1 blockade (Figure 11A–11I). However, we observed a significantly higher proximity of CD68+ myeloid cells to CD8+ T cells in nonresponders at the pretreatment and on-treatment time points for patients on PD-1 blockade (Figure 5,  $P < 0.05$ ).

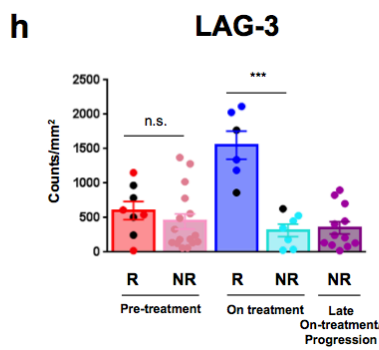
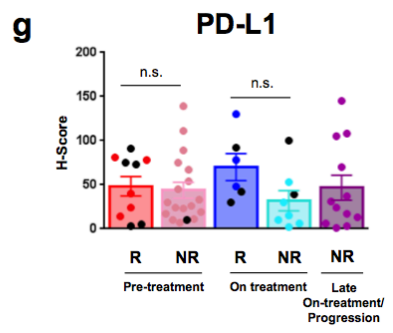
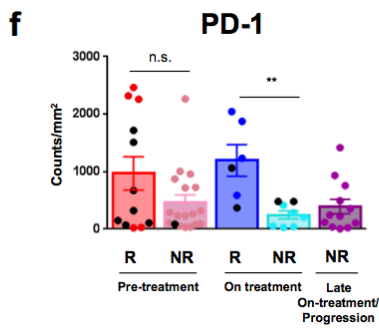
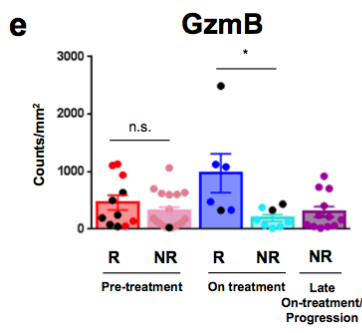
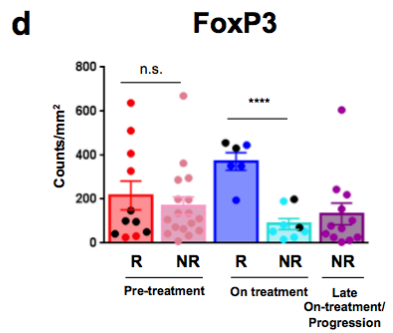
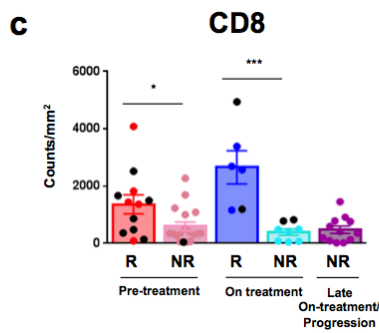
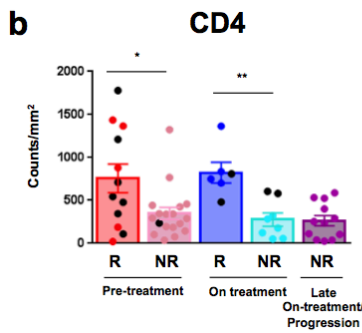
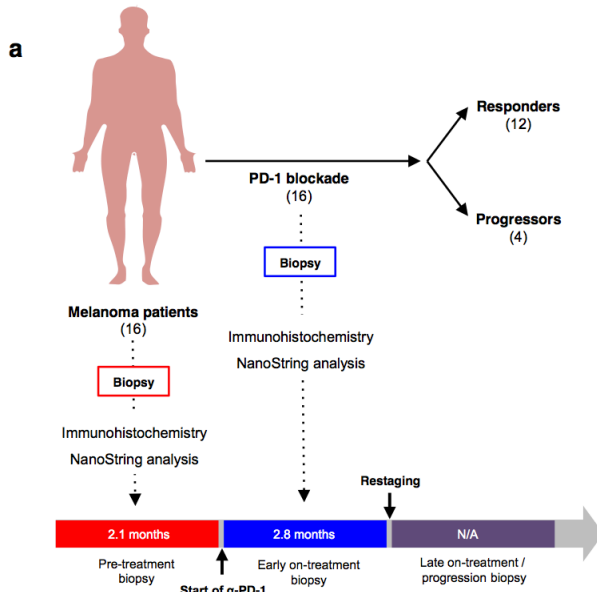


**Figure 10. Significant increase in immune infiltrate between responders and non-responders to PD-1 blockade in absence of prior anti-CTLA-4 therapy.** (a) Timeline illustrating breakdown of anti-CTLA-4-naïve patient samples by response and treatment time point and planned analyses. CD4 (b), CD8 (c), FoxP3 (d), GzmB (e), PD-1 (f), PD-L1 (g), and LAG-3 (h) were assessed for density by quantitative IHC. Error bars represent standard error mean. n.s.= not significant. Black dots depict anti-CTLA-4-naïve patients. \*=  $p \leq 0.05$ , \*\*=  $p \leq 0.01$ , \*\*\*=  $p \leq 0.001$ , n.s.= not significant.

(The experiment and analysis were done by Dr. Pei-Ling Chen. This figure was used with permission from Dr. Pei-Ling Chen.)

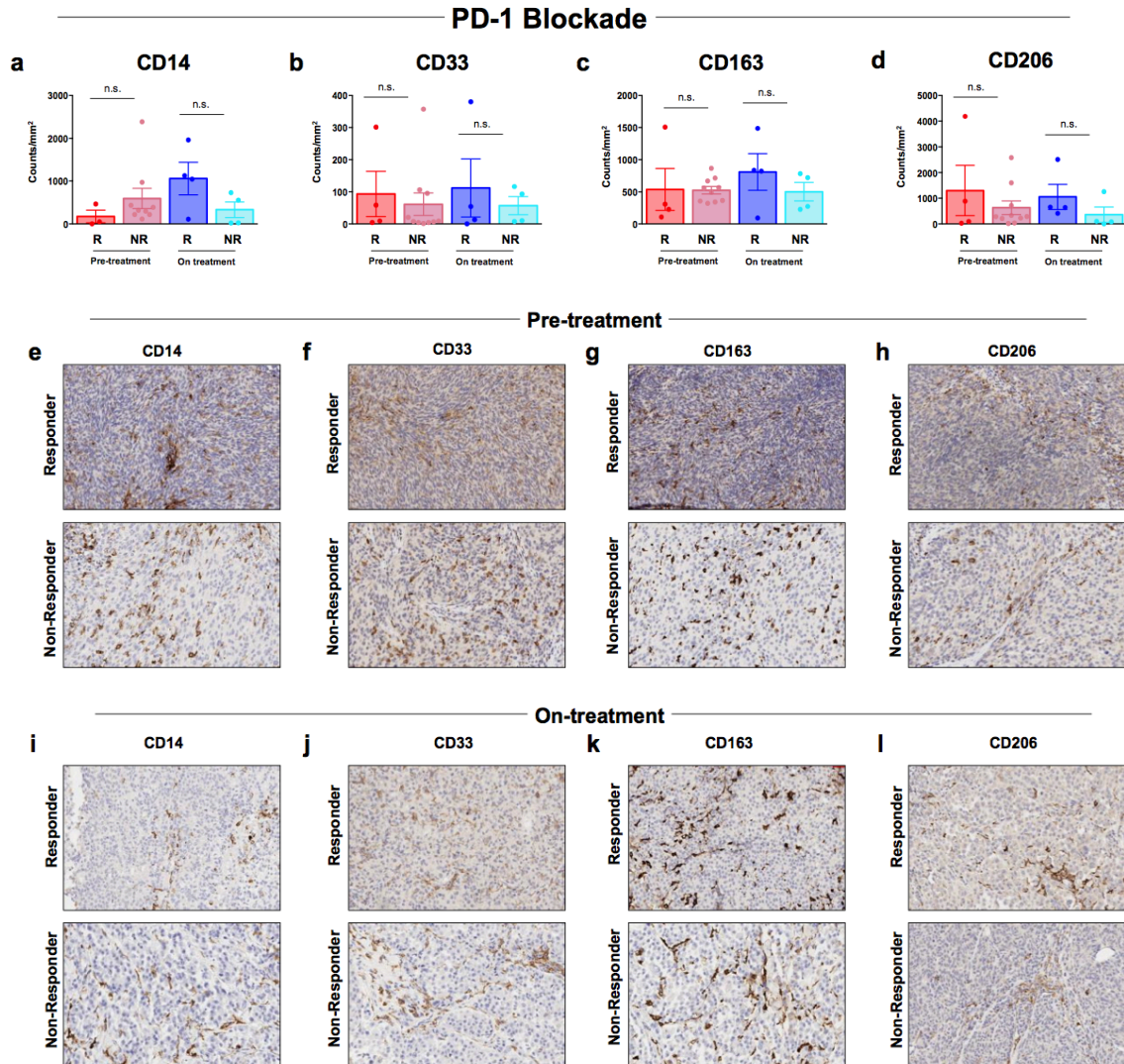


**Figure 11. Immune profiling of myeloid cells at pre-treatment and on-treatment PD-1 blockade time points by immunohistochemistry.** CD14 (a), CD33 (b), CD163 (c), and CD206 (d) were assessed for density by quantitative IHC. Shown in (e-h) and (i-l) are representative IHC images in responders and non-responders at the pre-treatment and on treatment timepoints, respectively. Error bars represent standard error mean. n.s.= not significant.

(The experiment and analysis were done by Dr. Pei-Ling Chen. This figure was used with permission from Dr. Pei-Ling Chen.)

### **3.2.4 Gene Expression Profiling in Longitudinal Tumor Biopsies Is Predictive of Response in Patients Treated with Sequential CTLA4 and PD-1 Blockade**

To further dissect the tumor microenvironment–mediated response and resistance to immune checkpoint blockade and to identify potential mechanisms of therapeutic resistance, we performed targeted gene expression profiling (GEP) via a custom 795-gene NanoString panel composed of immune-related genes and genes pertaining to common cancer signaling pathways in samples with available tissue. When comparing GEP results between responders and non-responders at each individual biopsy time point, no significant differences were found at pretreatment CTLA4 blockade, on- treatment CTLA4 blockade, and pretreatment PD-1 blockade. However, early on-treatment tumor samples of patients on anti– PD-1 therapy showed 411 significantly differentially expressed genes (DEG) in responders (FDR-adjusted  $P < 0.05$ ), mostly upregulated as compared with nonresponders (Figure 12A–D and Figure 13), including IHC markers represented in the NanoString code- set, cytolytic markers, HLA molecules, IFN $\gamma$  pathway effectors, chemokines and select adhesion molecules. Notably, a small number of DEGs ( $n = 6$ ) were lower in responders than in non-responders on PD-1 blockade and included vascular endothelial growth factor (VEGFA), suggesting a mechanism of therapeutic resistance and a potential target for therapy, which is corroborated by data from others implicating angiogenesis in resistance to immunotherapy (107-109). Notably, though only 10 of the 12 IHC markers were represented in the NanoString codeset, all 10

overlapping probes showed concordance with our IHC findings ([Figure 14A–14J](#) and [Figure 15](#)).

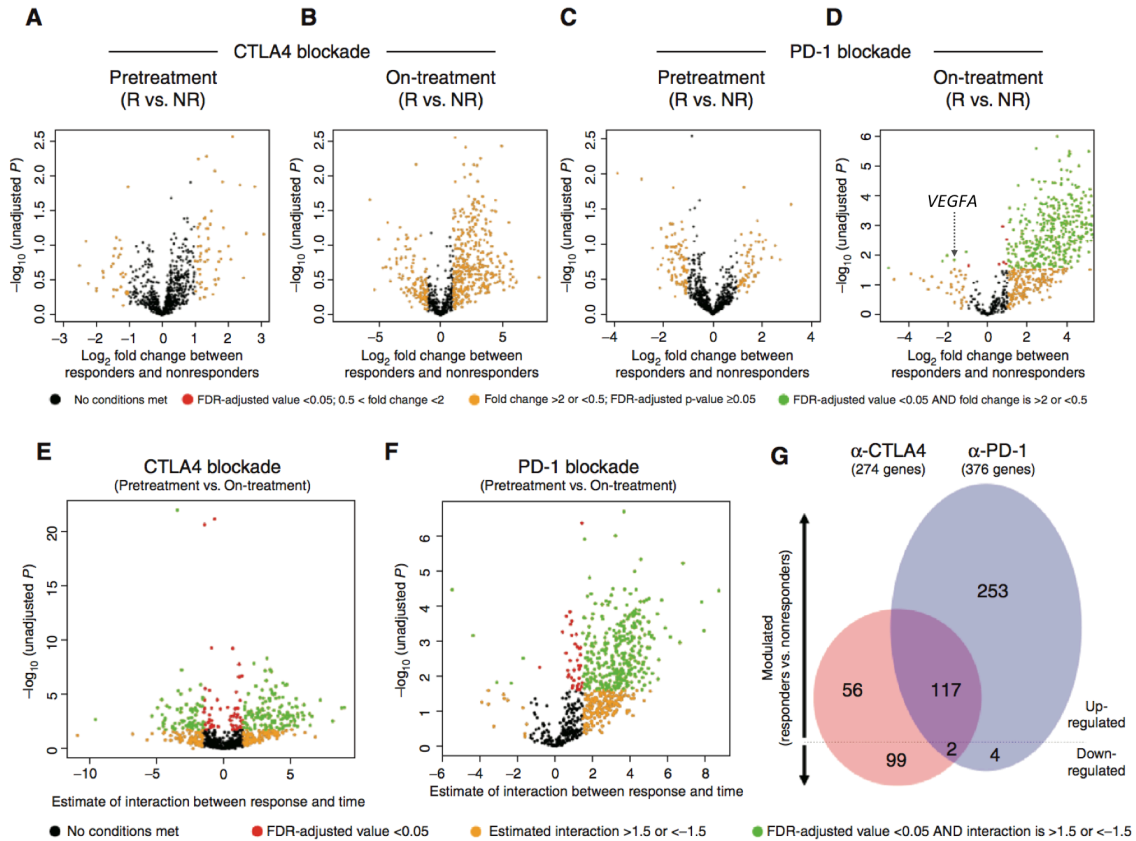


**Figure 12. Gene expression profiling in longitudinal tumor biopsies is predictive of response in a unique cohort of patients treated with sequential CTLA4 and PD-1 blockade.** Gene expression profiling was performed via NanoString in longitudinal tumor biopsies from patients treated with sequential CTLA4 and PD-1 blockade (n = 54), including pretreatment anti-CTLA4 [n = 16; 5 responders (R) and 11 nonresponders (NR)], on-treatment anti-CTLA4 (n = 5; 3 responders and 2 nonresponders), and progression anti-CTLA4 biopsies (n = 15), pretreatment anti-PD-1 (n = 16; 7 responders and 9 nonresponders), on-treatment anti-PD-1 (doses 2–3; n = 10; 5 responders and 5 nonresponders), and progression anti-PD-1 (n = 7) biopsies. Volcano plots illustrate the log<sub>2</sub> fold change (FC) in gene expression (responders vs. nonresponders) on the x-axis and unadjusted P values from Student t tests between responders and nonresponders on the y-axis. Differentially expressed genes (FDR-adjusted  $P < 0.05$  and FC >2 or

$<-1/2$ ) between responders and nonresponders were highlighted in green at the time of pretreatment (**A**) and on-treatment (**B**) CTLA4 blockade, pretreatment (**C**) and on-treatment (**D**) PD-1 blockade. Interaction of time covariate (pretreatment, on-treatment) and response covariate (responders, nonresponders) was illustrated in volcano plots. Genes with significant interaction were highlighted in green (FDR-adjusted  $P < 0.05$  and interaction  $>1.5$  or  $<-1.5$ ) for CTLA4 blockade (**E**) and PD-1 blockade (**F**). Venn diagram illustrates shared and unique genes upregulated and downregulated in CTLA4 (red) and PD-1 (blue) blockade over treatment time course (**G**).



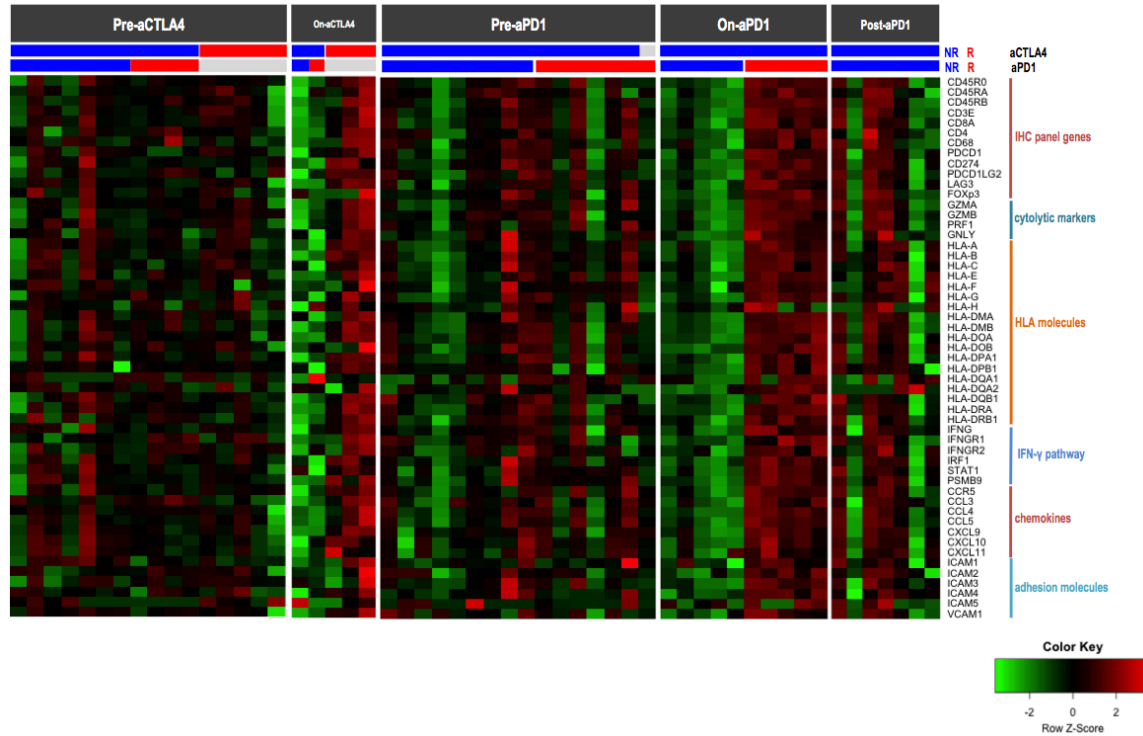


**Figure 13. Heatmap of 54 NanoString samples.** Values are log<sub>2</sub>-transformed normalized mRNA count. Samples are ordered by treatment time point and by responsiveness to anti-CTLA-4 or anti-PD-1 therapy. Color pattern is relative with respect to the row within each time point, with red indicating gene up-regulation and green indicating gene down-regulation.

## CTLA-4 Blockade

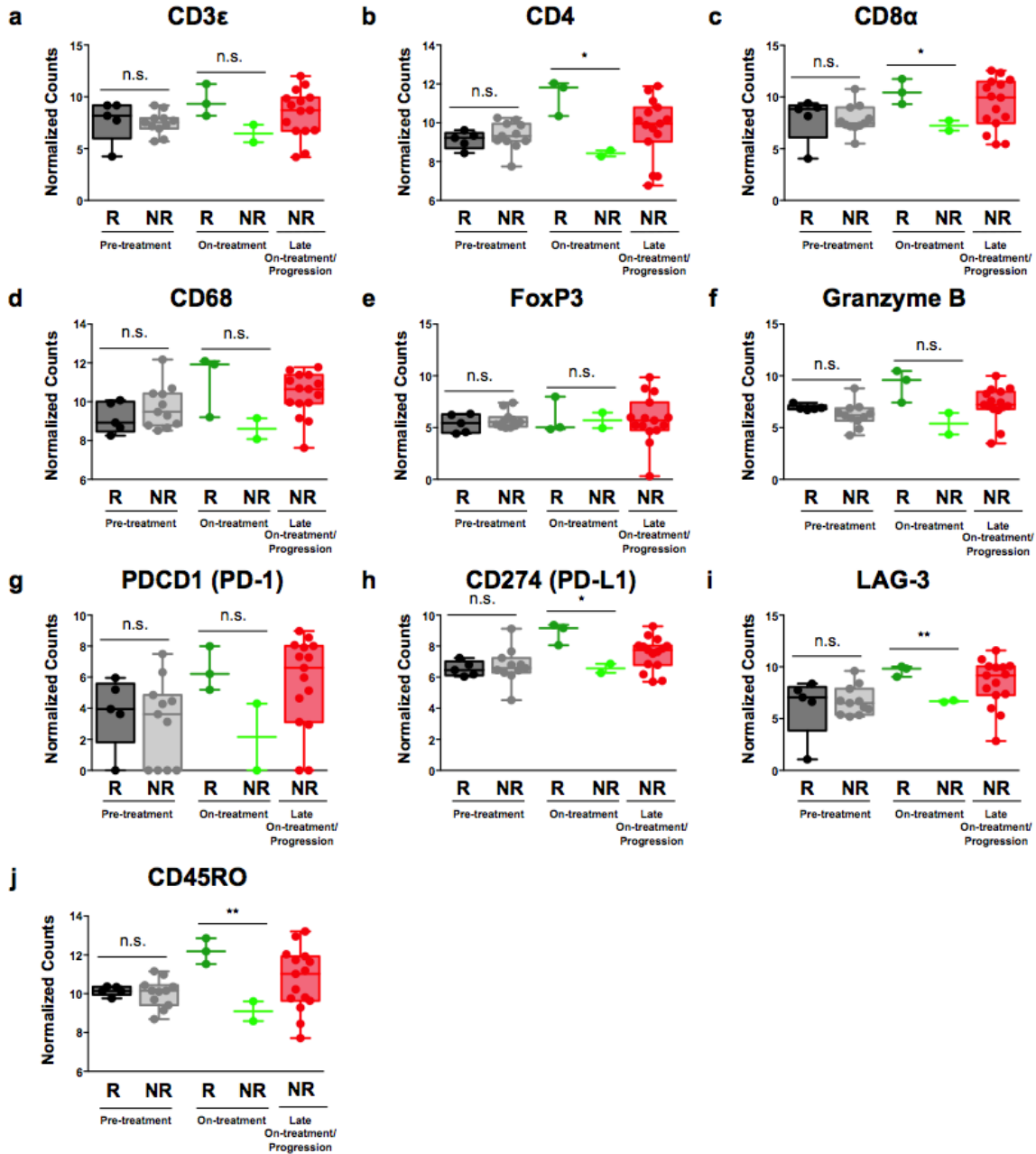


**Figure 14. Gene-specific NanoString concordance with immune profiling by IHC in pre-treatment, on-treatment and progression CTLA-4 blockade samples.** Gene expression profiling was performed via NanoString on 54 tumor biopsies. Of the custom-designed 795 probe code set, 10 probes were represented in our immune profiling analysis by IHC, namely CD3, CD4, CD8, CD45RO, CD68, FoxP3, Granzyme B, LAG-3,

PD-1 and PD-L1. All values represented by box and whisker plots. \*=  $p \leq 0.05$ , \*\*=  
 $p \leq 0.01$ , \*\*\*=  $p \leq 0.001$ , n.s.= not significant.

(The analysis was done by Dr. Pei-Ling Chen. This figure was used with permission from  
Dr. Pei-Ling Chen.)

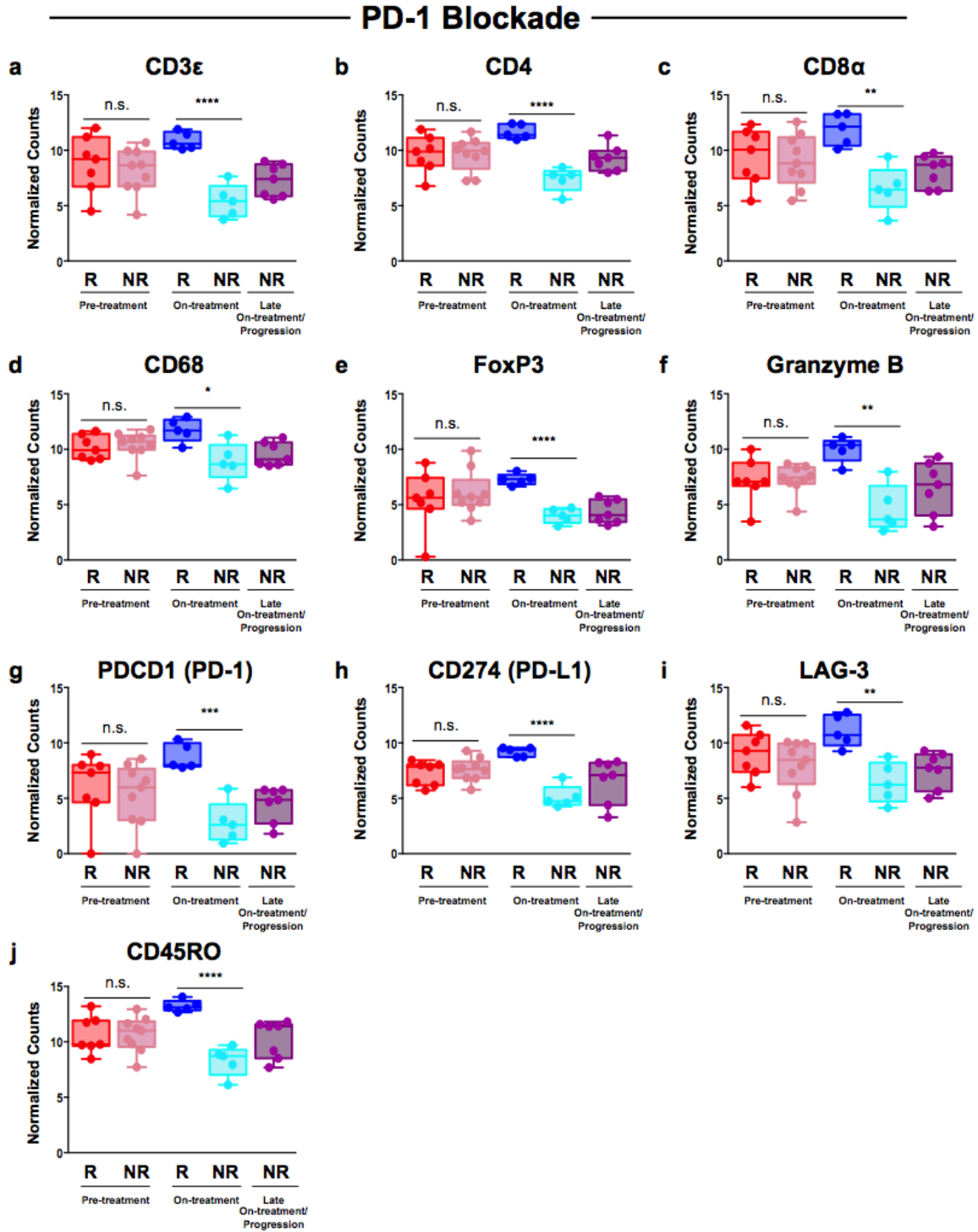


**Figure 15. Gene-specific NanoString concordance with immune profiling by IHC in pre-treatment, on-treatment and progression PD-1 blockade samples. Gene expression profiling was performed via NanoString on 54 tumor biopsies. Of the custom-**

designed 795 probe code set, 10 probes were represented in our immune profiling analysis by IHC, namely CD3, CD4, CD8, CD45RO, CD68, FoxP3, Granzyme B, LAG-3, PD-1 and PD-L1. All values represented by box and whisker plots.

\*=  $p \leq 0.05$ , \*\*=  $p \leq 0.01$ , \*\*\*=  $p \leq 0.001$ , n.s.= not significant.

(The analysis was done by Dr. Pei-Ling Chen. This figure was used with permission from Dr. Pei-Ling Chen.)

We next compared GEPs between pretreatment and on-treatment time points to identify dynamic changes in the tumor microenvironment associated with each form of immune checkpoint therapy. To do this, I used the linear mixed-effects model to test time trend of gene expression from pretreatment to on-treatment and its interaction with response status for CTLA4 and PD-1 blockade, respectively. With CTLA4 blockade, 173 upregulated DEGs and 101 downregulated DEGs were identified in responders versus nonresponders to therapy (Figure 12E), with upregulated DEGs similar to those described in previously published datasets (102). With PD-1 blockade, 370 upregulated DEGs and 6 downregulated DEGs were identified in responders versus nonresponders (Figure 12F). Upregulated DEGs related to processes such as antigen presentation, T-cell activation, and T-cell homing. Importantly, we did not observe significant differences in GEPs in PD-1-treated patients regardless of prior treatment with CTLA4 blockade (Figure 16); however, the cohort was admittedly small and we cannot exclude the possibility that these GEPs may in part be due to prior treatment with CTLA4 blockade.

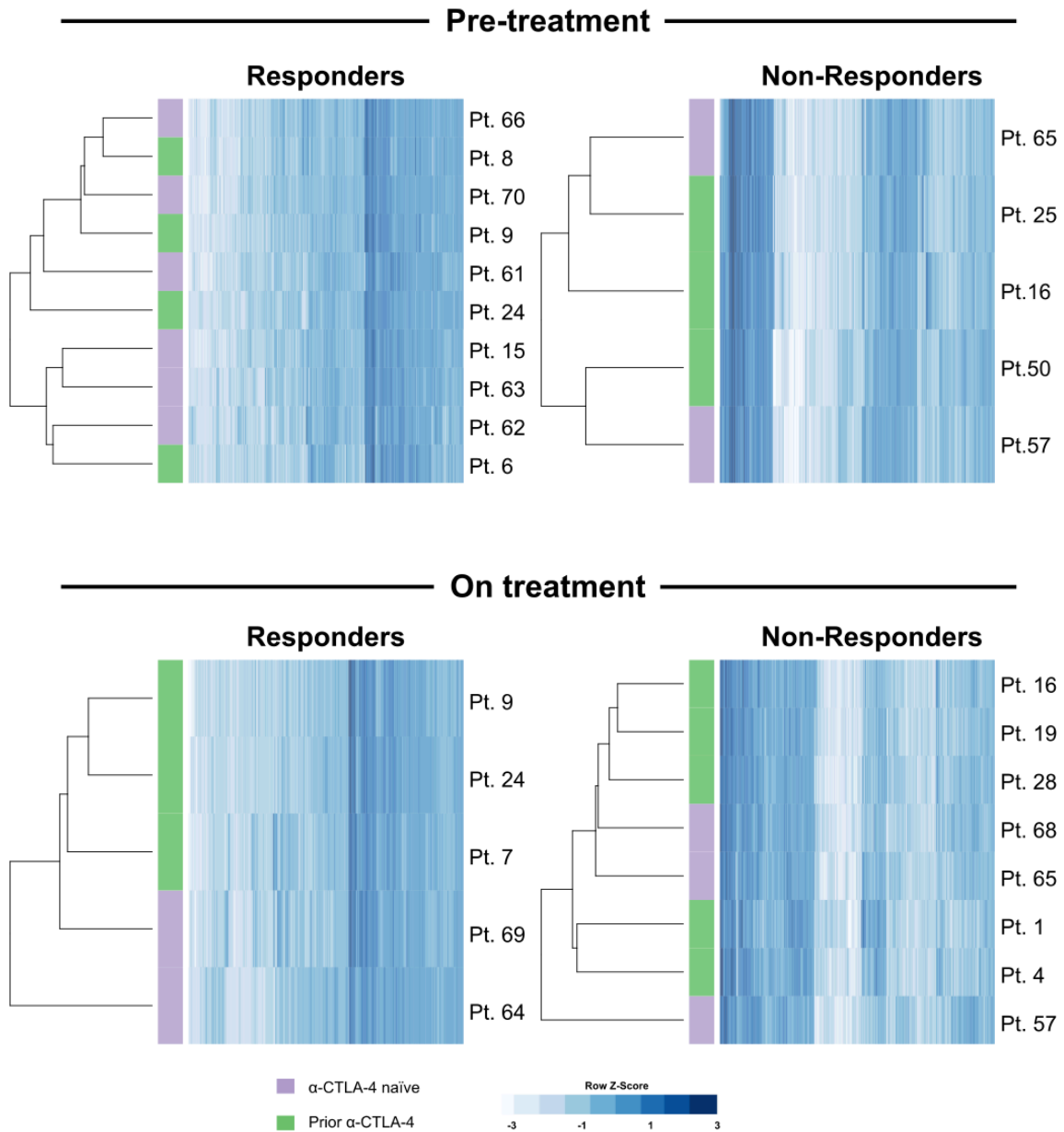


**Figure 16. Prior CTLA-4 blockade is not required for PD-1 early on-treatment profile.** Heatmap of 28 anti-PD-1 samples, which included 7 pre-treatment samples (4 responders, 3 non-responders) and 8 on-treatment samples (3 responders, 5 non-responders) with prior CTLA-4 exposure, as well as 8 pre-treatment samples (6 responders, 2 non-responders) and 5 on-treatment samples (2 responders and 3 non-responders) that were CTLA-4 blockade-naïve. Values are median-centered and log2-

transformed. Hierarchical clustering was performed on gene expression (higher expression in dark blue, lower expression in light blue).



To investigate mechanistic differences between the two forms of immune checkpoint blockade, we next compared the response-associated DEGs (from pretreatment to on-treatment) in tumor biopsies of CTLA4- versus PD-1–treated patients. In this comparison, only 117 shared DEGs were upregulated for both CTLA4 and PD-1 blockade (Figure 12G), with 56 upregulated DEGs unique to CTLA4 blockade, and 253 unique to PD-1 blockade (FDR-adjusted  $P < 0.05$ ). Analysis of shared downregulated DEGs revealed 99 that were unique to CTLA4 blockade and 4 that were unique to PD-1 blockade (FDR-adjusted  $P < 0.05$ ), with only two common DEGs in responders versus non- responders across both forms of therapy, including dual serine/threonine and tyrosine protein kinase (DSTYK) and S100 Calcium Binding Protein A1 (S100A1).

### 3.3 Discussion

Immune checkpoint blockade therapies have revolutionized the treatment of advanced melanoma and other cancer types; however, only a fraction of patients benefit from these treatments as monotherapy, and robust predictors of response and mechanisms of therapeutic resistance are currently lacking. Though data suggest a correlation among clinical response, preexisting tumor-infiltrating lymphocytes, T-cell repertoire, tumor-intrinsic mutational load, and neoantigens, the demonstrated biomarker profiles between responders and nonresponders are often overlapping and not very robust (97, 100).

Together, the studies presented herein build on collective efforts to identify biomarkers of response and resistance to immune checkpoint blockade (39, 48,

100), and provide novel evidence that assessment of adaptive immune responses early in the course of therapy is highly predictive of response—with nonoverlapping immune signatures in responders versus nonresponders, particularly to PD-1 blockade. These data have important clinical implications and suggest that immune signatures in tumor biopsies should be evaluated early after initiation of treatment with immune checkpoint blockade rather than in pretreatment tumor samples—at least until better predictive markers in pretreatment tissue and blood samples may be identified. This is highly relevant, as many clinical trials of immune checkpoint inhibitors currently mandate assessment of immune markers only in pretreatment tumor tissue; however, our findings suggest that we should reconsider this approach and assess adaptive immune responses in patients on therapy. Of note, we recognize the immune signatures observed in early on-treatment samples may simply be a consequence of the immune response to checkpoint inhibitors, and may not represent bona fide mechanisms of therapeutic response. Additional studies are needed to fully delineate whether these immune signatures are responsible for, or a product of, the mechanisms underlying the response—though are admittedly out of the context of the current study. Importantly, similar observations have been made in other tumor types (110), suggesting that such an approach could be applicable to other solid tumors—though this hypothesis needs to be tested more broadly.

These data also offer mechanistic insight into response to immune checkpoint blockade, suggesting that response to PD-1 blockade is related to

enhanced cytolytic activity, antigen processing, and IFN $\gamma$  pathway components (25, 101). Interestingly, VEGFA was decreased in responders and increased in nonresponders to therapy, suggesting a mechanism of therapeutic resistance as observed by others (107-109) and a potential target for therapy. The antiangiogenesis pathway has been shown to interact with antitumor immunity through multiple mechanisms. Previous studies demonstrate that increased VEGF secretion decreases T-cell effector function and trafficking to tumor (111, 112) and correlates with increased PD-1 expression on CD8 T cells (108). In addition to direct effect on T cells, VEGF also decreases the number of immature dendritic cells as well as T-cell priming ability of mature dendritic cells (113), further contributing to decreased effector T-cell function. Angiogenic factors have also been shown to expand T regulatory cell (114) and myeloid-derived suppressor cell populations. Based on these findings and preclinical and translational data supporting synergy between angiogenesis inhibitors and immunotherapies, multiple trials of combination therapy are under way, including bevacizumab with anti-PD-1 therapy (109). Phase I trial data from patients with advanced melanoma of bevacizumab and ipilimumab support synergy with this combination therapy, showing a 67% disease control rate, increased CD8 T-cell tumor infiltration, and circulating memory CD4 and CD8 T cells with combination therapy (109, 115). Our data are in line with these studies and reinforce the value in these combination anti-VEGF/anti-PD-1 clinical trials.

In addition, these data provide strong evidence regarding differential effects of distinct forms of immune checkpoint blockade on the tumor microenvironment,

with insight into distinct mechanisms of response and of therapeutic resistance, which is in line with prior published reports in mice (102) and in humans (103). These differences have important clinical implications and may help guide rational therapeutic combinations of distinct immune checkpoint inhibitors and immunomodulatory agents depending on the desired treatment effect.

An important consideration is that the differences in immune infiltrates observed in responders versus nonresponders to PD-1–based therapy could be related to prior treatment with CTLA4 blockade, though gene expression analyses and IHC results in CTLA4-naïve versus CTLA4-experienced patients did not differ significantly. This cohort is admittedly small and results need to be validated in larger cohorts and in other histologies. Based on available data from this and other groups, biopsies should be performed early on treatment (i.e., within 2 to 3 cycles of therapy) to validate these studies. In addition, though these novel findings are provocative, they may be difficult to validate in other solid tumor types where acquisition of early on-treatment biopsies may be less feasible. Nonetheless, there is a critical need to study this phenomenon in other solid tumors, as results from such studies may help usher in a new paradigm for immune monitoring in the setting of immune checkpoint blockade—with emphasis placed on assessment of an adaptive immune response in an early on-treatment biopsy rather than in pretreatment markers.

## **CHAPTER FOUR – GENOMIC PROFILING**

## Chapter 4 GENOMIC PROFILING

Content of this chapter is based on:

(\*Authors contributed equally)

From Whijae Roh\*, Pei-Ling Chen\*, Alexandre Reuben\*, Christine N. Spencer, Peter A. Prieto, John P. Miller, Vancheswaran Gopalakrishnan, Feng Wang, Zachary A. Cooper, Sangeetha M. Reddy, Curtis Gumbs, Latasha Little, Qing Chang, Wei-Shen Chen, Khalida Wani, Mariana Petaccia De Macedo, Eveline Chen, Jacob L. Austin-Breneman, Hong Jiang, Jason Roszik, Michael T. Tetzlaff, Michael A. Davies, Jeffrey E. Gershenwald, Hussein Tawbi, Alexander J. Lazar, Patrick Hwu, Wen-Jen Hwu, Adi Diab, Isabella C. Glitza, Sapna P. Patel, Scott E. Woodman, Rodabe N. Amaria, Victor G. Prieto, Jianhua Hu, Padmanee Sharma, James P. Allison, Lynda Chin, Jianhua Zhang, Jennifer A. Wargo, and P. Andrew Futreal, "Integrated molecular analysis of tumor biopsies on sequential CTLA-4 and PD-1 blockade reveals markers of response and resistance." *Science translational medicine* 9.379 (2017): eaah3560.

Reprinted with permission from AAAS.

### 4.1 Introductions and Rationale

Immune checkpoint blockade represents a major advancement in cancer therapy for advanced melanoma. However, durable clinical responses are seen in only a minority of patients treated with single-agent CTLA-4 (116) or PD-1 blockade (116, 117). Although higher response rates are achieved when CTLA-4 and PD-1 inhibitors are administered concurrently, this regimen also has greatly

increased toxicity (116, 118). There is a clinical need to predict who will benefit from immunotherapy and to understand mechanisms of therapeutic resistance to improve patient management and outcomes. Recently, evidence has pointed to a role of tumor molecular features (such as mutational load) (25, 41, 75, 119) and host immune infiltrates (40, 59, 86, 120) in response to therapy, though complexities exist with the predictive power of these markers (121). Studies have also begun to uncover mechanisms of resistance, including expression of immune checkpoint molecules (86, 122-129), insufficient infiltration of CD8+ T cells (86, 120), oncogenic pathways (43, 44, 130), transcriptomic resistance signatures (131), lack of sensitivity to interferon signaling (47, 132-135), defects in antigen processing and presentation (40, 47, 136, 137), diversity and abundance of bacteria within the gut microbiome (53, 138), and metabolism of cancer cells and T cells (139-141). However, additional insights are clearly needed for a more comprehensive understanding of resistance.

To further refine both host and tumor genomic contributions to resistance to checkpoint blockade, we assembled a cohort of longitudinal tissue samples from metastatic melanoma patients treated with sequential immune checkpoint blockade (CTLA-4 blockade followed by PD-1 blockade at time of progression). We previously performed deep immune profiling studies on these samples (via immunohistochemistry and gene expression profiling) and identified immune biomarkers of response and mechanisms of therapeutic resistance (87). To complement these studies, we report here the results of in-depth molecular analysis (via whole exome sequencing and T cell receptor sequencing) of these

longitudinal samples. These studies have identified putative genomic and molecular biomarkers of response and resistance to immune checkpoint blockade, demonstrating the complex interplay of host and tumor in treatment response.

## **4.2 Results**

### **4.2.1 T cell clonality predicts response to PD-1 blockade but not CTLA-4 blockade**

We studied a cohort of 56 patients who were first treated with CTLA-4 blockade, and then subsequently treated with PD-1 blockade at the time of progression, with longitudinal tumor samples collected as described in section 3.2.1 (Patient Cohort, Checkpoint Blockade Treatment, and Longitudinal Tumor Biopsies) (Figure 17A, Table 5) by performing whole exome sequencing (WES) and TCR sequencing (TCR-seq) on DNA from available tumor samples (Figure 17A, 18, 19, and Table 6). Responders were defined as patients who had complete resolution or partial reduction in the size of tumors by CAT scan-based imaging (by at least 30%), or who had prolonged stable disease (for at least 6 months). Non-responders were defined as patients who had tumor growth of at least 20% on CAT scan, or had stable disease lasting less than 6 months. I first compared the mutation status of common melanoma driver genes (78, 142) in pre-treatment samples, and also assessed interferon-gamma pathway genes, given the importance of defects in interferon-gamma signaling in resistance to immune checkpoint blockade (45, 47, 143, 144), and found no significant



differences between responders and non-responders to therapy with regard to somatic point mutations or indels (Fisher's exact test with a false discovery rate threshold of 0.05) ([Figure 17B](#)). Next, I compared the frequency of HLA somatic mutations (32) in pre-treatment samples and found that HLA somatic mutations were found in only one pre-treatment biopsy from a CTLA-4 blockade non-responder.

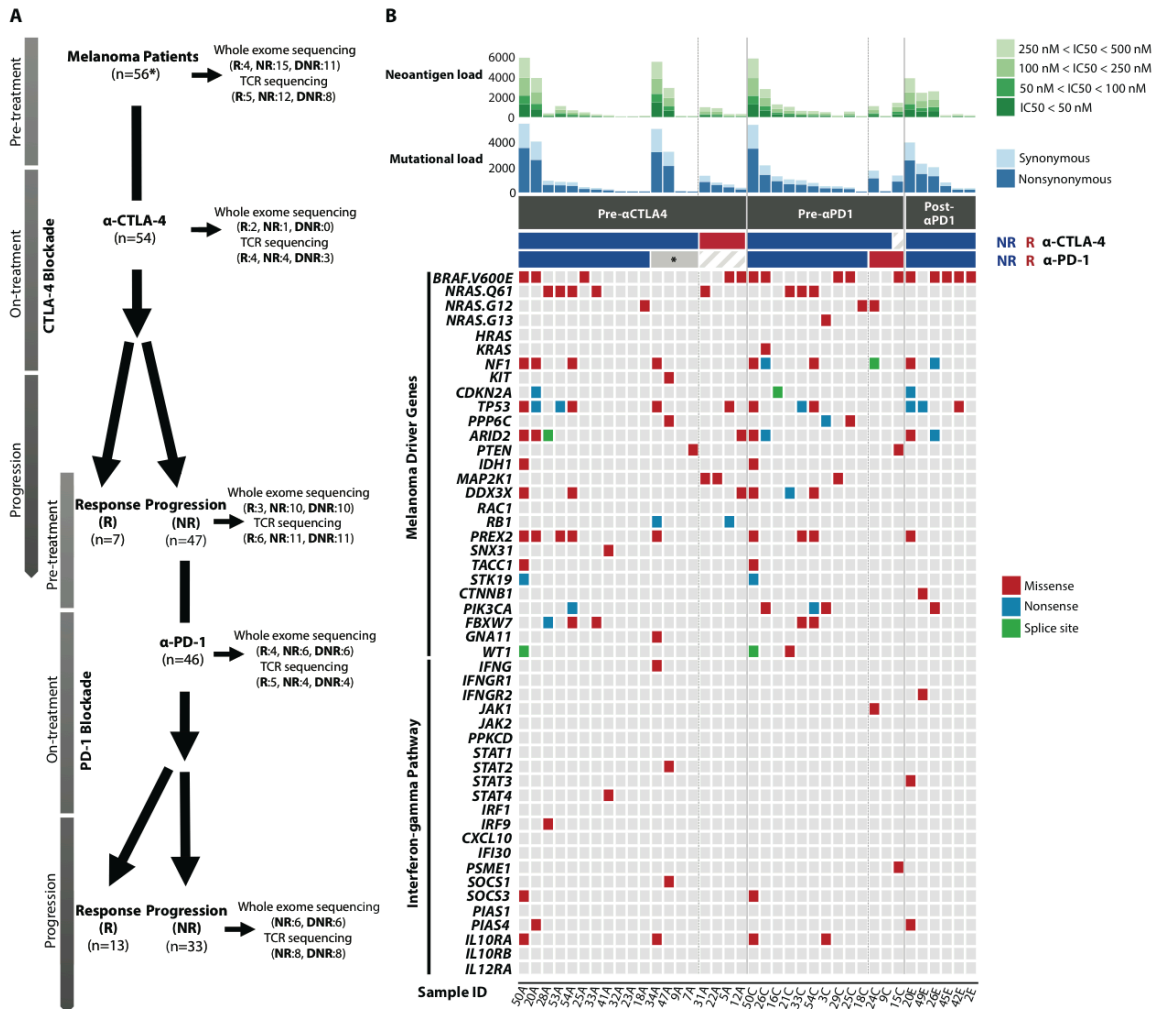


**Figure 17. Patient cohort diagram and genomic landscape of serial tumor**

**biopsies. (A)** Patients with metastatic melanoma were initially treated with CTLA-4 blockade (n=56\*: \* indicates that two of the 56 patients were CTLA-4 blockade naïve). Both responded to PD-1 blockade, and only pre-treatment samples were available for WES and TCR-seq). Non-responders to CTLA-4 blockade (n=47) were then treated with PD-1 blockade. Double non-responders progressed on CTLA-4 blockade first and then progressed on PD-1 blockade. Serial tumor biopsies were collected at multiple time points (pre-treatment, early on-treatment, and progression on CTLA-4 blockade and PD-1 blockade, respectively) when feasible. Whole exome sequencing and TCR sequencing were performed on these serial tumor biopsies. The numbers in parentheses indicate the

number of samples available for responders and non-responders after quality control of WES and TCR-seq data. R: responders, NR: non-responders, DNR: double non-responders. **(B)** For each sample (columns), genomic profiles (rows) were characterized. Column annotations represent biopsy time (Pre- $\alpha$ CTLA4: pre-CTLA-4 blockade samples, Pre- $\alpha$ PD1: pre-PD-1 blockade samples, Post- $\alpha$ PD1: post-PD-1 blockade samples) and response status (red: responders indicated as R, blue: non-responders indicated as NR, \*: failed CTLA-4 blockade but responded to PD-1 blockade) for each sample (Sample ID denotes patient ID followed by biopsy time: A=pre- $\alpha$ CTLA-4, C=post-CTLA-4/pre-PD-1, and E=post-PD-1). Shown at the top of the panel is mutational burden and neoantigen burden for each sample. Neoantigens were defined as having an  $IC_{50} < 500nM$ . Color scale shows the range of  $IC_{50}$  from 500nM to 50nM. Synonymous (light) and non-synonymous (dark) mutations are shown in different shades of blue. Additional genomic profiles included selected somatic point mutations, and indels. No indels were found among melanoma driver genes. When multiple mutations were found in one gene, the following precedence rule was applied: Nonsense mutation > Frame-shift indel > Splice site mutation > Missense mutation > In-frame indel.

sample	patient	time	aCTLA4_response	aPD1_response	tumor_purity	n_nonsynonymous	n_neoantigen	n_clones_by_expands	n_clones_by_sciclone	n_copy_gain	n_copy_loss
31A	31	preCTLA4	response	NA	0.85	819	997	9	2	88	0
34A	34	preCTLA4	nonresponse	response	0.85	3123	5628	17	6	917	1129
50A	50	preCTLA4	nonresponse	nonresponse	0.95	3445	6037	17	2	1008	1581
9A	9	preCTLA4	nonresponse	response	0.85	84	117	5	3	674	2400
5A	5	preCTLA4	response	NA	0.95	404	296	6	3	0	0
7A	7	preCTLA4	nonresponse	response	0.85	67	115	4	2	38	0
25A	25	preCTLA4	nonresponse	nonresponse	0.95	273	477	12	3	33	1675
32A	32	preCTLA4	nonresponse	nonresponse	0.75	77	72	5	2	359	2051
47A	47	preCTLA4	nonresponse	response	0.85	2047	2958	9	3	3	0
41A	41	preCTLA4	nonresponse	nonresponse	0.95	172	176	8	4	579	2285
20A	20	preCTLA4	nonresponse	nonresponse	0.9	2520	3982	14	2	0	161
33A	33	preCTLA4	nonresponse	nonresponse	0.9	232	266	5	1	31	0
12A	12	preCTLA4	response	NA	0.95	242	311	9	6	453	171
54A	54	preCTLA4	nonresponse	nonresponse	0.85	514	686	14	10	283	1012
18A	18	preCTLA4	nonresponse	nonresponse	0.95	71	124	7	2	715	110
28A	28	preCTLA4	nonresponse	nonresponse	0.6	596	372	12	5	0	993
53A	53	preCTLA4	nonresponse	nonresponse	0.9	555	1114	17	8	325	1481
22A	22	preCTLA4	response	NA	0.85	589	901	8	3	699	130
23A	23	preCTLA4	nonresponse	nonresponse	0.95	69	75	4	2	442	1326
6B	6	onCTLA4	nonresponse	response	0.85	63	52	6	2	14	45
22B	22	onCTLA4	response	NA	0.95	52	74	6	2	32	938
37B	37	onCTLA4	response	NA	0.5	78	155	3	1	62	0
18C	18	postCTLA4_prePD1	nonresponse	nonresponse	0.4	64	103	3	1	209	119
24C	24	postCTLA4_prePD1	nonresponse	response	0.95	1101	1110	17	5	1	0
33C	33	postCTLA4_prePD1	nonresponse	nonresponse	0.9	611	627	13	4	208	1106
50C	50	postCTLA4_prePD1	nonresponse	nonresponse	0.8	3388	5961	12	3	0	7
15C	15	postCTLA4_prePD1	NA	response	0.9	842	1453	11	5	827	995
9C	9	postCTLA4_prePD1	nonresponse	response	0.9	90	122	5	3	458	41
26C	26	postCTLA4_prePD1	nonresponse	nonresponse	0.85	1365	2852	15	5	56	4149
29C	29	postCTLA4_prePD1	nonresponse	nonresponse	0.95	316	161	10	6	362	0
25C	25	postCTLA4_prePD1	nonresponse	nonresponse	0.95	266	551	11	5	146	2716
16C	16	postCTLA4_prePD1	nonresponse	nonresponse	0.95	883	1286	15	6	1101	2194
21C	21	postCTLA4_prePD1	nonresponse	nonresponse	0.9	647	1039	12	4	464	0
54C	54	postCTLA4_prePD1	nonresponse	nonresponse	0.8	484	608	11	3	101	0
3C	3	postCTLA4_prePD1	nonresponse	nonresponse	0.8	328	499	11	6	0	217
4D	4	onPD1	nonresponse	nonresponse	0.85	128	301	9	5	6	1111
7D	7	onPD1	nonresponse	response	0.1	18	25	3	1	0	0
9D	9	onPD1	nonresponse	response	0.2	63	103	4	1	0	0
1D	1	onPD1	nonresponse	nonresponse	0.85	108	144	10	6	964	4919
16D	16	onPD1	nonresponse	nonresponse	0.95	895	1562	14	4	574	2
28D	28	onPD1	nonresponse	nonresponse	0.95	610	371	13	4	646	698
47D	47	onPD1	nonresponse	response	0.2	299	438	3	2	0	0
3D1	3	onPD1	nonresponse	response	0.45	119	144	3	2	4	0
3D2	3	onPD1	nonresponse	nonresponse	0.3	137	176	3	1	0	0
53D	53	onPD1	nonresponse	nonresponse	0.75	631	1416	13	8	402	1458
26E	26	postPD1	nonresponse	nonresponse	0.95	1259	2619	15	5	60	3665
49E	49	postPD1	nonresponse	nonresponse	0.9	1439	2473	16	3	158	2979
20E	20	postPD1	nonresponse	nonresponse	0.85	2484	3950	10	5	NA	NA
42E	42	postPD1	nonresponse	nonresponse	0.95	212	287	10	6	688	2989
45E	45	postPD1	nonresponse	nonresponse	0.85	499	184	12	1	NA	NA
2E	2	postPD1	nonresponse	nonresponse	0.9	211	172	11	3	1570	2815

**Table 5. Sample information, tumor purity, mutational load, neoantigen load, number of clones per tumor, and burden of copy number alterations**

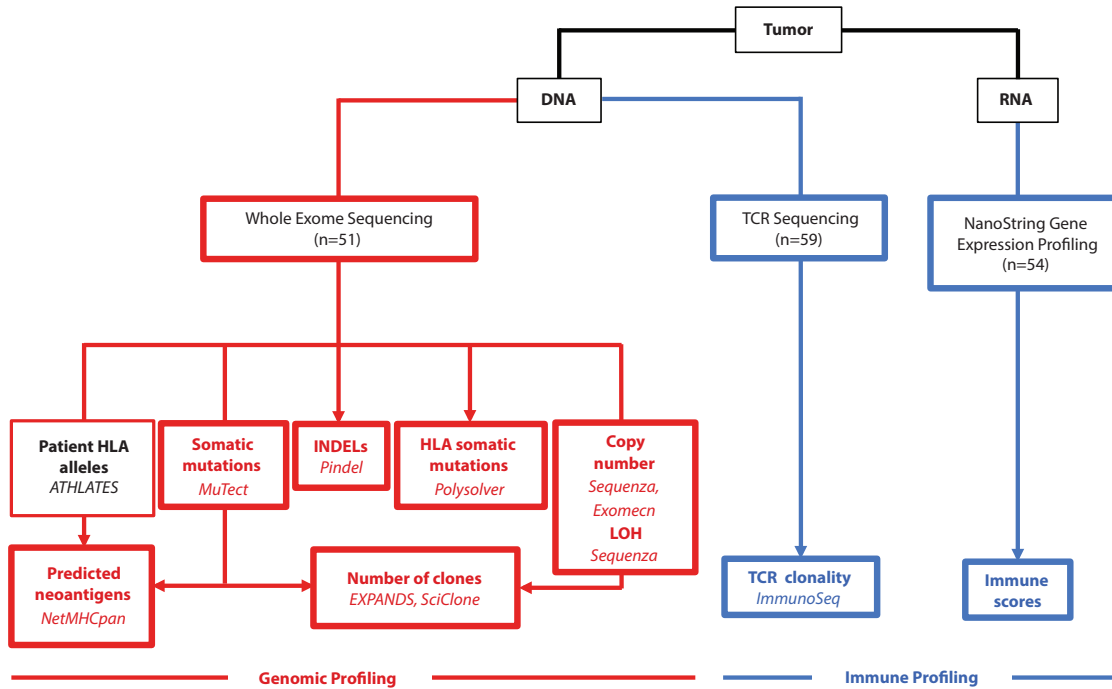


**Figure 18. Workflow diagram of multidimensional profiling analysis.** Peripheral blood and serial tumor biopsies were collected from patients (n=56). Using DNA and RNA extracted from formaldehyde fixed-paraffin embedded (FFPE) tumor tissues, we performed whole exome sequencing and TCR sequencing. NanoString gene expression profiling data were obtained from immune profiling. Genomic profiles (red) were characterized from whole exome sequencing data. Immune profiles (blue) were characterized from TCR sequencing data and NanoString gene expression data. Characterized genomic profiles included somatic point mutations, indels, HLA somatic mutations, copy number alterations, neoantigens, and intratumor heterogeneity measures (number of clones per tumor). TCR clonality was derived from enumeration of identified TCR clonotypes. Immune scores were calculated from gene expression of selected immune-related genes (cytolytic markers, HLA molecules, IFN- $\gamma$  pathway, chemokines, and adhesion molecules). Bolded text shows the variables analyzed. Italics show the software used to generate the associated variables

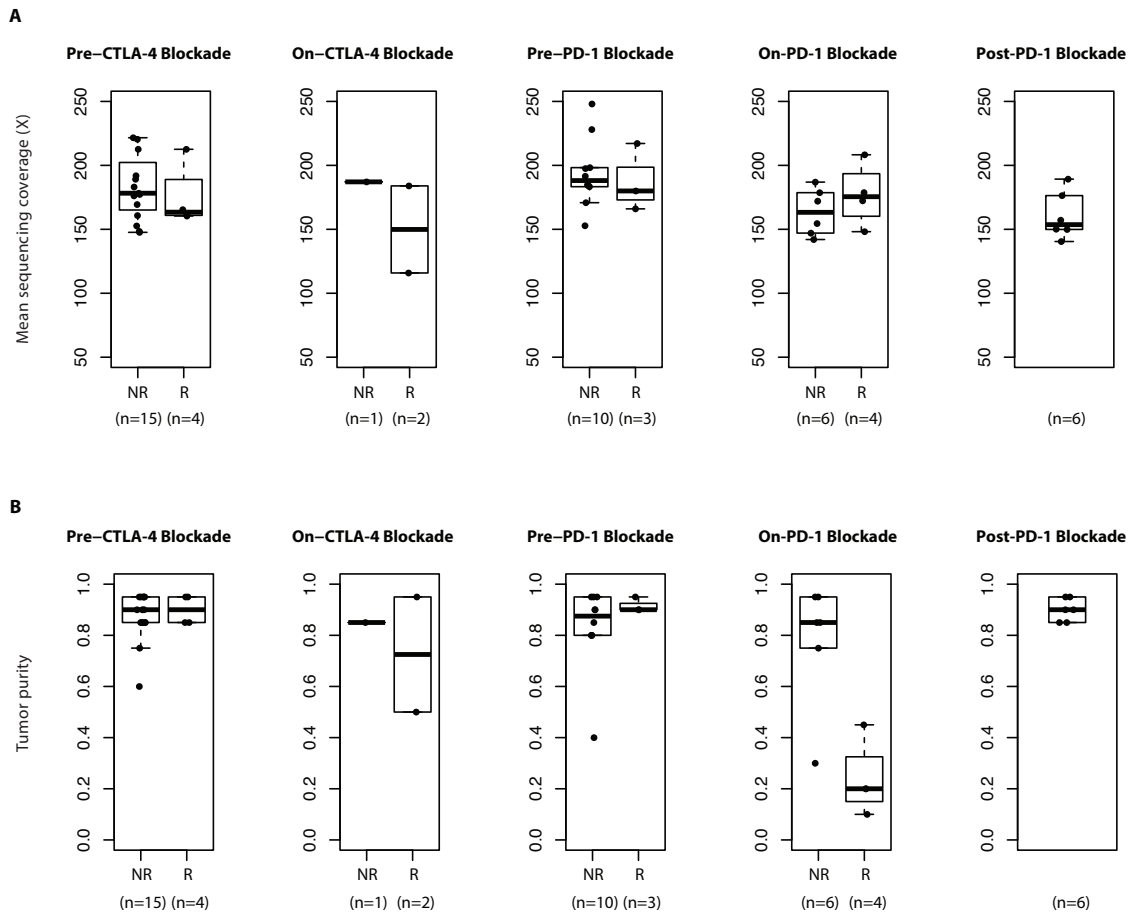


**Figure 19. Distribution of sequencing coverage and tumor purities across samples. (A)** The difference of mean sequencing coverage across groups stratified by five biopsy time points and response status (NR: non-responders, R: responders). **(B)** The difference of tumor purities across groups stratified by five biopsy time points and response status. Tumor purity was assessed by two pathologists.

Timepoint	Pre-CTLA-4	Pre-CTLA-4	On-CTLA-4	On-CTLA-4
Response	response	nonresponse	response	nonresponse
Mutational load	513 (248)	923 (1209)	65 (18)	63 (0)
Neoantigen load	626 (374)	1479 (2106)	114 (57)	52 (0)
Burden of copy number loss	75 (88)	1080 (856)	469 (663)	45 (0)
Immune scores	7 (0.6)	8 (0.54)	9.1 (0.98)	7.1 (0.85)
TCR clonality	0.013 (0.008)	0.02 (0.02)	0.158 (0.118)	0.044 (0.03)

Timepoint	Post-CTLA-4/Pre-PD-1	Post-CTLA-4/Pre-PD-1	On-PD-1	On-PD-1	Post-PD-1
Response	response	nonresponse	response	nonresponse	nonresponse
Mutational load	677 (525)	835 (969)	124 (123)	418 (337)	1017 (889)
Neoantigen load	895 (691)	1368 (1795)	177 (180)	661 (647)	1614 (1618)
Burden of copy number loss	345 (563)	1050 (1477)	0 (0)	1364 (1836)	3112 (377)
Immune scores	8 (1.5)	8.4 (1.3)	10.5 (0.48)	6.7 (0.94)	7.8 (1.2)
TCR clonality	0.11 (0.09)	0.041 (0.046)	0.145 (0.08)	0.015 (0.01)	0.074 (0.055)

\* Mean value (standard deviation)

**Table 6. Summary measure of the data across clinical subgroups**

In our cohort, we did not observe any statistically significant differences in mutational load or predicted neoantigen load in pre-treatment samples from responders versus non-responders to therapy by either CTLA-4 or PD-1 blockade ([Figure 20A-20B](#)) (mutational load:  $P = 0.597$  in pre-CTLA-4 blockade samples,  $P = 0.937$  in pre-PD-1 blockade samples; neoantigen load:  $P = 0.736$  in pre-CTLA-4 blockade samples,  $P = 0.937$  in pre-PD-1 blockade samples), which is in contrast to published literature (25, 41, 75, 119) and may be due to limited sample size. Further, no significant differences were observed in intratumor heterogeneity (ITH), estimated as the number of clones per tumor, between responders and non-responders to immune checkpoint blockade ([Figure 21](#)).



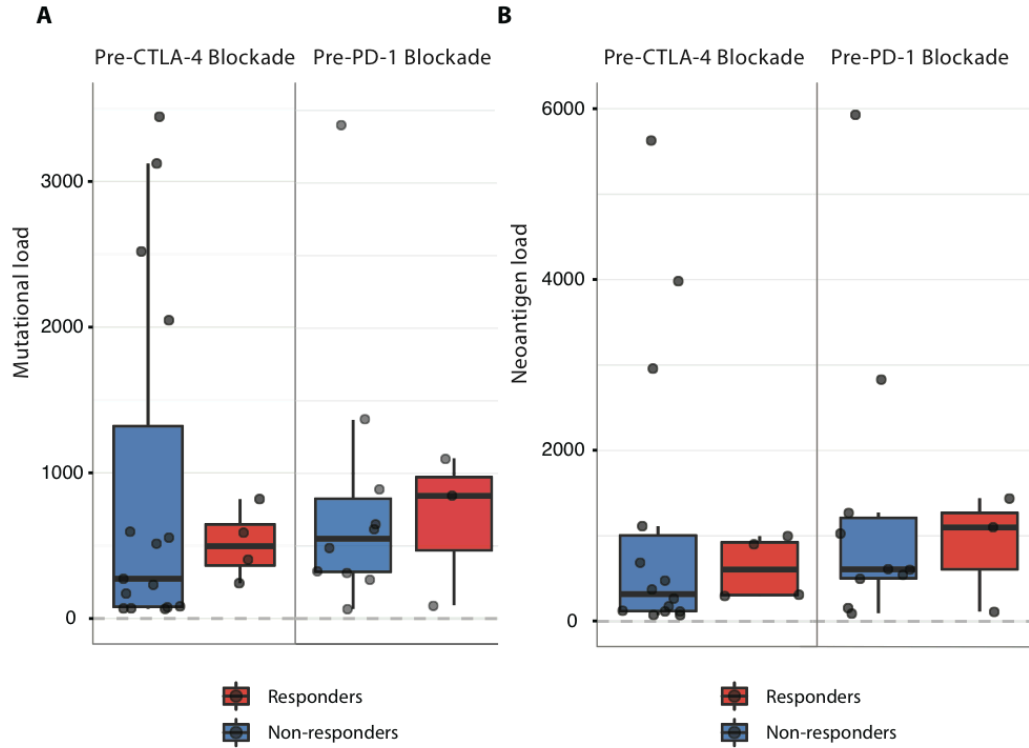


**Figure 20. Mutational load, neoantigen load, and clinical response.** Boxplots summarize mutational load (**A**) and neoantigen load (**B**) by response status (blue: non-responders, red: responders) in pre-CTLA-4 blockade samples and pre-PD-1 blockade samples; median values (lines) and interquartile range (whiskers) are indicated. *P* values were calculated using a two-sided Mann-Whitney *U* test ( $P = 0.597$  in pre-CTLA-4 blockade samples,  $P = 0.937$  in pre-PD-1 blockade samples for mutational load;  $P = 0.736$  in pre-CTLA-4 blockade samples,  $P = 0.937$  in pre-PD-1 blockade samples for neoantigen load).

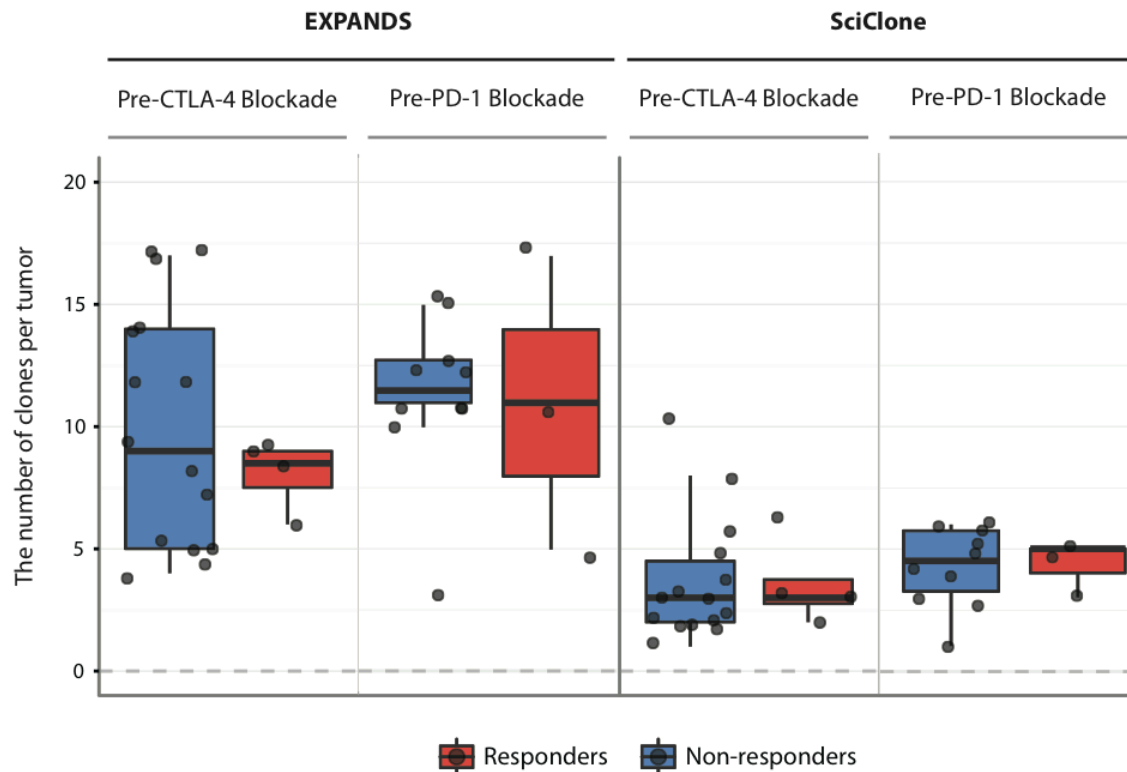


**Figure 21. Intratumor heterogeneity and clinical response.** Intratumor heterogeneity was estimated as the number of clones per tumor for each sample. The number of clones per tumor was estimated by EXPANDS and SciClone independently. There was moderate correlation between the estimated number of clones per tumor from two algorithms (correlation coefficient = 0.59; Spearman rank correlation,  $P = 0.00037$ ). Boxplots summarize the number of clones per tumor estimated from each software by response status (blue: non-responders, red: responders) in pre-CTLA-4 blockade samples and pre-PD-1 blockade samples; median values (lines) and interquartile range (whiskers) are indicated.  $P$  values were calculated using a two-sided Mann-Whitney  $U$  test ( $P > 0.05$  for all).

We next performed sequencing of the CDR3 variable region of the  $\beta$ -chain of the T cell receptor (TCR-seq) to understand the role of the T cell repertoire in response and resistance to checkpoint blockade (Table 7). Although no significant differences were observed in TCR clonality when comparing responders to non-responders in the context of CTLA-4 blockade at the pre-treatment ( $P = 0.96$ ) and on-treatment time points ( $P = 0.2$ ) (Figure 22), an increase in clonality was noted in a subset of patients treated with CTLA-4 blockade (Figure 23). Among 8 patients with matched longitudinal tumor samples (pre-CTLA-4 and pre-PD-1,  $n=8$ ) available, all three PD-1 blockade responders showed an increase in TCR clonality on CTLA-4 blockade, whereas this was the case in only 1 out of 5 non-responders to PD-1 blockade (Figure 23). The one patient (Patient 50) classified as a non-responder in the context of the trial criteria who demonstrated an increase in clonality appeared to have some clinical benefit from treatment with PD-1 blockade, as he continued on PD-1 blockade therapy for a total of 24 doses and had no evidence of disease at last follow up. Higher TCR clonality was observed in responders to PD-1 blockade at both pre- ( $P = 0.037$ ) and on-treatment ( $P = 0.032$ ) time points (Figure 22).

sample	patient	time	aCTLA4_response	aPD1_response	Clonality
10A		10 preCTLA4	response	NA	0.05527087
10B		10 onCTLA4	response	NA	0.04997955
12A		12 preCTLA4	response	NA	0.01794051
15C		15 postCTLA4_prePD1	NA	response	0.00582951
16C		16 postCTLA4_prePD1	nonresponse	nonresponse	0.01731895
16D		16 onPD1	nonresponse	nonresponse	0.01817108
18A		18 preCTLA4	nonresponse	nonresponse	0.0544221
18B		18 onCTLA4	nonresponse	nonresponse	0.01083352
18C		18 postCTLA4_prePD1	nonresponse	nonresponse	0.05261548
19D		19 onPD1	nonresponse	nonresponse	0.00829378
19E		19 postPD1	nonresponse	nonresponse	0.0546851
1B	1	onCTLA4	nonresponse	nonresponse	0.05518331
1D	1	onPD1	nonresponse	nonresponse	0.02867525
22B	22	onCTLA4	response	nonresponse	0.07514578
23A	23	preCTLA4	nonresponse	nonresponse	0.02615795
23B	23	onCTLA4	nonresponse	nonresponse	0.08747733
24A	24	preCTLA4	nonresponse	response	0.08637499
24C	24	postCTLA4_prePD1	nonresponse	response	0.14294231
24D	24	onPD1	nonresponse	response	0.23178676
25A	25	preCTLA4	nonresponse	nonresponse	0.02639377
25C	25	postCTLA4_prePD1	nonresponse	nonresponse	0.01237117
25E	25	postPD1	nonresponse	nonresponse	0.00649915
26E	26	postPD1	nonresponse	nonresponse	0.1357679
27B	27	onCTLA4	response	nonresponse	0.1382599
2A	2	preCTLA4	nonresponse	nonresponse	0.00428925
2E	2	postPD1	nonresponse	nonresponse	0.03395957
31A	31	preCTLA4	response	nonresponse	0.01887839
33C	33	postCTLA4_prePD1	nonresponse	nonresponse	0.07783938
37A	37	preCTLA4	response	NA	0.03382181
37B	37	onCTLA4	response	NA	0.24256822
3A	3	preCTLA4	nonresponse	nonresponse	0.01494006
3C	3	postCTLA4_prePD1	nonresponse	nonresponse	0.01626247
3D1	3	onPD1	nonresponse	response	0.02786906
40C	40	postCTLA4_prePD1	nonresponse	nonresponse	0.00144045
42C	42	postCTLA4_prePD1	nonresponse	nonresponse	0.04860959
42E	42	postPD1	nonresponse	nonresponse	0.02891788
45E	45	postPD1	nonresponse	nonresponse	0.05604353
47A	47	preCTLA4	nonresponse	response	0.01718291
47D	47	onPD1	nonresponse	response	0.17340681
49C	49	postCTLA4_prePD1	nonresponse	nonresponse	0.02107852
49E	49	postPD1	nonresponse	nonresponse	0.03817971
4A	4	preCTLA4	nonresponse	nonresponse	0.00437446
4C	4	postCTLA4_prePD1	nonresponse	nonresponse	0.0021321
4D	4	onPD1	nonresponse	nonresponse	0.00511381
50A	50	preCTLA4	nonresponse	nonresponse	0.02263149
50C	50	postCTLA4_prePD1	nonresponse	nonresponse	0.16309696
50E	50	postPD1	nonresponse	nonresponse	0.17025982
52C	52	postCTLA4_prePD1	nonresponse	response	0.17419149
54C	54	postCTLA4_prePD1	nonresponse	nonresponse	0.04147743
56D	56	onPD1	nonresponse	response	0.21286792
5A	5	preCTLA4	response	nonresponse	0.00323339
6B	6	onCTLA4	nonresponse	response	0.02449196
6C2	6	postCTLA4_prePD1	nonresponse	response	0.07375047
7A	7	preCTLA4	nonresponse	nonresponse	0.02885111
7D	7	onPD1	nonresponse	response	0.14695446
8A	8	preCTLA4	nonresponse	response	0.02901636
8C	8	postCTLA4_prePD1	nonresponse	response	0.25088206
9A	9	preCTLA4	nonresponse	response	0.02939994
9C	9	postCTLA4_prePD1	nonresponse	response	0.23396692

**Table 7. TCR clonality**

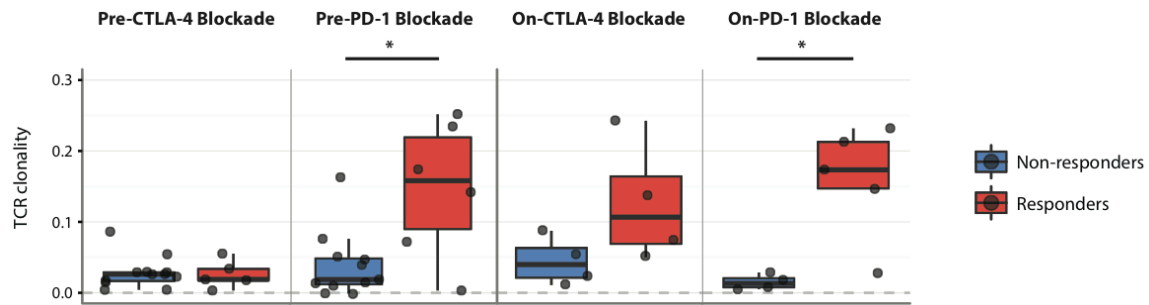


**Figure 22. TCR clonality and clinical response.** Boxplots summarize TCR clonality by response status (blue: non-responders, red: responders) in pre-CTLA-4 blockade samples, pre-PD-1 blockade samples, on-CTLA-4 blockade samples, and on-PD-1 blockade samples, respectively; median values (lines) and interquartile range (whiskers) are indicated.  $P$  values were calculated using a two-sided Mann-Whitney  $U$  test ( $P > 0.05$  for TCR clonality in pre-CTLA-4 blockade and on-CTLA-4 blockade samples,  $P = 0.037$  for TCR clonality in pre-PD-1 blockade samples and  $P = 0.032$  for TCR clonality in on-PD-1 blockade samples.).

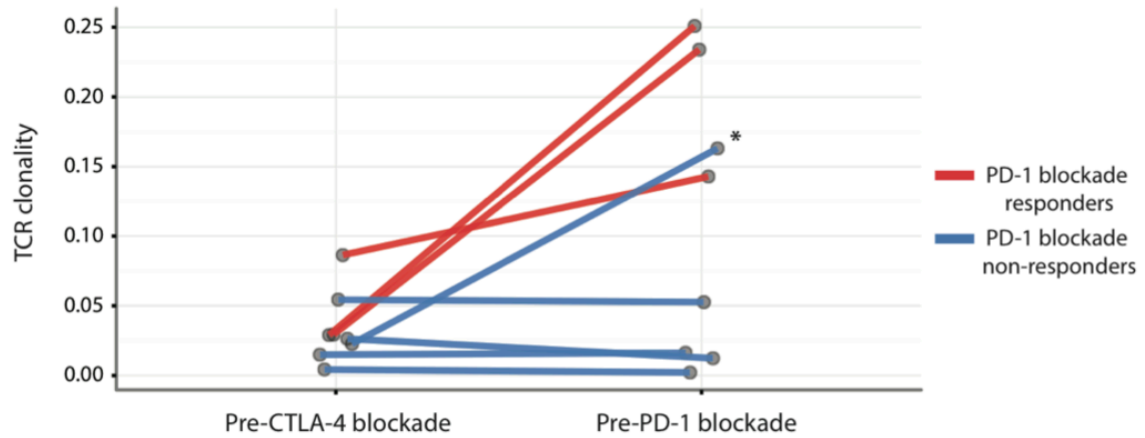


**Figure 23. The effects of previous CTLA-4 blockade exposure on the baseline TCR clonality of pre-PD-1 blockade samples.** Data show the patient-matched TCR clonality at two time points (pre-CTLA-4 and pre-PD-1) (red line: PD-1 blockade responders, blue line: PD-1 blockade non-responders, \*: PD-1 blockade non-responder, Patient 50, who continued on with pembrolizumab off protocol for a total of 24 doses and had no evidence of disease at last follow up).

Next, I sought to investigate the association between TCR clonality and immune activation in the tumor microenvironment. To do so, I first calculated the immune score from gene expression profiling data in our cohort. The immune score was defined as the geometric mean of gene expression in selected genes including cytolytic markers, HLA molecules, IFN- $\gamma$  pathway, selected chemokines, and adhesion molecules related to tumor rejection in the context of the immunologic constant of rejection (145, 146) (Table 8). Although no association was observed between TCR clonality and immune scores in pre-CTLA-4 blockade samples, a significant positive correlation was observed between TCR clonality and immune scores in pre-PD-1 blockade samples ( $P = 0.0018$ , Figure 24).

sample	immune score
5A	8.17
7A	8.55
8A	7.76
9A	7.83
10A	7.53
18A	7.82
19A	8.02
22A	6.86
23A	7.54
25A	8.8
31A	8.2
37A	8.23
42A	9.32
43A	7.21
47A	7.54
50A	7.13
6B	7.78
18B	6.57
22B	8.47
27B	10.45
37B	9.86
2C	10.12
3C	8.6
4C	7.59
6C1	7.22
6C2	6.08
8C	10.17
9C	9.84
15C	7.86
16C	7.62
18C	9.72
24C	9.31
25C	6.05
49C	8.3
50C	8.67
52C	9.88
54C	9.14
1D	6.45
3D1	10.04
4D	5.48
7D	10.48
9D	10.04
16D	8.08
19D	6.55
24D	11.22
40D	7.06
47D	10.5
2E	8.11
19E	5.84
26E	7.04
43E	6.03
45E	8.74
49E	9.06
50E	8.46

**Table 8. Immune scores (NanoString) in our cohort**



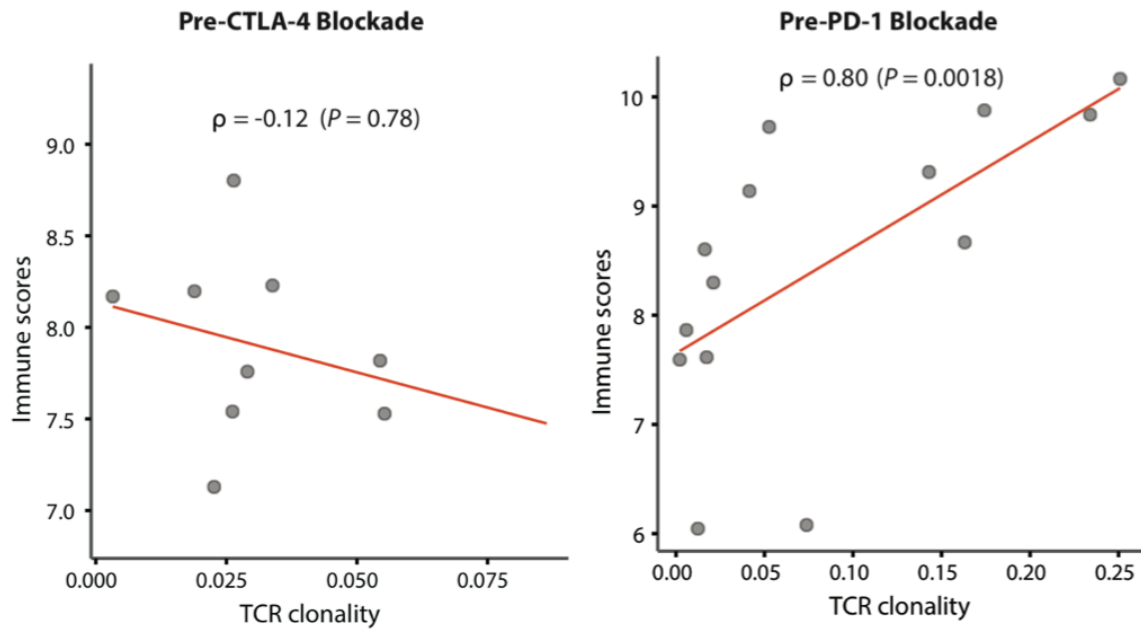


**Figure 24. The correlation between TCR clonality and immune scores.** Data show the correlation between TCR clonality and immune scores for the pre-CTLA-4 blockade biopsies and the pre-PD-1 blockade biopsies. Spearman rank correlation was used for correlation coefficient.

#### **4.2.2 High copy number loss burden is associated with poor response to immune checkpoint blockade**

Given the lack of clear differences in point mutation and indel status in driver genes between responders and non-responders to CTLA-4 and PD-1 blockade, I then investigated whether copy number alterations (CNAs) may play a role in response and resistance to CTLA-4 and PD-1 blockade. With regards to specific genes, I did not find any significant association between copy number gain or loss status and response to therapy in pre-treatment biopsies for either therapy (Fisher's exact test with a false discovery rate threshold of 0.05). Given a recent report demonstrating the impact of loss of HLA Class I and  $\beta$ 2-microglobulin in resistance to cytolytic activity (40), I next examined the relevance of copy number loss in these genes within our cohort. In this study, although we observed no significant loss of HLA class I genes, loss of  $\beta$ 2-microglobulin was detected in 4 non-responders to CTLA-4 blockade (with focal copy number loss in 2 patients and arm-level copy number loss in 2 patients). Focal copy number loss of  $\beta$ 2-microglobulin was also observed in 1 pre-treatment sample from a CTLA-4 blockade naïve PD-1 blockade responder. To assess CNAs at the whole genome sample level, I defined burden of CNAs as the total number of genes with copy number gain or loss per sample. On testing the association between burden of CNAs and response to therapy in pre-treatment biopsies of patients on CTLA-4 or PD-1 blockade, we observed no significant differences in burden of copy number gain or loss ( $P > 0.05$  for all comparisons) in the context of individual agent response (Figure 25). However, a

trend toward higher burden of copy number loss was observed in pre-CTLA-4 blockade biopsies from CTLA-4 blockade responders compared to CTLA-4 blockade non-responders, though statistical significance was not attained ( $P = 0.077$ ).

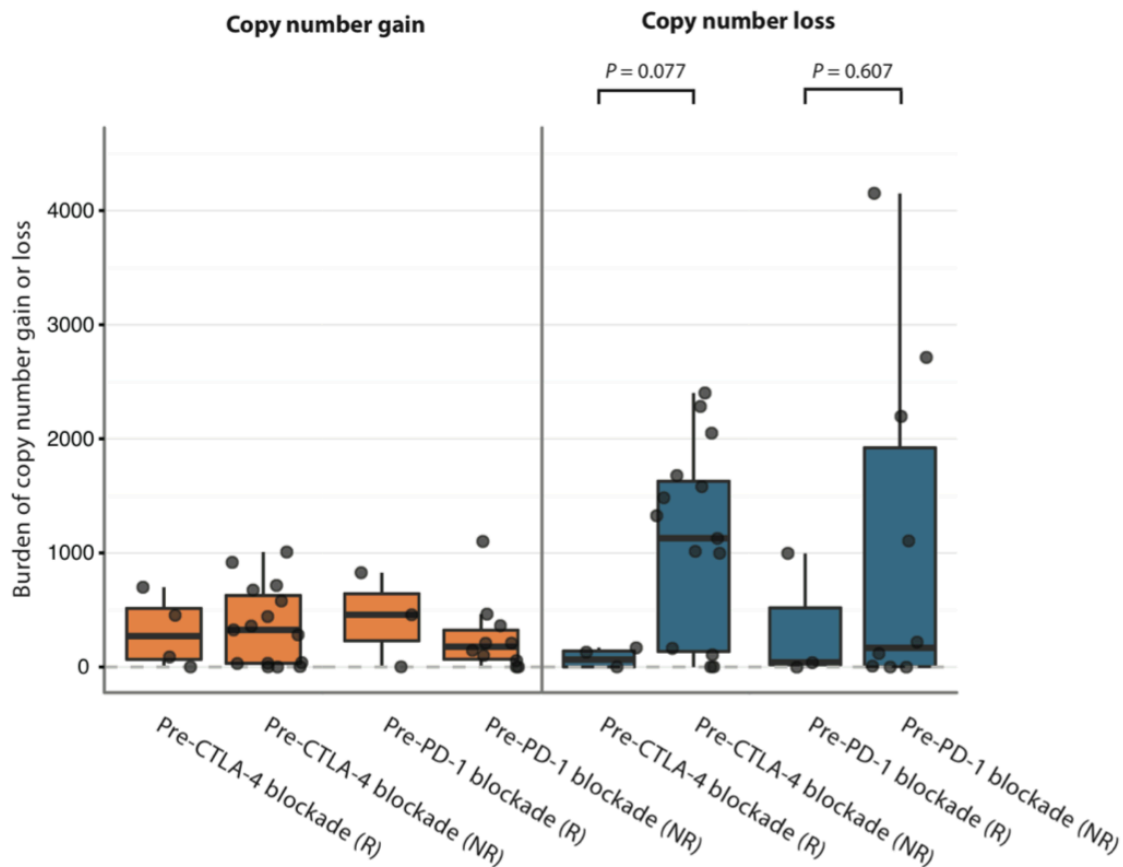


**Figure 25. Burden of copy number alterations in responders versus non-responders.** Boxplots summarize burden of copy number gain or loss in four groups of interest: pre-CTLA-4 blockade responders, pre-CTLA-4 blockade non-responders, pre-PD-1 blockade responders, and pre-PD-1 blockade non-responders; median values (lines) and interquartile range (whiskers) are indicated. *P* values were calculated using a two-sided Mann-Whitney *U* test. (*P* = 0.077 for pre-CTLA-4 blockade responders vs. non-responders, *P* = 0.607 for pre-PD-1 blockade responders vs. non-responders, and *P* > 0.05 for all others) NR: non-responders, R: responders.

I next investigated the burden of copy number alterations in pre-CTLA-4 blockade biopsies from patients who progressed on CTLA-4 blockade first and then progressed on PD-1 blockade, termed double non-responders (DNRs) because we hypothesized that the association between burden of copy number alterations and resistance might be stronger in patients with potentially more resistant phenotype (failure on both treatments) than in patients who failed a single agent. We observed no significant differences in burden of copy number *gain* but significantly higher burden of copy number *loss* in pre-CTLA-4 blockade biopsies from DNRs compared to pre-CTLA-4 blockade biopsies from CTLA-4 blockade responders ( $P = 0.042$ ) (Figure 26 and 27). We noted a strikingly higher burden of copy number loss in post-PD-1 blockade biopsies compared to pre-CTLA-4 blockade biopsies from CTLA-4 blockade responders ( $P = 0.029$ ) (Fig 2A, fig. S7). The burden of copy number loss was not correlated with mutational load at any of the time points studied (Figure 28), suggesting that the association is not readily attributable to decreased mutational burden.

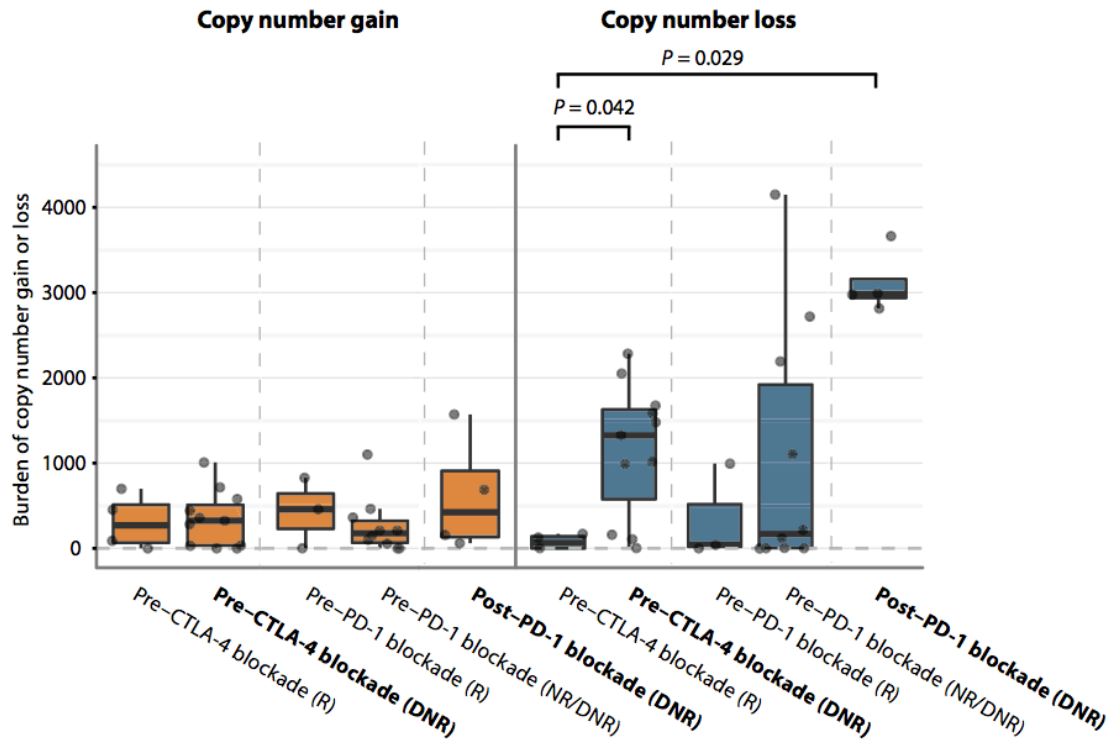


**Figure 26. Burden of copy number alterations in responders versus double non-responders.** Boxplots summarize burden of copy number gain or loss in five groups of interest: responders to CTLA-4 blockade at pre-treatment, pre-CTLA-4 blockade double non-responders, responders to PD-1 blockade at pre-treatment, pre-PD-1 blockade double non-responders, and post-PD-1 blockade double non-responders; median values (lines) and interquartile range (whiskers) are indicated. *P* values were calculated using a two-sided Mann-Whitney *U* test. (*P* = 0.042 for pre-CTLA-4 blockade responders vs. double non-responders, *P* = 0.029 for pre-CTLA-4 blockade responders vs. post-PD-1 blockade double non-responders, and *P* > 0.05 for all others) DNR: double non-responders, NR: non-responders, R: responders. In bold are highlighted the Pre-CTLA-4 blockade and Post-PD-1 blockade double non-responder (DNR) groups.

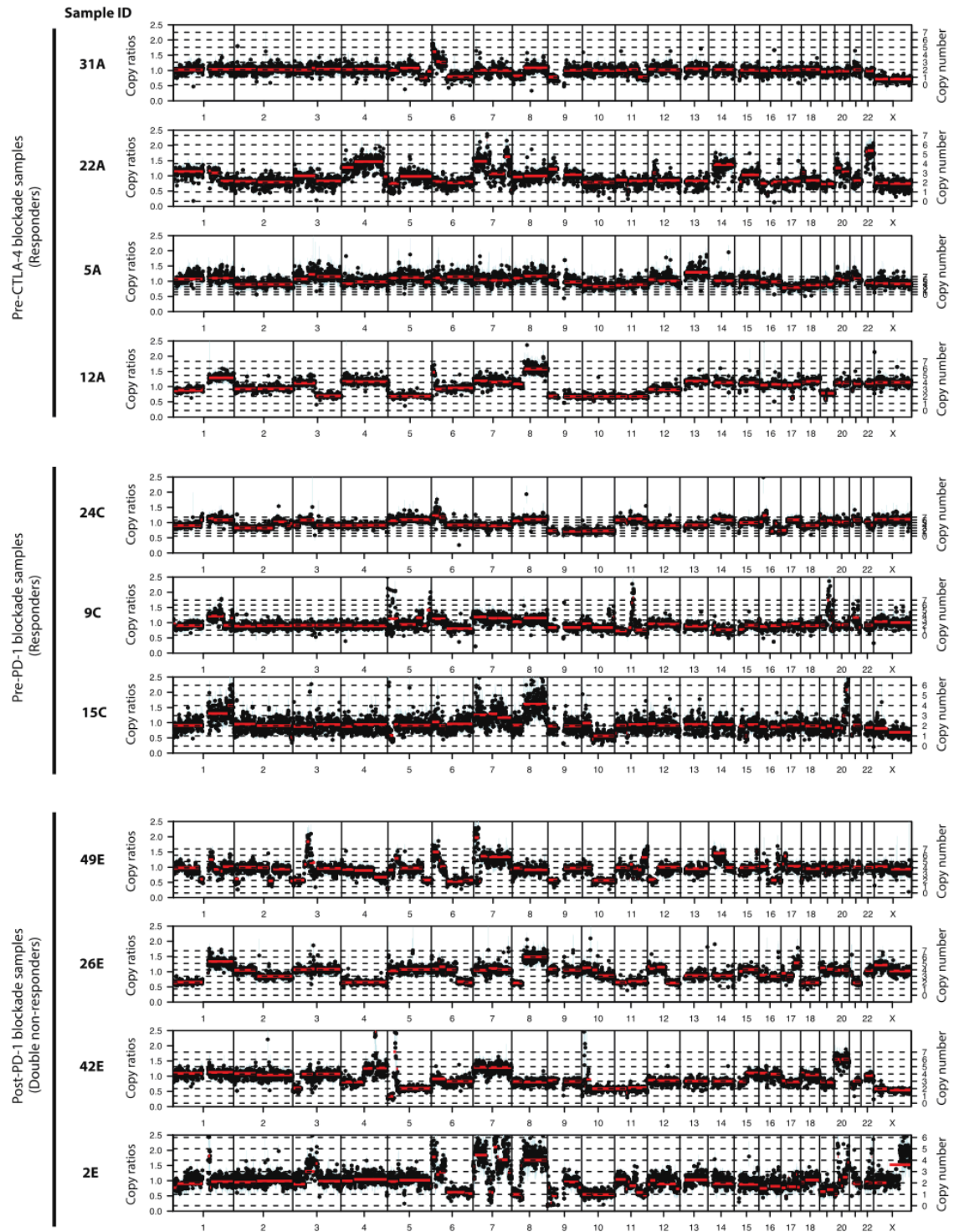


**Figure 27. Copy number profiles of responders and double non-responders.** Copy ratios (tumor/normal) were plotted in genomic coordinates for responders (pre-CTLA-4 blockade, pre-PD-1 blockade) and double non-responders (post-PD-1 blockade). Red

lines indicate copy number segmented values. The dotted lines indicate the copy number.



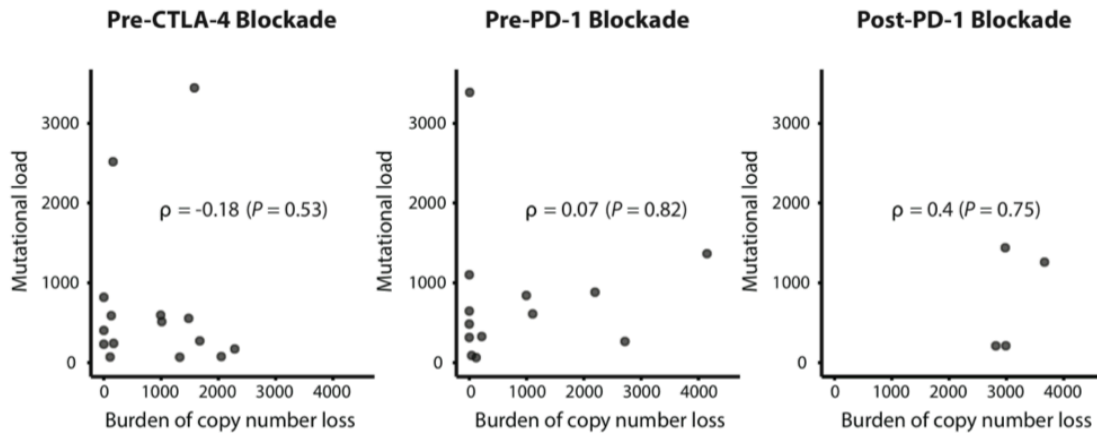


**Figure 28. Correlation between burden of copy number loss and mutational load.**

Data show the correlation between burden of copy number loss and mutational load.

Spearman rank correlation was used for correlation coefficient (correlation coefficient = -0.18; Spearman rank correlation,  $P = 0.53$  for pre-CTLA-4 blockade samples, correlation coefficient = 0.07,  $P = 0.82$  for pre-PD-1 blockade samples, correlation coefficient = 0.4,  $P = 0.75$  for post-PD-1 blockade double non-responder samples.).

To gain insight into mechanisms through which CNAs could influence response to therapy, I next investigated if there were any recurrent regions of copy number loss in double non-responders with high burden of copy number loss (> 2,000 genes with copy number loss). Recurrent copy number loss was observed at the arm level in chromosome 6q and 10q, and recurrent focal copy number loss was observed in 8p23.3, 11p15.5, 11q23, 11q24, and 11q25 (Figure 29, Table 9). In these regions with recurrent copy number loss, tumor suppressor genes were located in chromosomes 6q (*FOXO3*, *PRDM1*, *PTPRK*, *TNFAIP3*, and *ESR1*), 10q (*NCOA4*, *BMPR1A*, *PTEN*, *FAS*, *SUFU*, and *TCF7L2*), and 11q23.3 (*CBL*, *ARHGEF12*). These data suggest that high burden of copy number loss in double non-responders is associated with recurrent copy number loss in tumor suppressor genes located in chromosomes 6q, 10q, and 11q23.3.

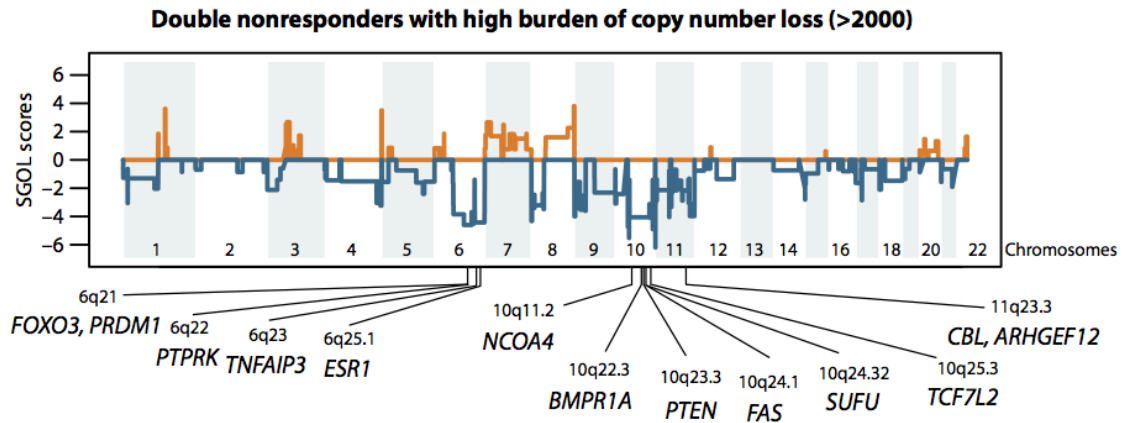


**Figure 29. Recurrent copy number loss in double non-responders.** Segment Gain or Loss (SGOL) scores were calculated for each copy number segments as sum of  $\log_2$  copy ratios (tumor/normal) of each copy number segment across all double non-responder samples with burden of copy number loss higher than 2,000 (n=9). Higher positive SGOL scores indicate higher copy number gain of copy number segments and lower negative SGOL scores indicate higher copy number loss of copy number segments. Tumor suppressor genes with recurrent copy number loss are indicated in chromosome 6q, 10q, and 11q23.3.

Recurrent Samples	Status	Chromosome	MCR.start	MCR.end	Cytobands
32A,41A,25C,49E,2E	loss	chr6	64694354	100061533	q12,q13,q14.1,q14.2,q14.3,q15,q16.1,q16.2
32A,41A,26C,25C,49E,2E	loss	chr6	100061533	126210395	q16.2,q16.3,q21,q22.1,q22.2,q22.31,q22.32
32A,41A,26C,25C,2E	loss	chr6	126210395	129722389	q22.32,q22.33
32A,41A,26C,25C,49E,2E	loss	chr6	129722389	134304023	q22.33,q23.1,q23.2
32A,41A,26C,49E,2E	loss	chr6	134304023	136359446	q23.2,q23.3
26E,32A,41A,26C,49E	loss	chr6	137026266	137519127	q23.3
26E,32A,41A,26C,49E,2E	loss	chr6	137519127	170190200	q23.3,q24.1,q24.2,q24.3,q25.1,q25.2,q25.3,q26,q27
32A,41A,26C,49E,2E	loss	chr6	170190200	170595317	q27
26E,41A,26C,49E,2E	loss	chr8	182934	2148771	p23.3
26E,32A,41A,26C,2E	gain	chr8	144789269	146115367	q24.3
41A,25C,16C,49E,42E,2E	loss	chr10	42965636	45939136	q11.21
41A,25C,49E,42E,2E	loss	chr10	45939136	45958881	q11.21
41A,25C,49E,42E,2E	loss	chr10	46965017	46965018	q11.22
41A,25C,16C,49E,42E,2E	loss	chr10	46965727	47000146	q11.22
41A,25C,49E,42E,2E	loss	chr10	47000146	47087609	q11.22
41A,25C,49E,42E,2E	loss	chr10	48429578	116251686	q11.22,q11.23,q21.1,q21.2,q21.3,q22.1,q22.2,q22.3,q23.1,q23.2
41A,25C,49E,42E,2E	loss	chr10	118355695	127436411	q25.3,q26.11,q26.12,q26.13
41A,25C,49E,42E,2E	loss	chr10	127461154	127530325	q26.13,q26.2
41A,16C,49E,42E,2E	loss	chr10	127708428	127734716	q26.2
41A,25C,16C,49E,42E,2E	loss	chr10	127734716	135216340	q26.2,q26.3
41A,25C,16C,49E,42E	loss	chr10	135216340	135269955	q26.3
26E,26C,25C,49E,42E	loss	chr11	1021268	1212967	p15.5
26E,26C,25C,49E,42E	loss	chr11	1213174	1213177	p15.5
26E,26C,25C,49E,42E	loss	chr11	1213204	1213245	p15.5
26E,41A,26C,25C,49E,42E	loss	chr11	1213245	1213533	p15.5
26E,26C,25C,49E,42E	loss	chr11	1215580	1253942	p15.5
26E,26C,25C,49E,42E	loss	chr11	1255773	1309956	p15.5
26C,25C,16C,42E,2E	loss	chr11	118765267	134202036	q23.3,q24.1,q24.2,q24.3,q25

\*MCR: Minimum Common Regions (by cghMCR)

**Table 9. Recurrent copy number alterations in double non-responders with burden of copy number loss > 2000**

### 4.2.3 An independent patient cohort shows copy number loss as a putative resistance mechanism

To investigate the impact of higher burden of copy number loss on resistance in another cohort of patients on immune checkpoint blockade, we obtained WES SAM files from 110 melanoma patients and RNA-seq data from a subset of 42 melanoma patients (25) and reanalyzed the data utilizing the same informatics pipeline and calling criteria. I then tested the association between the burden of CNAs (Table 10) and response to therapy in pre-treatment biopsies on CTLA-4 blockade using the same response criteria (clinical benefit, long-term survival with no clinical benefit, and minimal or no clinical benefit) as previously described (25). Although the burden of copy number gain was not significantly associated with clinical benefit from CTLA-4 blockade, a lower burden of copy number loss was significantly associated with clinical benefit ( $P = 0.016$ ) (Figure 30). As observed in our cohort, the burden of copy number loss once again did not correlate with mutational load (Figure 31). When examining the regions associated with recurrent copy number loss in the *no clinical benefit* subgroup, recurrent copy number loss was observed at arm level in chromosome 9p and 10q, and recurrent focal copy number loss was observed in 4q35.2, 6q25, 6q27, and 11p15.5 (Figure 32). Among these regions, tumor suppressor genes were observed in 6q25.1 (*ESR1*) and 10q (*NCOA4*, *BMPR1A*, *PTEN*, *FAS*, and *SUFU*), as seen within our cohort. Of note, no recurrent copy number loss was observed in any tumor suppressor gene in the *clinical benefit* subgroup and *long-term survival* subgroup.

<b>patient</b>	<b>group</b>	<b>n_copy_gain</b>	<b>n_copy_loss</b>
Pat02	response	27	1471
Pat03	nonresponse	0	865
Pat04	response	164	2971
Pat06	nonresponse	NA	NA
Pat07	response	820	753
Pat08	nonresponse	162	3976
Pat100	nonresponse	4	1099
Pat101	nonresponse	771	4100
Pat103	response	0	0
Pat104	nonresponse	1070	12
Pat105	response	0	0
Pat106	nonresponse	NA	NA
Pat109	nonresponse	0	328
Pat11	long-survival	27	0
Pat110	nonresponse	11	1152
Pat113	response	845	4053
Pat115	nonresponse	679	8146
Pat117	response	0	98
Pat118	nonresponse	430	65
Pat119	long-survival	157	2811
Pat121	nonresponse	NA	NA
Pat123	response	0	0
Pat124	nonresponse	1012	2573
Pat126	response	435	533
Pat127	nonresponse	937	6204
Pat128	nonresponse	1554	118
Pat129	nonresponse	683	1093
Pat13	long-survival	0	264
Pat130	nonresponse	344	6043
Pat131	nonresponse	29	0
Pat132	response	NA	NA
Pat133	nonresponse	329	695
Pat135	nonresponse	711	2929
Pat138	response	145	217
Pat139	nonresponse	755	4170
Pat14	nonresponse	356	132
Pat140	nonresponse	1076	453
Pat143	nonresponse	869	5385
Pat147	nonresponse	0	18
Pat148	nonresponse	13	1576
Pat15	nonresponse	1466	4970
Pat151	nonresponse	198	1722
Pat157	nonresponse	642	2619
Pat159	long-survival	123	2002
Pat16	long-survival	318	2139
Pat160	nonresponse	2780	2244
Pat162	nonresponse	767	2096
Pat163	long-survival	149	2910
Pat165	nonresponse	NA	NA
Pat166	nonresponse	NA	NA
Pat167	nonresponse	884	2319
Pat168	nonresponse	1308	3186
Pat17	nonresponse	155	1948
Pat170	nonresponse	0	1893

Pat171	nonresponse	NA	NA
Pat174	response	0	65
Pat175	nonresponse	NA	NA
Pat18	long-survival	304	246
Pat19	nonresponse	141	183
Pat21	response	125	0
Pat24	response	367	660
Pat25	nonresponse	0	0
Pat27	long-survival	456	0
Pat28	long-survival	0	0
Pat29	response	84	0
Pat32	nonresponse	451	2
Pat33	nonresponse	122	329
Pat36	nonresponse	34	0
Pat37	nonresponse	1281	3368
Pat38	response	253	72
Pat39	response	12	0
Pat40	nonresponse	177	1779
Pat41	nonresponse	0	1883
Pat43	nonresponse	799	1059
Pat44	nonresponse	0	1310
Pat45	nonresponse	513	5015
Pat46	nonresponse	296	1497
Pat47	response	177	1727
Pat49	response	285	0
Pat50	nonresponse	246	4819
Pat54	nonresponse	7	1861
Pat55	nonresponse	141	1174
Pat56	nonresponse	684	5341
Pat57	nonresponse	669	1403
Pat58	nonresponse	198	4857
Pat59	nonresponse	106	0
Pat60	nonresponse	443	131
Pat62	nonresponse	0	1658
Pat63	response	317	1213
Pat64	nonresponse	1207	1429
Pat66	response	1073	100
Pat67	nonresponse	404	1795
Pat70	nonresponse	452	1502
Pat71	nonresponse	0	10
Pat73	response	NA	NA
Pat74	nonresponse	267	1468
Pat76	nonresponse	0	84
Pat77	response	0	27
Pat78	nonresponse	NA	NA
Pat79	response	472	2815
Pat80	response	1211	3403
Pat81	nonresponse	NA	NA
Pat82	nonresponse	297	2101
Pat83	long-survival	448	0
Pat85	nonresponse	143	0
Pat86	nonresponse	682	3385
Pat88	response	621	2017
Pat90	response	978	6764
Pat92	nonresponse	NA	NA
Pat98	nonresponse	471	1635

**Table 10. Burden of copy number alterations in the Van Allen cohort**

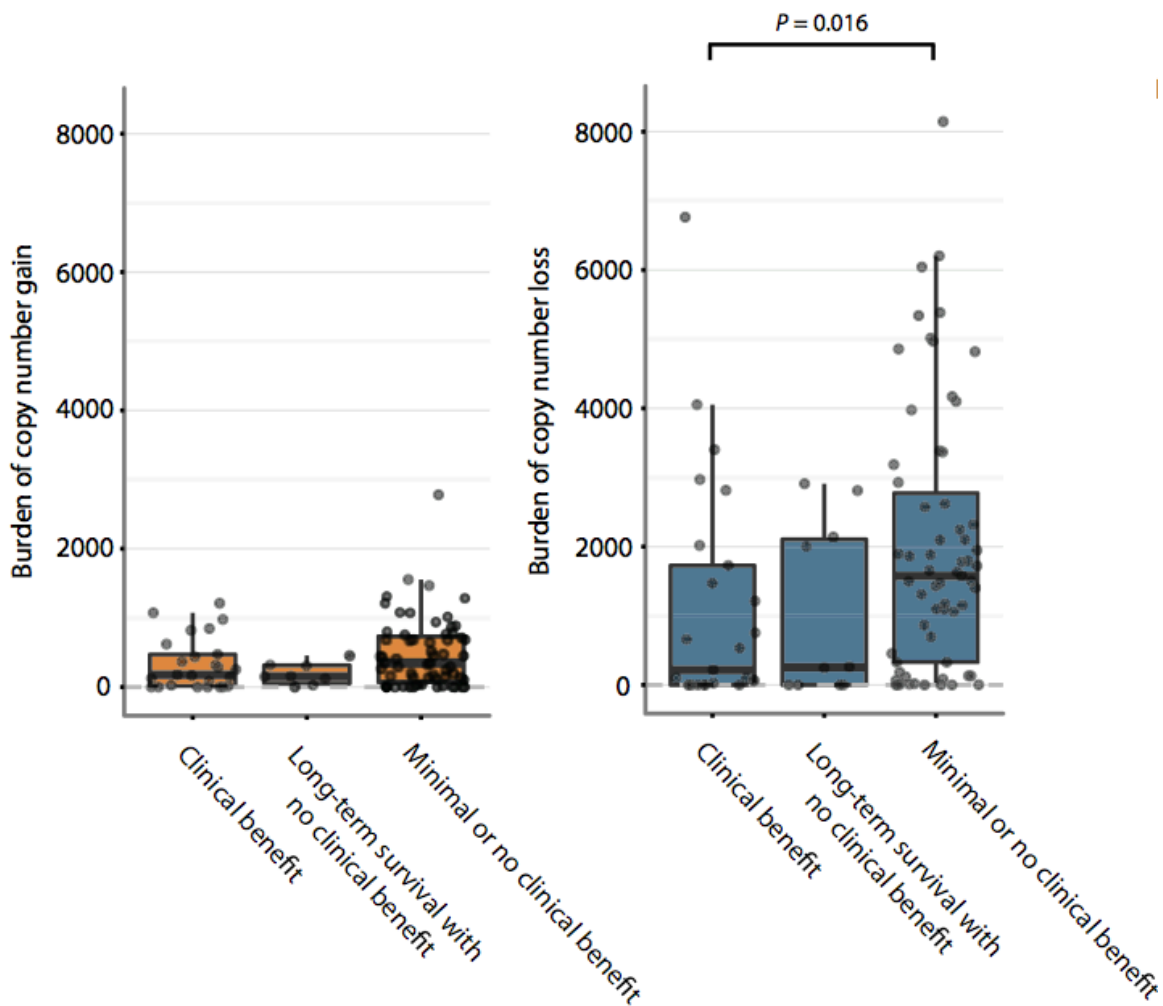


**Figure 30. Burden of copy number alterations in each clinical response group from an independent cohort.** Boxplots summarize burden of copy number gain or loss in three patient subgroups from the Van Allen cohort: clinical benefit, long-term survival with no clinical benefit, and minimal or no clinical benefit; median values (lines) and interquartile range (whiskers) are indicated. *P* values were calculated using a two-sided Mann-Whitney *U* test ( $P = 0.016$  for burden of copy number loss in clinical benefit vs. minimal or no clinical benefit, and  $P > 0.05$  for all others).



**Van Allen cohort**

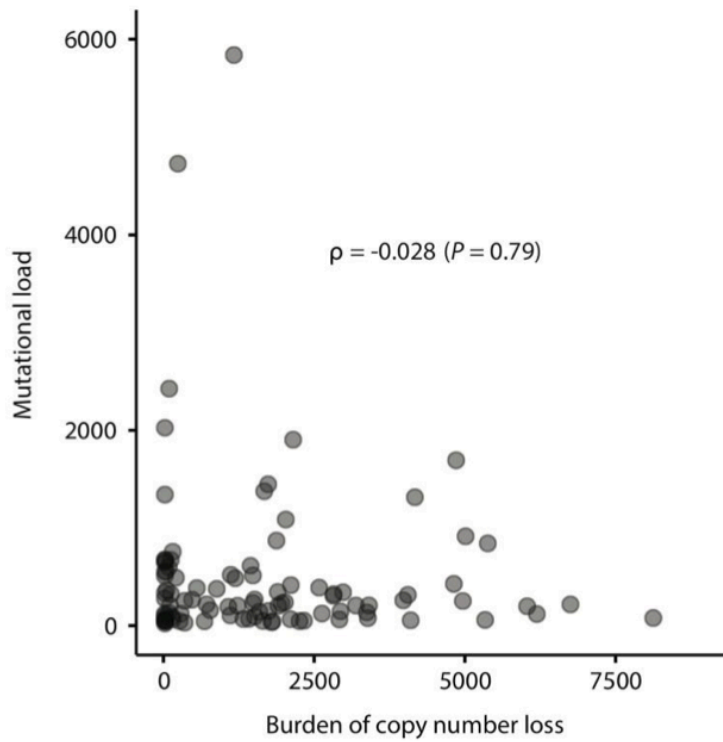


**Figure 31. Correlation between burden of copy number loss and mutational load in the Van Allen cohort.** Data show the correlation between burden of copy number loss and mutational load in Van Allen cohort. Spearman rank correlation was used for correlation coefficient (correlation coefficient = -0.028,  $P = 0.79$ ).

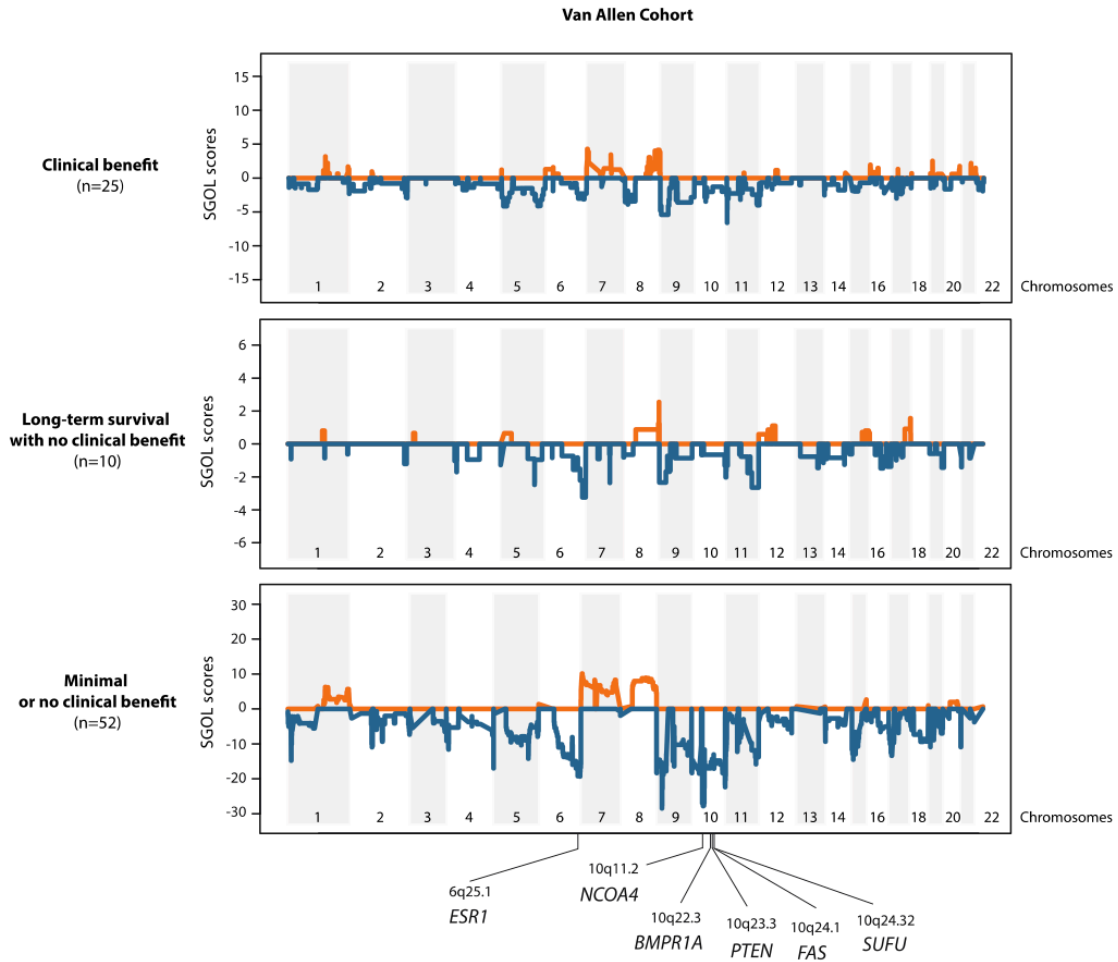


**Figure 32. Segment Gain or Loss (SGOL) scores in three patient subgroups from the Van Allen cohort.** Plots show the recurrent copy number alterations in genomic coordinates. SGOL scores were calculated as sum of  $\log_2$  copy ratios of copy number segment in each group (sample size of each group is indicated in parentheses). In minimal or no clinical benefit group, samples with burden of copy number loss lower than 100 (Pat25, Pat32, Pat36, Pat59, Pat71, Pat76, Pat85, Pat104, Pat118, Pat131, and Pat147) were excluded from analysis. Higher positive SGOL scores indicate higher copy number gain in copy number segments, and lower negative SGOL scores indicate higher copy number loss in copy number segments. Copy number segments with both copy number gain and copy number loss present were excluded. Tumor suppressor genes with recurrent copy number loss are indicated.

Next, I investigated whether the recurrent region of copy number loss identified in our cohort (Table 9) is also associated with CTLA-4 blockade resistance in this independent cohort (Van Allen cohort). To do so, I calculated the burden of copy number loss in this independent cohort as the total number of genes with copy number loss in the recurrent regions of copy number loss identified in our cohort. We observed a significantly higher burden of copy number loss in the minimal or no clinical benefit groups compared to the clinical benefit group ( $P = 0.0034$ ) (Figure 33). This result suggests that the recurrent regions of copy number loss in our cohort are also associated with CTLA-4 blockade resistance in this independent cohort.

### Van Allen cohort

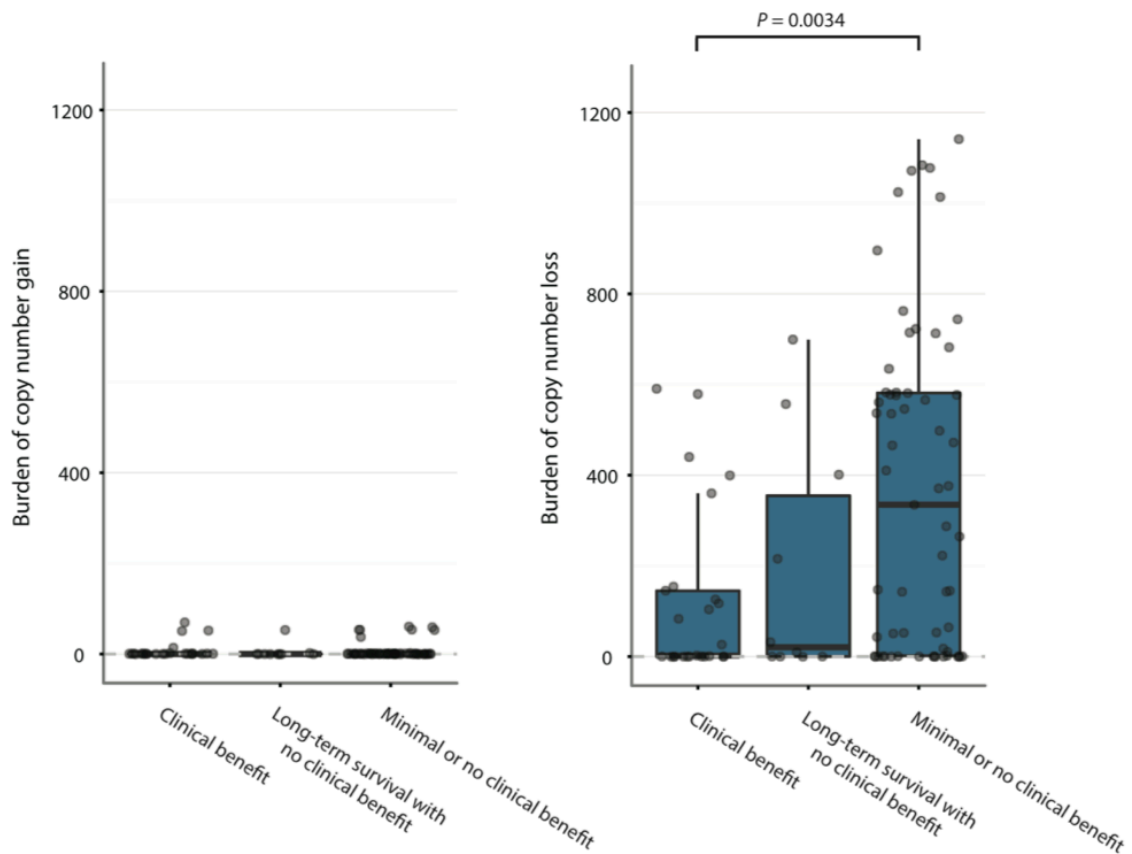


**Figure 33. Burden of recurrent CNAs in patients in Van Allen cohort.** Boxplots summarize burden of copy number gain or loss in recurrent regions of copy number loss identified from our cohort in each response group from the Van Allen cohort; median values (lines) and interquartile range (whiskers) are indicated.  $P$  values were calculated using a two-sided Mann-Whitney  $U$  test. ( $P = 0.0034$  for clinical benefit group vs. minimal or no clinical benefit group, and  $P > 0.05$  for all others)

I next sought to determine the relative contribution of copy number loss burden from chromosome 10 in CTLA-4 blockade resistance. I was specifically interested in copy number loss from chromosome 10 because a recent study (147) showed functional evidence that recurrent loss of the entire chromosome 10 can result in collective repression of multiple tumor suppressor genes. This is also consistent with the observation that chromosome 10 harbored the largest number of tumor suppressor genes with recurrent copy number loss in both our cohort (Figure 29) and the independent cohort (Figure 32). The logistic regression model showed that the odds of resistance to CTLA-4 blockade were  $\exp(1.504) = 4.5$  (95% CI: 1.56 – 13) times greater in patients with high burden of copy number loss in chromosome 10 than in patients with low burden of copy number loss in chromosome 10 (Table 11) and the odds of resistance were  $\exp(1.069) = 2.91$  (95% CI: 1.07 – 7.89) times greater in patients with high burden of copy number loss outside chromosome 10 than in patients with low burden of copy number loss outside chromosome 10 (Table 12). Therefore, the relative contribution of copy number loss burden from chromosome 10 in CTLA-4 blockade resistance was higher than copy number loss burden outside chromosome 10. I further investigated the extent to which *PTEN* loss in chromosome 10 is associated with CTLA-4 blockade resistance (44). In our data, the odds of resistance were 5.58 times greater in patients with *PTEN* loss than in patients with no *PTEN* loss (95% CI: 1.19 - 26.20) (Table 13), suggesting that *PTEN* loss is likely to be one of the driver resistance mechanisms exploited by tumors with high burden of copy number loss on chromosome 10.

	Estimate	SE	Z-value	P-value
Intercept	1.922	1.136	1.691	0.091
Log2(Mutational load)	-0.206	0.135	-1.52	0.128
Burden of copy number loss (high or low) : chr10 only	1.504	0.541	2.779	0.005

**Table 11. Relative contribution of copy number loss burden by chromosome 10 in CTLA-4 blockade resistance**

	Estimate	SE	Z-value	P-value
Intercept	2.448	1.134	2.159	0.031
Log2(Mutational load)	-0.254	0.137	-1.85	0.065
Burden of copy number loss (high or low) : outside chr10	1.069	0.509	2.1	0.036

**Table 12. Relative contribution of copy number loss burden outside chromosome 10 in CTLA-4 blockade resistance**

	Estimate	SE	Z-value	P-value
Intercept	2.227	1.124	1.982	0.048
Log2(Mutational load)	-0.207	0.135	-1.53	0.126
PTEN loss (loss or no loss)	1.719	0.789	2.178	0.029

**Table 13. Relative contribution of PTEN loss in CTLA-4 blockade resistance**



#### **4.2.4 Integrated analysis reveals putative mechanisms through which CNAs may influence response to therapy**

In addition to studying the influence of copy number loss on molecular features such as tumor suppressor genes, I sought to study the relationship of these alterations with the immune tumor microenvironment. To do so, I examined the correlation between burden of copy number loss and immune scores. Although we observed no correlation between the burden of copy number loss and immune scores in pre-CTLA-4 blockade biopsies in our cohort (correlation coefficient = -0.13; Spearman rank correlation,  $P = 0.79$ ), a moderate negative correlation between the burden of copy number loss and immune scores calculated by ESTIMATE (88) was identified in the Van Allen cohort (correlation coefficient = -0.41; Spearman rank correlation,  $P = 0.011$ ) (25) (Figure 34A). In pre-PD-1 blockade biopsies in our cohort, we also observed a negative correlation between the burden of copy number loss and immune scores (correlation coefficient = -0.63; Spearman rank correlation,  $P = 0.091$ ) (Figure 34B), although this could not be investigated in post-PD-1 blockade biopsies due to sample size. Our immune scores and those calculated by ESTIMATE (Table 14) showed a strong positive correlation (correlation coefficient = 0.91; Spearman rank correlation,  $P < 2.2e-16$ ) in the independent cohort (Figure 34C), suggesting concordance between immune scores.

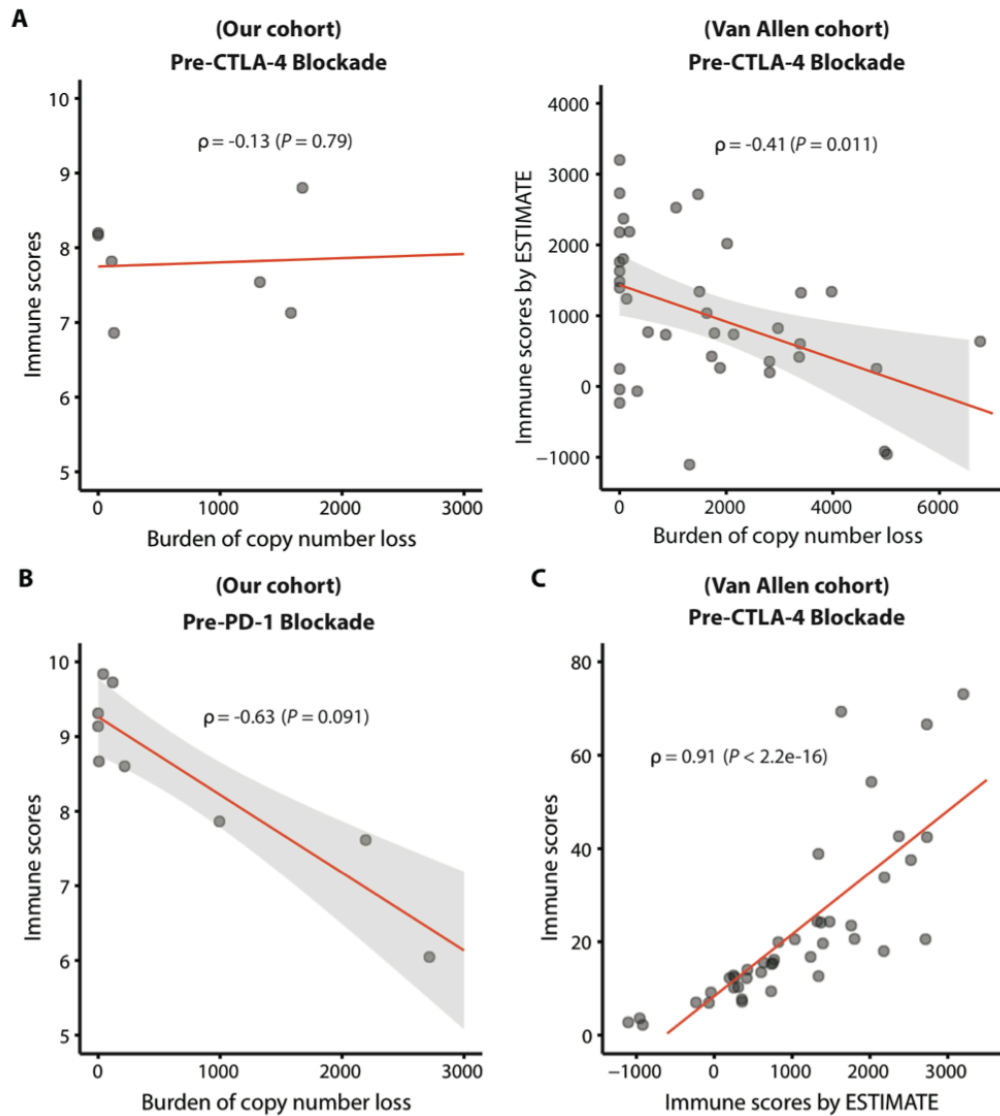


**Figure 34. Correlation between burden of copy number loss and immune scores.**

Data show **(A)** the correlation between burden of copy number loss and immune scores for the pre-CTLA-4 blockade biopsies in our cohort, and the correlation between burden of copy number loss and immune scores calculated by ESTIMATE in patients with matched copy number data and RNA-seq data available ( $n=38$ ) from Van Allen cohort, **(B)** the correlation between burden of copy number loss and immune scores for the pre-PD-1 blockade biopsies in our cohort, and **(C)** the correlation between immune scores

and immune scores calculated by ESTIMATE in Van Allen cohort. Spearman rank correlation was used for correlation coefficient.

patient	immune_score_ESTIMATE
Pat02	2714.41
Pat03	730.23
Pat04	822.98
Pat06	2731.64
Pat08	1338.68
Pat118	1801.37
Pat119	353.57
Pat123	-43.53
Pat126	768.27
Pat14	1238.3
Pat15	-919.35
Pat16	735.31
Pat19	2186.07
Pat20	307.95
Pat25	247.77
Pat27	1394.39
Pat28	1630
Pat29	1759.46
Pat33	-68.31
Pat36	-233.77
Pat37	416.22
Pat38	2371.01
Pat39	2177.73
Pat40	752.89
Pat41	263
Pat43	2526.03
Pat44	-1105.11
Pat45	-957.69
Pat46	1339.92
Pat47	424.87
Pat49	2730.05
Pat50	252.84
Pat79	197.48
Pat80	1323.28
Pat81	356.89
Pat83	1481.38
Pat85	3198.89
Pat86	601.73
Pat88	2018.3
Pat90	635.76
Pat91	1370.99
Pat98	1035.48

**Table 14. Immune scores (RNA-seq) in the Van Allen cohort**

I further sought to determine which pathways or gene ontologies (GO) were enriched in up/down-regulated genes at the mRNA expression level in the high burden of copy number loss (n=10; mean: 4149, range: 2815 to 6764) versus low burden of copy number loss (n=10; mean: 0) groups within the Van Allen cohort. Gene set enrichment analysis (GSEA) (89) showed that immune-related pathways were enriched among down-regulated genes, whereas cell cycle-related pathways were enriched among up-regulated genes (Figure 35 and 36A). Similar results were found with GO terms (Figure 36B). Collectively, these data suggest that high burden of copy number loss may be associated with down-regulation of immune-related pathways.

**High burden of copy number loss versus low burden of copy number loss  
Enriched KEGG pathway gene sets ( $q < 0.001$ )**

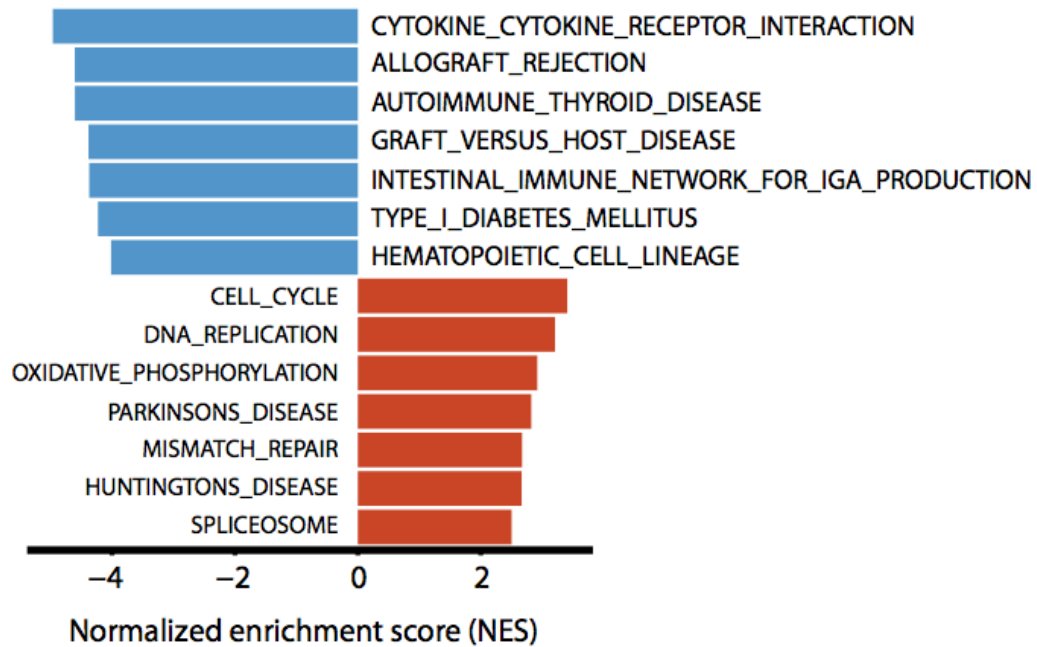
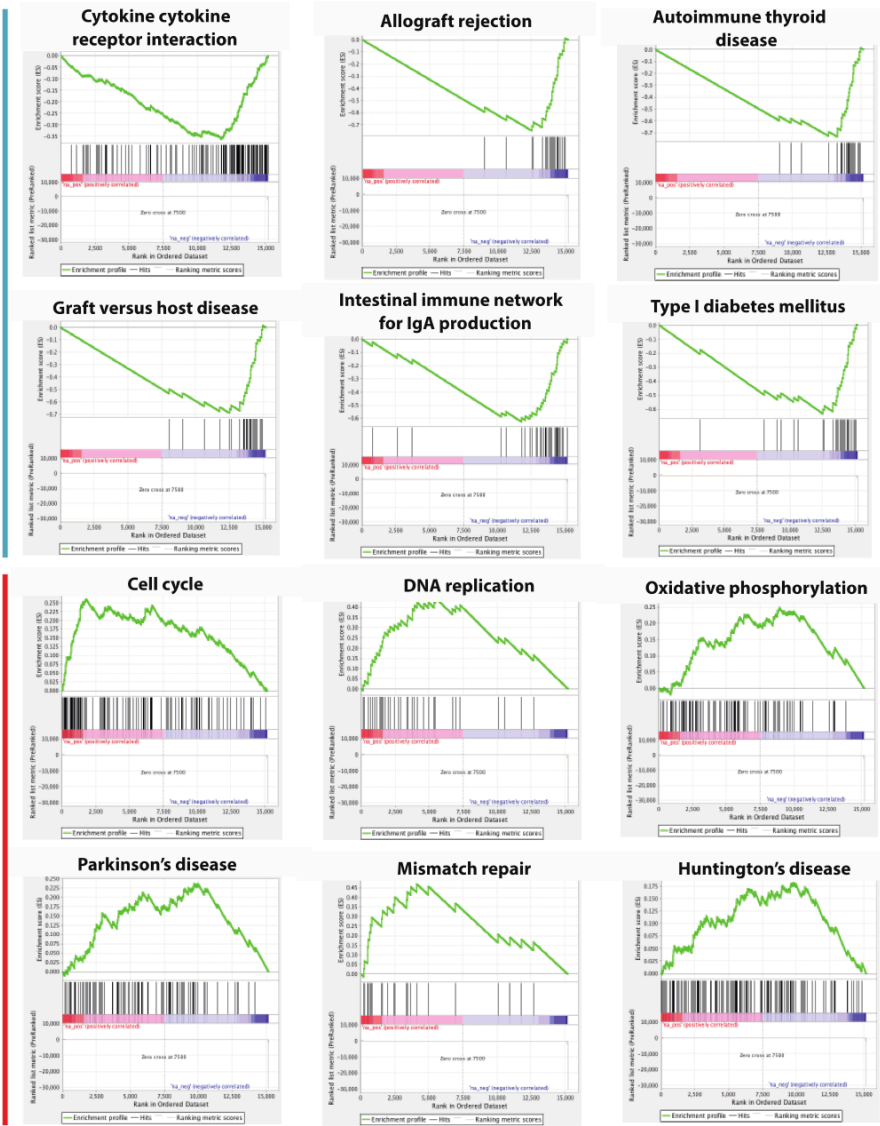


**Figure 35. Gene set enrichment analysis of differentially expressed genes between tumors with high burden of copy number loss and those with low burden of copy number loss.** Gene set enrichment analysis (GSEA) results show top enriched KEGG pathways from down-regulated genes (blue bars) and up-regulated genes (red bars) in high burden of copy number loss group versus low burden of copy number loss group (FDR-adjusted  $P < 0.001$ ).

A

Down-regulated in high burden of copy number loss vs. low burden of copy number loss



Up-regulated in high burden of copy number loss vs. low burden of copy number loss

B

High burden of copy number loss vs. low burden of copy number loss  
Enriched Gene Ontology gene sets (q<0.001)

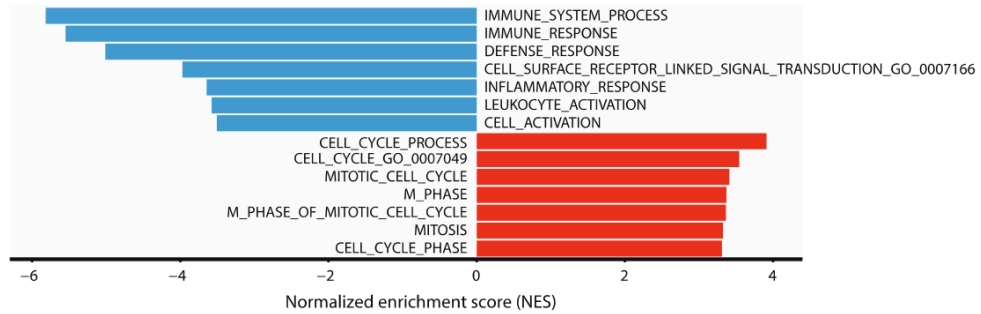


Figure 36. Up and down-regulated pathways in patients with high versus low copy number loss in the Van Allen cohort. (A) Data show enrichment plots for top enriched

KEGG pathways from down-regulated genes (upper panel) and up-regulated genes (lower panel) in high burden of copy number loss group versus low burden of copy number loss group (FDR-adjusted  $P < 0.001$ ). **(B)** Gene set enrichment analysis (GSEA) results show top enriched Gene Ontology (biological process) terms from down-regulated genes (blue bar) and up-regulated genes (red bar) in high burden of copy number loss group versus low burden of copy number loss group (FDR-adjusted  $P < 0.001$ ).



#### **4.2.5 Mutational load and burden of copy number loss may allow better patient stratification for response than either correlate alone**

Finally, I was interested in determining if the effect of mutational load and burden of copy number loss on clinical response was non-redundant. Using the reanalyzed data from the Van Allen cohort, I first stratified patients into four subgroups based on mutational load (high or low) and burden of copy number loss (low or high) (Figure 37). Within each subgroup, I then calculated the proportion of patients with *clinical benefit*, *long-term survival*, and *no clinical benefit*, respectively (Figure 38). The proportion of patients with clinical benefit was higher in the subgroup of patients with high mutational load and low burden of copy number loss (11 out of 26) compared to the subgroup of patients with low mutational load and high burden of copy number loss (4 out of 26) ( $P = 0.064$ , Fisher's exact test). Similarly, the proportion of patients with no clinical benefit was significantly higher in the subgroup of patients with low mutational load and high burden of copy number loss (21 out of 26) compared to the subgroup of patients with high mutational load and low burden of copy number loss (13 out of 26) ( $P = 0.04$ , Fisher's exact test). I then performed a logistic regression on response status (clinical response or no clinical response) with the  $\log_2$ -transformed mutational load and  $\log_2$ -transformed burden of copy number loss as covariates, and found an additive effect of mutational load (coefficient = 0.266,  $z = 1.939$ ,  $P = 0.053$ ) and burden of copy number loss (coefficient = -0.149,  $z = -2.55$ ,  $P = 0.011$ ) on clinical response (Table 15). This suggests that the effects of mutational load and burden of copy number loss on clinical response are likely

non-redundant. Collectively, the above data demonstrate the potential utility of a combinatorial biomarker using mutational load and copy number loss burden.

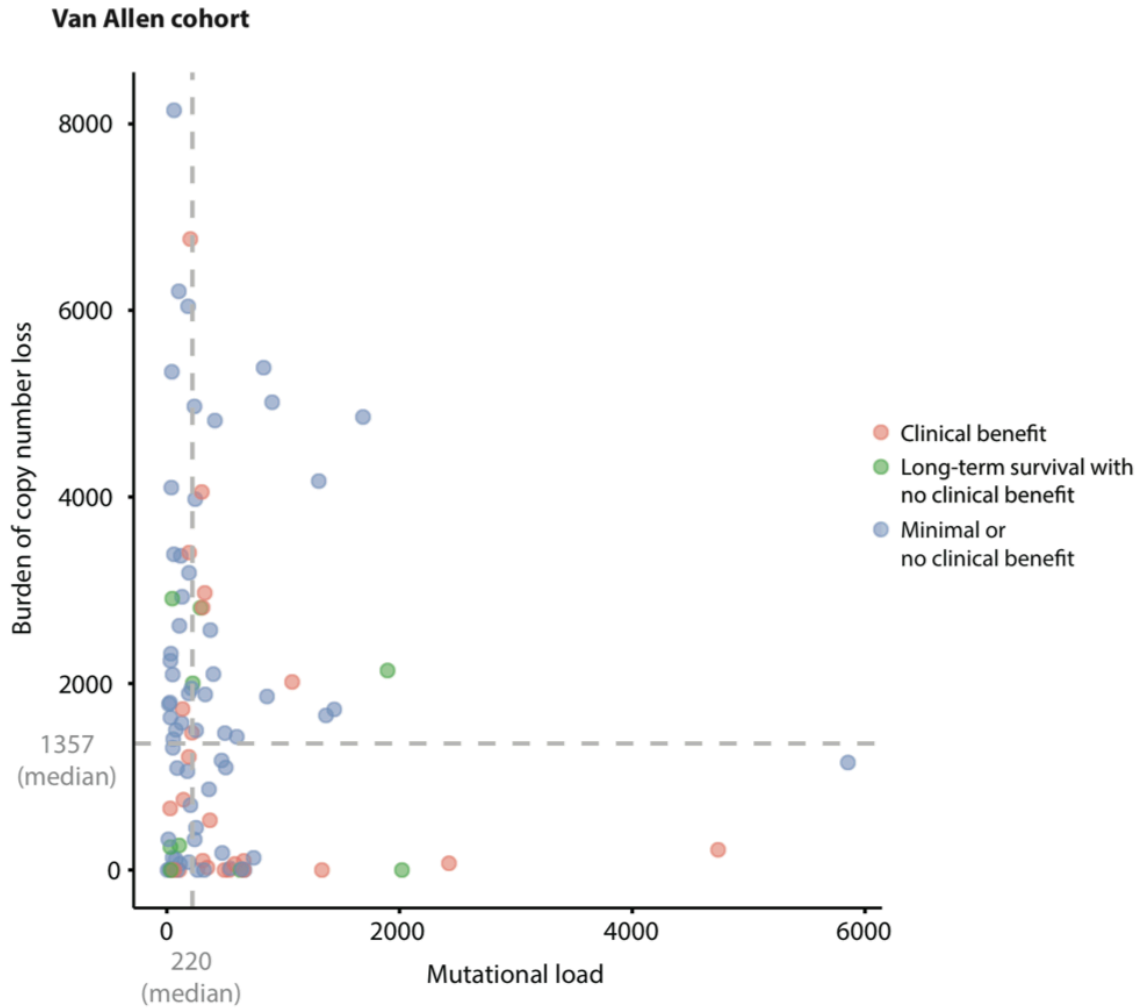


**Figure 37. Patient stratification based on mutational load and burden of copy number loss in the Van Allen cohort.** Patients were stratified into four subgroups based on mutational load and burden of copy number loss: high mutational load (>median, 220) and low burden of copy number loss ( $\leq$ median, 1357) (n=26), high mutational load and high burden of copy number loss (n=23), low mutational load and low burden of copy number loss (n=23), and low mutational load and high burden of copy number loss (n=26). Within each subgroup, response status of each patient is color-coded.

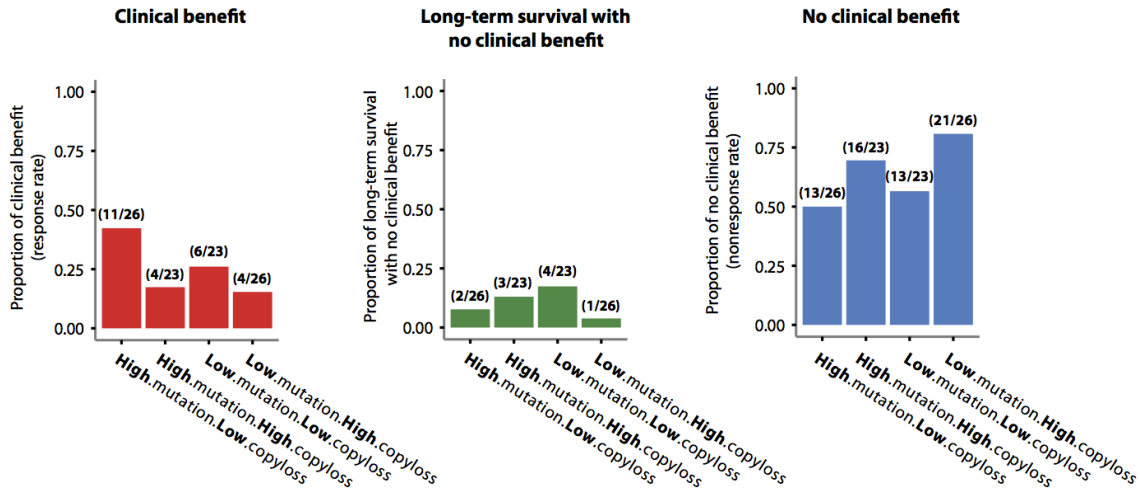


**Figure 38. Clinical response rate in patient subgroups stratified by mutational load and burden of copy number loss.** Proportions of patients with clinical benefit, long-term survival with no clinical benefit, and minimal or no clinical benefit were calculated within each of the four patient subgroups: high mutational load and low burden of copy number loss, high mutational load and high burden of copy number loss, low mutational load and low burden of copy number loss, and low mutational load and high burden of copy number loss. The numbers in parentheses indicate the number of patients with different levels of response (clinical benefit, long-term survival, and no clinical benefit) out of the total number of patients in each of the four patient subgroups.

	<b>Estimate</b>	<b>Z-value</b>	<b>P-value</b>
<b>Intercept</b>	-1.821	-1.556	0.12
<b>Log2(Mutational load)</b>	0.266	1.939	0.053
<b>Log2(Burden of copy number loss)</b>	-0.149	-2.55	0.011

**Table 15. Additive effect of high mutational load and low burden of copy number loss on response to CTLA-4 blockade.**

### 4.3 Discussion

There is now abundant evidence that both tumor- (25, 41, 43, 44, 75, 119) and host-related factors (40, 59, 86, 120) can influence heterogeneous response and resistance to immune checkpoint blockade. Here, we report genomic characterization of tumors from a cohort of metastatic melanoma patients in the context of sequential immune checkpoint blockade. This study builds on our prior immune profiling of tumors within the same cohort of metastatic melanoma patients (87), allowing for a more fully integrated analysis in this particular cohort.

In tumor compartment-specific analyses, we observed a higher burden of copy number loss in non-responders compared to responders on CTLA-4 blockade. This finding is in line with those in prior studies that have reported that the burden of copy number alterations increases in advanced melanoma and is implicated in melanoma progression (148-151). The association between burden of copy number loss and clinical response observed here suggests that melanoma progression may be associated with resistance to immune mediated tumor control. Furthermore, investigation of the findings reported here in a first line treatment setting will help delineate the value of these potential associations.

We also identified genomic regions of recurrent copy number loss in patients with high burden of copy number loss and determined that several tumor suppressor genes were located within these genomic regions. This suggests that loss of function in these tumor suppressor genes could potentially influence therapeutic resistance. In keeping with this suggestion, previous studies in preclinical models of melanoma with *PTEN* loss showed inhibition of T cell-

mediated tumor killing and decrease in T cell trafficking into tumors (44). *PTEN* was one of the tumor suppressor genes with recurrent copy number loss from patients with high burden of copy number loss in this study as well. A correlation between copy number loss burden and down-regulation of immune-related gene expression was found, suggesting that there may be gene expression sequelae of extensive copy number loss, including *PTEN* loss. More extensive analyses on larger cohorts with matched WES and RNA-seq data are needed to expand on these findings and develop an integrated expression/copy number evaluation approach to validate and potentially exploit the correlation seen here.

We also observed that the effects of low copy number loss burden and high mutational load on clinical response are non-redundant, suggesting the possibility of a combinatorial biomarker using copy number loss burden and mutational load. From a clinical perspective, the optimal cutoffs for high or low copy number loss burden and mutational load will need to be further validated if they are to impact improved patient stratification in the clinical setting.

Our work also confirms previous reports that TCR clonality is correlated with response to PD-1 blockade (86). A combinatorial biomarker approach of TCR clonality and genomic correlates such as mutational load and copy number loss burden needs to be further tested in a large cohort with pre-PD-1 blockade biopsies available.

Additionally, we observed increased TCR clonality after CTLA-4 blockade treatment in all PD-1 blockade responders with paired pre-CTLA-4 and pre-PD-1 blockade biopsies available. Prior work has shown that TCR clonality at the pre-

PD-1 time point was not significantly different ( $P = 0.1604$ ) between anti-CTLA-4-treated PD-1 blockade responders and anti-CTLA-4-naïve PD-1 blockade responders (86). Therefore, CTLA-4 blockade treatment may increase TCR clonality to a level high enough to mediate response to subsequent PD-1 blockade in certain patients. This result suggests that responders to PD-1 blockade may derive clinical benefit from prior CTLA-4 blockade, substantiating the utility of sequential CTLA-4 and PD-1 blockade. From a clinical perspective, sequential CTLA-4 and PD-1 blockade treatment might be able to increase the number of patients with high baseline TCR clonality prior to PD-1 blockade compared with PD-1 blockade monotherapy.

What emerges from this and other work regarding immune checkpoint responder/non-responder identification is a complex picture likely involving the interplay of tumor genomic characteristics, tumor modulation of the local microenvironment, and the extent of immune surveillance in the tumor milieu at the time of initiation of therapy. Furthermore, several intriguing questions emerge from this and other work. What is the effect of CTLA-4 blockade on the molecular profile of anti-PD-1 responders? Do the data reported hold true when applied to CTLA-4 blockade treatment-naïve patients? To what extent do the data emerging from melanoma studies apply to other tumor treatment contexts? There will likely be a need to develop integrated molecular phenotyping approaches to more accurately delineate responders/non-responders and develop tractable predictive models for these promising therapies.



## **CHAPTER FIVE – DISCUSSION, CONCLUSIONS AND FUTURE DIRECTIONS**

## **Chapter 5 DISCUSSION, CONCLUSIONS AND FUTURE DIRECTIONS**

### **5.1 Discussion and Conclusions**

The recent development of immunotherapy and cancer immunogenomics has changed the treatment landscape in metastatic melanoma. Immune checkpoint blockade has now become the front-line treatment for melanoma demonstrating prolonged survival and durable response. However, the response rate and the toxicity vary among individuals. Therefore, biomarkers are needed to predict patients who are more likely to respond and experience lower toxicity. In addition to biomarker discovery, identifying mechanisms of resistance to immune checkpoint blockade can further the development of novel combination therapy increasing the response rate. In this dissertation, I attempted to identify novel biomarkers and resistance mechanisms of immune checkpoint blockade (CTLA-4 and PD-1 blockade) by performing multidimensional profiling of longitudinal tumor biopsies (pre-, on-, and post-treatment) from metastatic melanoma patients treated with sequential immune checkpoint blockade.

In Chapter 3, we applied the immune profiling approach by immunohistochemistry staining of 12 markers and NanoString Gene Expression Profiling of 795 tumor microenvironment gene panels composed of immune-related genes and common cancer signaling pathway genes. The characterization of tumor microenvironment at multiple time points revealed that early on-treatment (as early as 2 to 3 doses after PD-1 blockade treatment) tumor biopsies show significantly increased expression of adaptive immune signature in responders versus nonresponders. This observation suggests that

assessment of adaptive immune signatures by early on-treatment biopsies can help identify patients who will respond to PD-1 blockade. By predicting response at early on-treatment time point, we can reduce the unnecessary burden of treatment cost and toxicity in patients who are not likely to respond to PD-1 blockade. Another major finding of immune profiling was that VEGFA expression was significantly higher in nonresponders versus responders in PD-1 blockade on-treatment biopsies suggesting the potential mechanism of therapeutic resistance mediated by tumor angiogenesis. Our finding is consistent with the results from the recent preclinical studies showing the efficacy of combination therapy of PD-1 blockade and antiangiogenic therapy (152, 153). Several clinical trials of combined PD-1 blockade and antiangiogenic therapy are also ongoing, and a phase I study combining bevacizumab and ipilimumab showed an objective response rate of 19.6% and a median survival of 25.1 months, which is roughly twice expectation for ipilimumab monotherapy in metastatic melanoma (109, 154). Additionally, we observed the increased intratumoral interaction between CD8+ T cells and CD68+ myeloid cells in both pre-treatment and on-treatment biopsies from nonresponders to PD-1 blockade. A recent study showed that tumor-associated macrophages (TAMs) physically remove the anti-PD-1 antibodies from the surface of T cells, which leads to resistance to PD-1 blockade treatment (51). They also showed that uptake of anti-PD-1 antibodies by TAMs depends on the crystallizable fragment (Fc) domain of the anti-PD-1 monoclonal antibodies and on Fc $\gamma$  receptors (Fc $\gamma$ Rs) expressed by TAMs. This mechanism might explain why nonresponders to PD-1 blockade have the

increased intratumoral interaction between CD8+ T cells and CD68+ myeloid cells. This finding suggests that combining PD-1 blockade with blockade of Fc $\gamma$  receptors (Fc $\gamma$ Rs) might be therapeutically effective in metastatic melanoma patients with increased intratumoral interaction between CD8+ T cells and CD68+ myeloid cells.

However, there are some caveats and biases in interpreting immune profiling data in our study. First, identifying an immune cell subset based on the staining of one marker using immunohistochemistry can bias the quantification of immune cell subset proportion in tumor microenvironment. Multiplexed marker imaging approach such as Vectra would provide more unbiased picture of immune cell subset representation in a tissue. Second, NanoString tumor microenvironment gene panels cannot capture the unbiased genome-wide transcriptome profiles in the tumor microenvironment because the composition of gene panels is based on immune-related genes. Therefore, RNA-seq data would have provided unbiased enrichment of certain pathways in differential gene expression analysis and analysis of differential longitudinal gene expression change between responders and nonresponders by linear mixed effects model.

In Chapter 4, we performed genomic profiling of tumor biopsies from the same cohort of patients in Chapter 3. TCR sequencing of tumor biopsies showed higher TCR clonality in responders versus nonresponders at pre-/on-PD-1 blockade time point. This result suggests that pre-existing clonal T clones actively suppressed in tumor microenvironment are crucial in mediating antitumor response after PD-1 blockade treatment. We also observed increased TCR

clonality after CTLA-4 blockade treatment in all PD-1 blockade responders whereas this longitudinal TCR clonality pattern could not be observed in nonresponders. This data suggest that prior CTLA-4 blockade treatment can be beneficial for subset of patients by preparing clonal baseline T cell repertoire in tumor microenvironment for the success of subsequent PD-1 blockade treatment.

Analysis of whole exome sequencing data revealed the novel tumor-intrinsic resistance mechanism driven by high burden of copy number loss in tumors. Of note, recurrent copy number loss was observed in certain genomic regions (arm level loss in 6q and 10q) contributing to major therapeutic resistance. Mechanistically, tumors with high burden of copy number loss showed decreased expression of immune-related genes. Our finding is consistent with the result from an independent study showing that tumor aneuploidy is associated with immune evasion in multiple cancer types (155). Since aneuploidy is associated with worse prognosis in general, it would be of interest to investigate the extent to which resistance to immune checkpoint blockade leads to worse prognosis in patients with high burden of copy number loss (156). Finally, I showed that combining burden of copy number loss with mutational load provided better predictive power than either alone.

However, there were some technical difficulties in the analysis of genome profiling data. First, the detection of CNAs in tumors with high level of tumor-infiltrating lymphocytes is challenging due to low sensitivity to detect CNAs in low tumor purity samples by current CNA detection algorithms. Therefore, the observation of higher immune cell infiltration in tumors with lower burden of copy

number loss might have been confounded by this technical limitation to some extent. Single cell exome sequencing of tumor cells with varying degree of immune cell infiltration would provide more accurate relationship between tumor aneuploidy and immune evasion. Second, it is difficult to extract accurate tumor-intrinsic transcriptome profiles from the bulk tumor RNA-seq data. Therefore, differential gene expression profiles between tumors with high versus low copy number loss might have not captured important tumor-intrinsic differentially expressed genes. Single-cell RNA-seq of tumor cells would provide more accurate tumor-intrinsic differential transcriptome profiles between tumor cells with high versus low burden of copy number loss because arm level loss can be computationally detected from single-cell RNA-seq data. Differential gene expression analysis of single-cell RNA-seq data might shed light on the detailed mechanism of immune evasion by tumor aneuploidy.

In conclusion, our study is one the first longitudinal studies investigating the molecular interplay between immune cells and tumor cells in the context of sequential immune checkpoint blockade treatment. First, I could identify biomarkers to PD-1 blockade such as early on-treatment adaptive immune signatures, clonal T cell repertoire in tumor microenvironment, and increase in TCR clonality after CTLA-4 blockade treatment. The combinatory biomarker approach of mutational load and burden of copy number loss was also suggested. Second, I identified resistance mechanisms such as increased VEGFA expression in nonresponders to PD-1 blockade and the association between higher burden of copy number loss and immune evasion leading to lack

of response. Our study sets the framework for discovery of novel biomarkers and resistance mechanisms of immune checkpoint blockade by integrative and longitudinal analysis of genomic and immune components.

## **5.2 Future Directions**

Immune profiling results showed that early adaptive immune signatures could be observed in responders in Chapter 3. Interestingly, previous study reported that early on-treatment biopsies (n=21) within 2 months from initiation of PD-1 blockade treatment showed a significant infiltration of intratumoral CD3+, CD8+, and CD68+ macrophages in responders, but not in nonresponders (157). Therefore, it would be interesting to determine how early these adaptive immune signatures can be observed in responders after treatment, which will allow nonresponders to change with other treatment options. This early biomarker will reduce the unnecessary treatment cost and toxicity from patients.

Additionally, it would be of interest to investigate whether early adaptive immune signatures can also be seen in other solid cancers. However, it is often more difficult to obtain post-treatment samples in other solid cancers. The recent study showed that tumor-infiltrating CD8+ T cells with neoantigen specificity can express PD-1 and the same PD-1 expressing T cells can also be found in the blood of melanoma patients (158). Therefore, we might be able to use liquid biopsy as a post-treatment monitoring tool and investigate whether early adaptive immune signatures can be observed in the blood.

In Chapter 3, spatial analysis of immunohistochemistry data revealed differential ratio of CD8+ T cells at the tumor center versus margin between responders and nonresponders. It might be interesting to compare transcriptional state between CD8+ T cells at the tumor center and those at the tumor margin by spatially resolved single-cell RNA-seq in intact tissues.

From longitudinal analysis of TCR sequencing data, I observed increased TCR clonality in subset of patients after CTLA-4 blockade treatment. This increase in TCR clonality was high enough to mediate response to subsequent PD-1 blockade treatment. From a clinical perspective, it would be useful to know which patients will be more likely to experience increase TCR clonality after CTLA-4 blockade treatment. Such biomarkers will then be used as a screening tool for sequential CTLA-4 and PD-1 blockade treatment.

Finally, our study shows that both immune and tumor component plays a critical role in response and resistance to immune checkpoint blockade. For example, pre-existing clonal T cell clones in tumor microenvironment were associated with better response to PD-1 blockade whereas tumors with higher burden of copy number loss showed lower immune cell infiltration leading to lack of response. The dynamic change in immune component also contributed to response and resistance. Increased expression of VEGFA in nonresponders to PD-1 blockade at on-treatment time point showed adaptive resistance to PD-1 blockade. On the other hand, increase in TCR clonality after CTLA-4 blockade treatment was associated with response to PD-1 blockade. Therefore, integrative analysis of immune and tumor component at both pre-treatment time point and



on-/post-treatment time point should be performed for biomarker discovery and identification of resistance mechanisms. In future studies, we need to take two different integrative analysis approaches for deeper understanding of cancer immunology as well as clinical utility of biomarkers. The first approach would be to understand mechanistic link between immune and tumor component in the context of immune checkpoint blockade. A large number of studies have found many potential biomarkers of response and resistance to immune checkpoint blockade. However, few studies have investigated the correlation between those biomarkers and their mechanistic link. Deeper understanding of relationship between biomarkers might provide new insights into cancer immunology. The second approach would be to build a predictive model based on immune and tumor component in a large cohort. This will allow us to find the most predictive combination and relative importance of each immune and tumor component in predicting response to immune checkpoint blockade. The predictive model trained with all the known biomarkers in a large cohort of patients will provide the robust clinical framework for treatment guidance of this therapy.

## References

1. D. Schadendorf, D. E. Fisher, C. Garbe, J. E. Gershenwald, J.-J. Grob, A. Halpern, M. Herlyn, M. A. Marchetti, G. McArthur, A. Ribas, Melanoma. *Nature reviews Disease primers* **1**, 15003 (2015).
2. D. Schadendorf, A. Hauschild, Melanoma in 2013: Melanoma [mdash] the run of success continues. *Nature Reviews Clinical Oncology* **11**, 75-76 (2014).
3. M. S. Lawrence, P. Stojanov, P. Polak, G. V. Kryukov, K. Cibulskis, A. Sivachenko, S. L. Carter, C. Stewart, C. H. Mermel, S. A. Roberts, Mutational heterogeneity in cancer and the search for new cancer genes. *Nature* **499**, 214 (2013).
4. M. S. Stark, S. L. Woods, M. G. Gartside, V. F. Bonazzi, K. Dutton-Regester, L. G. Aoude, D. Chow, C. Sereduk, N. M. Niemi, N. Tang, Frequent somatic mutations in MAP3K5 and MAP3K9 in metastatic melanoma identified by exome sequencing. *Nature genetics* **44**, 165-169 (2012).
5. E. Hodis, I. R. Watson, G. V. Kryukov, S. T. Arold, M. Imielinski, J.-P. Theurillat, E. Nickerson, D. Auclair, L. Li, C. Place, A landscape of driver mutations in melanoma. *Cell* **150**, 251-263 (2012).
6. M. Krauthammer, Y. Kong, B. H. Ha, P. Evans, A. Bacchiocchi, J. P. McCusker, E. Cheng, M. J. Davis, G. Goh, M. Choi, Exome sequencing identifies recurrent somatic RAC1 mutations in melanoma. *Nature genetics* **44**, 1006-1014 (2012).

7. A. P. Albino, R. Le Strange, A. I. Oliff, M. E. Furth, L. J. Old, Transforming ras genes from human melanoma: a manifestation of tumour heterogeneity? *Nature* **308**, 69-72 (1984).
8. H. Davies, G. R. Bignell, C. Cox, P. Stephens, Mutations of the BRAF gene in human cancer. *Nature* **417**, 949 (2002).
9. J. M. Stahl, A. Sharma, M. Cheung, M. Zimmerman, J. Q. Cheng, M. W. Bosenberg, M. Kester, L. Sandirasegarane, G. P. Robertson, Deregulated Akt3 activity promotes development of malignant melanoma. *Cancer research* **64**, 7002-7010 (2004).
10. M. Stark, N. Hayward, Genome-wide loss of heterozygosity and copy number analysis in melanoma using high-density single-nucleotide polymorphism arrays. *Cancer research* **67**, 2632-2642 (2007).
11. C. G. A. Network, Genomic classification of cutaneous melanoma. *Cell* **161**, 1681-1696 (2015).
12. P. B. Chapman, A. Hauschild, C. Robert, J. B. Haanen, P. Ascierto, J. Larkin, R. Dummer, C. Garbe, A. Testori, M. Maio, Improved survival with vemurafenib in melanoma with BRAF V600E mutation. *New England Journal of Medicine* **364**, 2507-2516 (2011).
13. A. Hauschild, J.-J. Grob, L. V. Demidov, T. Jouary, R. Gutzmer, M. Millward, P. Rutkowski, C. U. Blank, W. H. Miller, E. Kaempgen, Dabrafenib in BRAF-mutated metastatic melanoma: a multicentre, open-label, phase 3 randomised controlled trial. *The Lancet* **380**, 358-365 (2012).

14. J. A. Lo, D. E. Fisher, The melanoma revolution: from UV carcinogenesis to a new era in therapeutics. *Science* **346**, 945-949 (2014).
15. G. V. Long, D. Stroyakovskiy, H. Gogas, E. Levchenko, F. de Braud, J. Larkin, C. Garbe, T. Jouary, A. Hauschild, J. J. Grob, Combined BRAF and MEK inhibition versus BRAF inhibition alone in melanoma. *New England Journal of Medicine* **371**, 1877-1888 (2014).
16. D. S. Chen, I. Mellman, Oncology meets immunology: the cancer-immunity cycle. *Immunity* **39**, 1-10 (2013).
17. D. S. Chen, I. Mellman, Elements of cancer immunity and the cancer-immune set point. *Nature* **541**, 321-330 (2017).
18. G. P. Dunn, A. T. Bruce, H. Ikeda, L. J. Old, R. D. Schreiber, Cancer immunoediting: from immunosurveillance to tumor escape. *Nature immunology* **3**, 991-998 (2002).
19. P. Sharma, J. P. Allison, The future of immune checkpoint therapy. *Science* **348**, 56-61 (2015).
20. S. L. Topalian, J. M. Taube, R. A. Anders, D. M. Pardoll, Mechanism-driven biomarkers to guide immune checkpoint blockade in cancer therapy. *Nature reviews. Cancer* **16**, 275 (2016).
21. F. S. Hodi, S. J. O'day, D. F. McDermott, R. W. Weber, J. A. Sosman, J. B. Haanen, R. Gonzalez, C. Robert, D. Schadendorf, J. C. Hassel, Improved survival with ipilimumab in patients with metastatic melanoma. *N Engl J Med* **2010**, 711-723 (2010).

22. C. Robert, G. V. Long, B. Brady, C. Dutriaux, M. Maio, L. Mortier, J. C. Hassel, P. Rutkowski, C. McNeil, E. Kalinka-Warzocha, Nivolumab in previously untreated melanoma without BRAF mutation. *New England journal of medicine* **372**, 320-330 (2015).
23. C. Robert, J. Schachter, G. V. Long, A. Arance, J. J. Grob, L. Mortier, A. Daud, M. S. Carlino, C. McNeil, M. Lotem, Pembrolizumab versus ipilimumab in advanced melanoma. *New England Journal of Medicine* **372**, 2521-2532 (2015).
24. H. Hackl, P. Charoentong, F. Finotello, Z. Trajanoski, Computational genomics tools for dissecting tumour-immune cell interactions. *Nature Reviews Genetics* **17**, 441-458 (2016).
25. E. M. Van Allen, D. Miao, B. Schilling, S. A. Shukla, C. Blank, L. Zimmer, A. Sucker, U. Hillen, M. H. G. Foppen, S. M. Goldinger, Genomic correlates of response to CTLA-4 blockade in metastatic melanoma. *Science* **350**, 207-211 (2015).
26. W. H. Fridman, F. Pages, C. Sautes-Fridman, J. Galon, The immune contexture in human tumours: impact on clinical outcome. *Nature reviews. Cancer* **12**, 298 (2012).
27. B. A. Kidd, L. A. Peters, E. E. Schadt, J. T. Dudley, Unifying immunology with informatics and multiscale biology. *Nature immunology* **15**, 118-127 (2014).
28. T. Gong, J. D. Szustakowski, DeconRNASeq: a statistical framework for deconvolution of heterogeneous tissue samples based on mRNA-Seq data. *Bioinformatics* **29**, 1083-1085 (2013).

29. A. M. Newman, C. L. Liu, M. R. Green, A. J. Gentles, W. Feng, Y. Xu, C. D. Hoang, M. Diehn, A. A. Alizadeh, Robust enumeration of cell subsets from tissue expression profiles. *Nature methods* **12**, 453-457 (2015).
30. B. Li, E. Severson, J.-C. Pignon, H. Zhao, T. Li, J. Novak, P. Jiang, H. Shen, J. C. Aster, S. Rodig, Comprehensive analyses of tumor immunity: implications for cancer immunotherapy. *Genome biology* **17**, 174 (2016).
31. A. Snyder, T. A. Chan, Immunogenic peptide discovery in cancer genomes. *Current opinion in genetics & development* **30**, 7-16 (2015).
32. S. A. Shukla, M. S. Rooney, M. Rajasagi, G. Tiao, P. M. Dixon, M. S. Lawrence, J. Stevens, W. J. Lane, J. L. Dellagatta, S. Steelman, C. Sougnez, K. Cibulskis, A. Kiezun, N. Hacohen, V. Brusic, C. J. Wu, G. Getz, Comprehensive analysis of cancer-associated somatic mutations in class I HLA genes. *Nat Biotechnol* **33**, 1152-1158 (2015).
33. A. Szolek, B. Schubert, C. Mohr, M. Sturm, M. Feldhahn, O. Kohlbacher, OptiType: precision HLA typing from next-generation sequencing data. *Bioinformatics* **30**, 3310-3316 (2014).
34. R. Vita, L. Zarebski, J. A. Greenbaum, H. Emami, I. Hoof, N. Salimi, R. Damle, A. Sette, B. Peters, The immune epitope database 2.0. *Nucleic acids research* **38**, D854-D862 (2009).
35. D. A. Bolotin, S. Poslavsky, I. Mitrophanov, M. Shugay, I. Z. Mamedov, E. V. Putintseva, D. M. Chudakov, MiXCR: software for comprehensive adaptive immunity profiling. *Nature methods* **12**, 380-381 (2015).

36. B. Li, T. Li, J.-C. Pignon, B. Wang, J. Wang, S. Shukla, R. Dou, Q. Chen, F. S. Hodi, T. K. Choueiri, Landscape of tumor-infiltrating T cell repertoire of human cancers. *Nature genetics* **48**, 725 (2016).
37. P. Sharma, S. Hu-Lieskovan, J. A. Wargo, A. Ribas, Primary, adaptive, and acquired resistance to cancer immunotherapy. *Cell* **168**, 707-723 (2017).
38. A. Snyder Charen, V. Makarov, T. Merghoub, L. Walsh, J. Yuan, M. Miller, K. Kannan, M. A. Postow, C. Elipenahli, C. Liu. (American Society of Clinical Oncology, 2014).
39. A. Snyder, V. Makarov, T. Merghoub, J. Yuan, J. M. Zaretsky, A. Desrichard, L. A. Walsh, M. A. Postow, P. Wong, T. S. Ho, Genetic basis for clinical response to CTLA-4 blockade in melanoma. *New England Journal of Medicine* **371**, 2189-2199 (2014).
40. M. S. Rooney, S. A. Shukla, C. J. Wu, G. Getz, N. Hacohen, Molecular and genetic properties of tumors associated with local immune cytolytic activity. *Cell* **160**, 48-61 (2015).
41. N. A. Rizvi, M. D. Hellmann, A. Snyder, P. Kvistborg, V. Makarov, J. J. Havel, W. Lee, J. Yuan, P. Wong, T. S. Ho, Mutational landscape determines sensitivity to PD-1 blockade in non-small cell lung cancer. *Science* **348**, 124-128 (2015).
42. C. Liu, W. Peng, C. Xu, Y. Lou, M. Zhang, J. A. Wargo, J. Q. Chen, H. S. Li, S. S. Watowich, Y. Yang, BRAF inhibition increases tumor infiltration by T cells and enhances the antitumor activity of adoptive immunotherapy in mice. *Clinical cancer research* **19**, 393-403 (2013).

43. S. Spranger, R. Bao, T. F. Gajewski, Melanoma-intrinsic beta-catenin signalling prevents anti-tumour immunity. *Nature* **523**, 231-235 (2015).
44. W. Peng, J. Q. Chen, C. Liu, S. Malu, C. Creasy, M. T. Tetzlaff, C. Xu, J. A. McKenzie, C. Zhang, X. Liang, L. J. Williams, W. Deng, G. Chen, R. Mbofung, A. J. Lazar, C. A. Torres-Cabala, Z. A. Cooper, P. L. Chen, T. N. Tieu, S. Spranger, X. Yu, C. Bernatchez, M. A. Forget, C. Haymaker, R. Amaria, J. L. McQuade, I. C. Glitza, T. Cascone, H. S. Li, L. N. Kwong, T. P. Heffernan, J. Hu, R. L. Bassett, Jr., M. W. Bosenberg, S. E. Woodman, W. W. Overwijk, G. Lizee, J. Roszik, T. F. Gajewski, J. A. Wargo, J. E. Gershenwald, L. Radvanyi, M. A. Davies, P. Hwu, Loss of PTEN Promotes Resistance to T Cell-Mediated Immunotherapy. *Cancer Discov* **6**, 202-216 (2016).
45. J. Gao, L. Z. Shi, H. Zhao, J. Chen, L. Xiong, Q. He, T. Chen, J. Roszik, C. Bernatchez, S. E. Woodman, Loss of IFN- $\gamma$  pathway genes in tumor cells as a mechanism of resistance to anti-CTLA-4 therapy. *Cell* **167**, 397-404. e399 (2016).
46. D. S. Shin, J. M. Zaretsky, H. Escuin-Ordinas, A. Garcia-Diaz, S. Hu-Lieskovan, A. Kalbasi, C. S. Grasso, W. Hugo, S. Sandoval, D. Y. Torrejon, Primary resistance to PD-1 blockade mediated by JAK1/2 mutations. *Cancer discovery* **7**, 188-201 (2017).
47. J. M. Zaretsky, A. Garcia-Diaz, D. S. Shin, H. Escuin-Ordinas, W. Hugo, S. Hu-Lieskovan, D. Y. Torrejon, G. Abril-Rodriguez, S. Sandoval, L. Barthly, Mutations Associated with Acquired Resistance to PD-1 Blockade in Melanoma. *New England Journal of Medicine*, (2016).



48. P. C. Tumeh, C. L. Harview, J. H. Yearley, I. P. Shintaku, E. J. Taylor, L. Robert, B. Chmielowski, M. Spasic, G. Henry, V. Ciobanu, PD-1 blockade induces responses by inhibiting adaptive immune resistance. *Nature* **515**, 568 (2014).
49. J. Gao, J. F. Ward, C. A. Pettaway, L. Z. Shi, S. K. Subudhi, L. M. Vence, H. Zhao, J. Chen, H. Chen, E. Efstathiou, VISTA is an inhibitory immune checkpoint that is increased after ipilimumab therapy in patients with prostate cancer. *Nature Medicine* **23**, 551-555 (2017).
50. S. Koyama, E. A. Akbay, Y. Y. Li, G. S. Herter-Sprie, K. A. Buczkowski, W. G. Richards, L. Gandhi, A. J. Redig, S. J. Rodig, H. Asahina, Adaptive resistance to therapeutic PD-1 blockade is associated with upregulation of alternative immune checkpoints. *Nature communications* **7**, (2016).
51. S. P. Arlauckas, C. S. Garris, R. H. Kohler, M. Kitaoka, M. F. Cuccarese, K. S. Yang, M. A. Miller, J. C. Carlson, G. J. Freeman, R. M. Anthony, In vivo imaging reveals a tumor-associated macrophage-mediated resistance pathway in anti-PD-1 therapy. *Science translational medicine* **9**, eaal3604 (2017).
52. S. R. Gordon, R. L. Maute, B. W. Dulken, G. Hutter, B. M. George, M. N. McCracken, R. Gupta, J. M. Tsai, R. Sinha, D. Corey, PD-1 expression by tumour-associated macrophages inhibits phagocytosis and tumour immunity. *Nature* **545**, 495-499 (2017).
53. M. Vétizou, J. M. Pitt, R. Daillère, P. Lepage, N. Waldschmitt, C. Flament, S. Rusakiewicz, B. Routy, M. P. Roberti, C. P. Duong, Anticancer immunotherapy

- by CTLA-4 blockade relies on the gut microbiota. *Science* **350**, 1079-1084 (2015).
54. K. M. Drescher, P. Sharma, P. Watson, Z. Gatalica, S. N. Thibodeau, H. T. Lynch, Lymphocyte recruitment into the tumor site is altered in patients with MSI-H colon cancer. *Familial cancer* **8**, 231-239 (2009).
55. D. T. Le, J. N. Uram, H. Wang, B. R. Bartlett, H. Kemberling, A. D. Eyring, A. D. Skora, B. S. Luber, N. S. Azad, D. Laheru, PD-1 blockade in tumors with mismatch-repair deficiency. *New England Journal of Medicine* **372**, 2509-2520 (2015).
56. D. A. Landau, S. L. Carter, P. Stojanov, A. McKenna, K. Stevenson, M. S. Lawrence, C. Sougnez, C. Stewart, A. Sivachenko, L. Wang, Evolution and impact of subclonal mutations in chronic lymphocytic leukemia. *Cell* **152**, 714-726 (2013).
57. D. A. Landau, E. Tausch, A. N. Taylor-Weiner, C. Stewart, J. G. Reiter, J. Bahlo, S. Kluth, I. Bozic, M. Lawrence, S. Böttcher, Mutations driving CLL and their evolution in progression and relapse. *Nature* **526**, 525 (2015).
58. M. Greaves, Evolutionary determinants of cancer. *Cancer discovery* **5**, 806-820 (2015).
59. M. Angelova, P. Charoentong, H. Hackl, M. L. Fischer, R. Snajder, A. M. Krogsdam, M. J. Waldner, G. Bindea, B. Mlecnik, J. Galon, Z. Trajanoski, Characterization of the immunophenotypes and antigenomes of colorectal cancers reveals distinct tumor escape mechanisms and novel targets for immunotherapy. *Genome Biol* **16**, 64 (2015).

60. N. McGranahan, A. J. Furness, R. Rosenthal, S. Ramskov, R. Lyngaa, S. K. Saini, M. Jamal-Hanjani, G. A. Wilson, N. J. Birkbak, C. T. Hiley, Clonal neoantigens elicit T cell immunoreactivity and sensitivity to immune checkpoint blockade. *Science* **351**, 1463-1469 (2016).
61. E. Eisenhauer, P. Therasse, J. Bogaerts, L. Schwartz, D. Sargent, R. Ford, J. Dancey, S. Arbuck, S. Gwyther, M. Mooney, New response evaluation criteria in solid tumours: revised RECIST guideline (version 1.1). *European journal of cancer* **45**, 228-247 (2009).
62. D. Waggott, K. Chu, S. Yin, B. G. Wouters, F.-F. Liu, P. C. Boutros, NanoStringNorm: an extensible R package for the pre-processing of NanoString mRNA and miRNA data. *Bioinformatics* **28**, 1546-1548 (2012).
63. J. Vandesompele, K. De Preter, F. Pattyn, B. Poppe, N. Van Roy, A. De Paepe, F. Speleman, Accurate normalization of real-time quantitative RT-PCR data by geometric averaging of multiple internal control genes. *Genome biology* **3**, research0034. 0031 (2002).
64. Y. Benjamini, Y. Hochberg, Controlling the false discovery rate: a practical and powerful approach to multiple testing. *Journal of the royal statistical society. Series B (Methodological)*, 289-300 (1995).
65. S. Pounds, S. W. Morris, Estimating the occurrence of false positives and false negatives in microarray studies by approximating and partitioning the empirical distribution of p-values. *Bioinformatics* **19**, 1236-1242 (2003).
66. D. Bates, M. Mächler, B. Bolker, S. Walker, Fitting linear mixed-effects models using lme4. *arXiv preprint arXiv:1406.5823*, (2014).

67. H. Li, R. Durbin, Fast and accurate short read alignment with Burrows-Wheeler transform. *Bioinformatics* **25**, 1754-1760 (2009).
68. A. McKenna, M. Hanna, E. Banks, A. Sivachenko, K. Cibulskis, A. Kernytzky, K. Garimella, D. Altshuler, S. Gabriel, M. Daly, M. A. DePristo, The Genome Analysis Toolkit: a MapReduce framework for analyzing next-generation DNA sequencing data. *Genome Res* **20**, 1297-1303 (2010).
69. M. A. DePristo, E. Banks, R. Poplin, K. V. Garimella, J. R. Maguire, C. Hartl, A. A. Philippakis, G. del Angel, M. A. Rivas, M. Hanna, A. McKenna, T. J. Fennell, A. M. Kernytzky, A. Y. Sivachenko, K. Cibulskis, S. B. Gabriel, D. Altshuler, M. J. Daly, A framework for variation discovery and genotyping using next-generation DNA sequencing data. *Nat Genet* **43**, 491-498 (2011).
70. G. A. Auwera, M. O. Carneiro, C. Hartl, R. Poplin, G. del Angel, A. Levy - Moonshine, T. Jordan, K. Shakir, D. Roazen, J. Thibault, From FastQ data to high - confidence variant calls: the genome analysis toolkit best practices pipeline. *Current protocols in bioinformatics*, 11.10. 11-11.10. 33 (2013).
71. K. Cibulskis, M. S. Lawrence, S. L. Carter, A. Sivachenko, D. Jaffe, C. Sougnez, S. Gabriel, M. Meyerson, E. S. Lander, G. Getz, Sensitive detection of somatic point mutations in impure and heterogeneous cancer samples. *Nat Biotechnol* **31**, 213-219 (2013).
72. K. Ye, M. H. Schulz, Q. Long, R. Apweiler, Z. Ning, Pindel: a pattern growth approach to detect break points of large deletions and medium sized insertions from paired-end short reads. *Bioinformatics* **25**, 2865-2871 (2009).

73. N. Andor, J. V. Harness, S. Muller, H. W. Mewes, C. Petritsch, EXPANDS: expanding ploidy and allele frequency on nested subpopulations. *Bioinformatics* **30**, 50-60 (2014).
74. C. A. Miller, B. S. White, N. D. Dees, M. Griffith, J. S. Welch, O. L. Griffith, R. Vij, M. H. Tomasson, T. A. Graubert, M. J. Walter, M. J. Ellis, W. Schierding, J. F. DiPersio, T. J. Ley, E. R. Mardis, R. K. Wilson, L. Ding, SciClone: inferring clonal architecture and tracking the spatial and temporal patterns of tumor evolution. *PLoS Comput Biol* **10**, e1003665 (2014).
75. A. Snyder, T. A. Chan, Immunogenic peptide discovery in cancer genomes. *Curr Opin Genet Dev* **30**, 7-16 (2015).
76. C. Liu, X. Yang, B. Duffy, T. Mohanakumar, R. D. Mitra, M. C. Zody, J. D. Pfeifer, ATHLATES: accurate typing of human leukocyte antigen through exome sequencing. *Nucleic Acids Res* **41**, e142 (2013).
77. I. Hoof, B. Peters, J. Sidney, L. E. Pedersen, A. Sette, O. Lund, S. Buus, M. Nielsen, NetMHCpan, a method for MHC class I binding prediction beyond humans. *Immunogenetics* **61**, 1-13 (2009).
78. N. Cancer Genome Atlas, Genomic Classification of Cutaneous Melanoma. *Cell* **161**, 1681-1696 (2015).
79. F. Favero, T. Joshi, A. M. Marquard, N. J. Birkbak, M. Krzystanek, Q. Li, Z. Szallasi, A. C. Eklund, Sequenza: allele-specific copy number and mutation profiles from tumor sequencing data. *Ann Oncol* **26**, 64-70 (2015).

80. J. Zhang, CNTools: Convert segment data into a region by sample matrix to allow for other high level computational analyses. *R package (Version 1.6. 0.)*, (2014).
81. J. Zhang, B. Feng, M. J. Zhang, C. biocViews Microarray, Package 'cghMCR'. (2013).
82. S. A. Forbes, D. Beare, P. Gunasekaran, K. Leung, N. Bindal, H. Boutselakis, M. Ding, S. Bamford, C. Cole, S. Ward, C. Y. Kok, M. Jia, T. De, J. W. Teague, M. R. Stratton, U. McDermott, P. J. Campbell, COSMIC: exploring the world's knowledge of somatic mutations in human cancer. *Nucleic Acids Res* **43**, D805-811 (2015).
83. M. Zhao, J. Sun, Z. Zhao, TSGene: a web resource for tumor suppressor genes. *Nucleic Acids Res* **41**, D970-976 (2013).
84. H. S. Robins, P. V. Campregher, S. K. Srivastava, A. Wachter, C. J. Turtle, O. Kahsai, S. R. Riddell, E. H. Warren, C. S. Carlson, Comprehensive assessment of T-cell receptor beta-chain diversity in alphabeta T cells. *Blood* **114**, 4099-4107 (2009).
85. C. S. Carlson, R. O. Emerson, A. M. Sherwood, C. Desmarais, M. W. Chung, J. M. Parsons, M. S. Steen, M. A. LaMadrid-Herrmannsfeldt, D. W. Williamson, R. J. Livingston, D. Wu, B. L. Wood, M. J. Rieder, H. Robins, Using synthetic templates to design an unbiased multiplex PCR assay. *Nat Commun* **4**, 2680 (2013).
86. P. C. Tumeh, C. L. Harview, J. H. Yearley, I. P. Shintaku, E. J. Taylor, L. Robert, B. Chmielowski, M. Spasic, G. Henry, V. Ciobanu, A. N. West, M. Carmona, C.

- Kivork, E. Seja, G. Cherry, A. J. Gutierrez, T. R. Grogan, C. Mateus, G. Tomasic, J. A. Glaspy, R. O. Emerson, H. Robins, R. H. Pierce, D. A. Elashoff, C. Robert, A. Ribas, PD-1 blockade induces responses by inhibiting adaptive immune resistance. *Nature* **515**, 568-571 (2014).
87. P.-L. Chen, W. Roh, A. Reuben, Z. A. Cooper, C. N. Spencer, P. A. Prieto, J. P. Miller, R. L. Bassett, V. Gopalakrishnan, K. Wani, Analysis of immune signatures in longitudinal tumor samples yields insight into biomarkers of response and mechanisms of resistance to immune checkpoint blockade. *Cancer Discovery* **6**, 827-837 (2016).
88. K. Yoshihara, M. Shahmoradgoli, E. Martinez, R. Vegesna, H. Kim, W. Torres-Garcia, V. Trevino, H. Shen, P. W. Laird, D. A. Levine, S. L. Carter, G. Getz, K. Stemke-Hale, G. B. Mills, R. G. Verhaak, Inferring tumour purity and stromal and immune cell admixture from expression data. *Nat Commun* **4**, 2612 (2013).
89. V. K. Mootha, C. M. Lindgren, K.-F. Eriksson, A. Subramanian, S. Sihag, J. Lehar, P. Puigserver, E. Carlsson, M. Ridderstråle, E. Laurila, PGC-1 $\alpha$ -responsive genes involved in oxidative phosphorylation are coordinately downregulated in human diabetes. *Nature genetics* **34**, 267-273 (2003).
90. S. L. Topalian, F. S. Hodi, J. R. Brahmer, S. N. Gettinger, D. C. Smith, D. F. McDermott, J. D. Powderly, R. D. Carvajal, J. A. Sosman, M. B. Atkins, Safety, activity, and immune correlates of anti-PD-1 antibody in cancer. *N Engl J Med* **2012**, 2443-2454 (2012).

91. R. H. Andtbacka, H. L. Kaufman, F. Collichio, T. Amatruda, N. Senzer, J. Chesney, K. A. Delman, L. E. Spitler, I. Puzanov, S. S. Agarwala, Talimogene laherparepvec improves durable response rate in patients with advanced melanoma. *Journal of clinical oncology* **33**, 2780-2788 (2015).
92. J. Larkin, V. Chiarion-Sileni, R. Gonzalez, J. J. Grob, C. L. Cowey, C. D. Lao, D. Schadendorf, R. Dummer, M. Smylie, P. Rutkowski, Combined nivolumab and ipilimumab or monotherapy in untreated melanoma. *New England journal of medicine* **373**, 23-34 (2015).
93. M. A. Postow, J. Chesney, A. C. Pavlick, C. Robert, K. Grossmann, D. McDermott, G. P. Linette, N. Meyer, J. K. Giguere, S. S. Agarwala, Nivolumab and ipilimumab versus ipilimumab in untreated melanoma. *New England Journal of Medicine* **372**, 2006-2017 (2015).
94. J. D. Wolchok, H. Kluger, M. K. Callahan, M. A. Postow, N. A. Rizvi, A. M. Lesokhin, N. H. Segal, C. E. Ariyan, R.-A. Gordon, K. Reed, Nivolumab plus ipilimumab in advanced melanoma. *New England Journal of Medicine* **369**, 122-133 (2013).
95. J. R. Brahmer, S. S. Tykodi, L. Q. Chow, W.-J. Hwu, S. L. Topalian, P. Hwu, C. G. Drake, L. H. Camacho, J. Kauh, K. Odunsi, Safety and activity of anti-PD-L1 antibody in patients with advanced cancer. *N Engl J Med* **2012**, 2455-2465 (2012).
96. B. D. Curti, M. Kovacsovic-Bankowski, N. Morris, E. Walker, L. Chisholm, K. Floyd, J. Walker, I. Gonzalez, T. Meeuwsen, B. A. Fox, OX40 is a potent



- immune-stimulating target in late-stage cancer patients. *Cancer research* **73**, 7189-7198 (2013).
97. S. L. Topalian, M. Sznol, D. F. McDermott, H. M. Kluger, R. D. Carvajal, W. H. Sharfman, J. R. Brahmer, D. P. Lawrence, M. B. Atkins, J. D. Powderly, Survival, durable tumor remission, and long-term safety in patients with advanced melanoma receiving nivolumab. *Journal of clinical oncology* **32**, 1020-1030 (2014).
98. J. D. Wolchok, J. S. Weber, M. Maio, B. Neyns, K. Harmankaya, K. Chin, L. Cykowski, V. de Pril, R. Humphrey, C. Lebbé, Four-year survival rates for patients with metastatic melanoma who received ipilimumab in phase II clinical trials. *Annals of oncology* **24**, 2174-2180 (2013).
99. D. Schadendorf, F. S. Hodi, C. Robert, J. S. Weber, K. Margolin, O. Hamid, D. Patt, T.-T. Chen, D. M. Berman, J. D. Wolchok, Pooled analysis of long-term survival data from phase II and phase III trials of ipilimumab in unresectable or metastatic melanoma. *Journal of clinical oncology* **33**, 1889-1894 (2015).
100. J. M. Taube, A. P. Klein, J. R. Brahmer, H. Xu, X. Pan, J. H. Kim, L. Chen, D. M. Pardoll, S. L. Topalian, R. A. Anders, Association of PD-1, PD-1 ligands, and other features of the tumor immune microenvironment with response to anti-PD-1 therapy. *Clinical cancer research*, clincanres. 3271.2013 (2014).
101. W. Hugo, J. M. Zaretsky, L. Sun, C. Song, B. H. Moreno, S. Hu-Lieskovan, B. Berent-Maoz, J. Pang, B. Chmielowski, G. Cherry, Genomic and transcriptomic features of response to anti-PD-1 therapy in metastatic melanoma. *Cell* **165**, 35-44 (2016).

102. M. M. Gubin, X. Zhang, H. Schuster, E. Caron, J. P. Ward, T. Noguchi, Y. Ivanova, J. Hundal, C. D. Arthur, W.-J. Krebber, Checkpoint blockade cancer immunotherapy targets tumour-specific mutant antigens. *Nature* **515**, 577-581 (2014).
103. R. Das, R. Verma, M. Sznol, C. S. Boddupalli, S. N. Gettinger, H. Kluger, M. Callahan, J. D. Wolchok, R. Halaban, M. V. Dhodapkar, Combination therapy with anti-CTLA-4 and anti-PD-1 leads to distinct immunologic changes in vivo. *The Journal of Immunology* **194**, 950-959 (2015).
104. M. S. Rooney, S. A. Shukla, C. J. Wu, G. Getz, N. Hacohen, Molecular and genetic properties of tumors associated with local immune cytolytic activity. *Cell* **160**, 48-61 (2015).
105. S. Spranger, R. Bao, T. F. Gajewski, Melanoma-intrinsic [beta]-catenin signalling prevents anti-tumour immunity. *Nature* **523**, 231 (2015).
106. R. R. Huang, J. Jalil, J. S. Economou, B. Chmielowski, R. C. Koya, S. Mok, H. Sazegar, E. Seja, A. Villanueva, J. Gomez-Navarro, CTLA4 blockade induces frequent tumor infiltration by activated lymphocytes regardless of clinical responses in humans. *Clinical Cancer Research* **17**, 4101-4109 (2011).
107. N. Ferrara, R. S. Kerbel, Angiogenesis as a therapeutic target. *Nature* **438**, 967 (2005).
108. T. Voron, O. Colussi, E. Marcheteau, S. Pernot, M. Nizard, A.-L. Pointet, S. Latreche, S. Bergaya, N. Benhamouda, C. Tanchot, VEGF-A modulates expression of inhibitory checkpoints on CD8+ T cells in tumors. *Journal of Experimental Medicine* **212**, 139-148 (2015).

109. P. A. Ott, F. S. Hodi, E. I. Buchbinder, Inhibition of immune checkpoints and vascular endothelial growth factor as combination therapy for metastatic melanoma: an overview of rationale, preclinical evidence, and initial clinical data. *Frontiers in oncology* **5**, (2015).
110. J. R. Westin, F. Chu, M. Zhang, L. E. Fayad, L. W. Kwak, N. Fowler, J. Romaguera, F. Hagemeister, M. Fanale, F. Samaniego, Safety and activity of PD1 blockade by pidilizumab in combination with rituximab in patients with relapsed follicular lymphoma: a single group, open-label, phase 2 trial. *The lancet oncology* **15**, 69-77 (2014).
111. G. T. Motz, S. P. Santoro, L.-P. Wang, T. Garrabrant, R. R. Lastra, I. S. Hagemann, P. Lal, M. D. Feldman, F. Benencia, G. Coukos, Tumor endothelium FasL establishes a selective immune barrier promoting tolerance in tumors. *Nature medicine* **20**, 607-615 (2014).
112. J. E. Ohm, D. I. Gabrilovich, G. D. Sempowski, E. Kisseleva, K. S. Parman, S. Nadaf, D. P. Carbone, VEGF inhibits T-cell development and may contribute to tumor-induced immune suppression. *Blood* **101**, 4878-4886 (2003).
113. D. Gabrilovich, T. Ishida, T. Oyama, S. Ran, V. Kravtsov, S. Nadaf, D. P. Carbone, Vascular endothelial growth factor inhibits the development of dendritic cells and dramatically affects the differentiation of multiple hematopoietic lineages in vivo. *Blood* **92**, 4150-4166 (1998).
114. M. Terme, S. Pernet, E. Marcheteau, F. Sandoval, N. Benhamouda, O. Colussi, O. Dubreuil, A. F. Carpentier, E. Tartour, J. Taieb, VEGFA-VEGFR pathway

- blockade inhibits tumor-induced regulatory T-cell proliferation in colorectal cancer. *Cancer research* **73**, 539-549 (2013).
115. F. S. Hodi, D. Lawrence, C. Lezcano, X. Wu, J. Zhou, T. Sasada, W. Zeng, A. Giobbie-Hurder, M. B. Atkins, N. Ibrahim, Bevacizumab plus ipilimumab in patients with metastatic melanoma. *Cancer immunology research* **2**, 632-642 (2014).
116. J. Larkin, V. Chiarion-Sileni, R. Gonzalez, J. J. Grob, C. L. Cowey, C. D. Lao, D. Schadendorf, R. Dummer, M. Smylie, P. Rutkowski, P. F. Ferrucci, A. Hill, J. Wagstaff, M. S. Carlino, J. B. Haanen, M. Maio, I. Marquez-Rodas, G. A. McArthur, P. A. Ascierto, G. V. Long, M. K. Callahan, M. A. Postow, K. Grossmann, M. Sznol, B. Dreno, L. Bastholt, A. Yang, L. M. Rollin, C. Horak, F. S. Hodi, J. D. Wolchok, Combined Nivolumab and Ipilimumab or Monotherapy in Untreated Melanoma. *N Engl J Med* **373**, 23-34 (2015).
117. S. L. Topalian, F. S. Hodi, J. R. Brahmer, S. N. Gettinger, D. C. Smith, D. F. McDermott, J. D. Powderly, R. D. Carvajal, J. A. Sosman, M. B. Atkins, Safety, activity, and immune correlates of anti-PD-1 antibody in cancer. *New England Journal of Medicine* **366**, 2443-2454 (2012).
118. J. D. Wolchok, H. Kluger, M. K. Callahan, M. A. Postow, N. A. Rizvi, A. M. Lesokhin, N. H. Segal, C. E. Ariyan, R. A. Gordon, K. Reed, M. M. Burke, A. Caldwell, S. A. Kronenberg, B. U. Agunwamba, X. Zhang, I. Lowy, H. D. Inzunza, W. Feely, C. E. Horak, Q. Hong, A. J. Korman, J. M. Wigginton, A. Gupta, M. Sznol, Nivolumab plus ipilimumab in advanced melanoma. *N Engl J Med* **369**, 122-133 (2013).

119. D. T. Le, J. N. Uram, H. Wang, B. R. Bartlett, H. Kemberling, A. D. Eyring, A. D. Skora, B. S. Lubber, N. S. Azad, D. Laheru, B. Biedrzycki, R. C. Donehower, A. Zaheer, G. A. Fisher, T. S. Crocenzi, J. J. Lee, S. M. Duffy, R. M. Goldberg, A. de la Chapelle, M. Koshiji, F. Bhajee, T. Huebner, R. H. Hruban, L. D. Wood, N. Cuka, D. M. Pardoll, N. Papadopoulos, K. W. Kinzler, S. Zhou, T. C. Cornish, J. M. Taube, R. A. Anders, J. R. Eshleman, B. Vogelstein, L. A. Diaz, Jr., PD-1 Blockade in Tumors with Mismatch-Repair Deficiency. *N Engl J Med* **372**, 2509-2520 (2015).
120. O. Hamid, C. Robert, A. Daud, F. S. Hodi, W. J. Hwu, R. Kefford, J. D. Wolchok, P. Hersey, R. W. Joseph, J. S. Weber, R. Dronca, T. C. Gangadhar, A. Patnaik, H. Zarour, A. M. Joshua, K. Gergich, J. Elassaiss-Schaap, A. Algazi, C. Mateus, P. Boasberg, P. C. Tume, B. Chmielowski, S. W. Ebbinghaus, X. N. Li, S. P. Kang, A. Ribas, Safety and tumor responses with lambrolizumab (anti-PD-1) in melanoma. *N Engl J Med* **369**, 134-144 (2013).
121. T. N. Schumacher, C. Kesmir, M. M. van Buuren, Biomarkers in cancer immunotherapy. *Cancer Cell* **27**, 12-14 (2015).
122. J. Matsuzaki, S. Gnjatic, P. Mhawech-Fauceglia, A. Beck, A. Miller, T. Tsuji, C. Eppolito, F. Qian, S. Lele, P. Shrikant, L. J. Old, K. Odunsi, Tumor-infiltrating NY-ESO-1-specific CD8<sup>+</sup> T cells are negatively regulated by LAG-3 and PD-1 in human ovarian cancer. *Proc Natl Acad Sci U S A* **107**, 7875-7880 (2010).
123. K. Sakuishi, L. Apetoh, J. M. Sullivan, B. R. Blazar, V. K. Kuchroo, A. C. Anderson, Targeting Tim-3 and PD-1 pathways to reverse T cell exhaustion and restore anti-tumor immunity. *J Exp Med* **207**, 2187-2194 (2010).

124. H. Li, K. Wu, K. Tao, L. Chen, Q. Zheng, X. Lu, J. Liu, L. Shi, C. Liu, G. Wang, W. Zou, Tim-3/galectin-9 signaling pathway mediates T-cell dysfunction and predicts poor prognosis in patients with hepatitis B virus-associated hepatocellular carcinoma. *Hepatology* **56**, 1342-1351 (2012).
125. S.-R. Woo, M. E. Turnis, M. V. Goldberg, J. Bankoti, M. Selby, C. J. Nirschl, M. L. Bettini, D. M. Gravano, P. Vogel, C. L. Liu, Immune inhibitory molecules LAG-3 and PD-1 synergistically regulate T-cell function to promote tumoral immune escape. *Cancer research* **72**, 917-927 (2012).
126. T. Powles, J. P. Eder, G. D. Fine, F. S. Braiteh, Y. Loriot, C. Cruz, J. Bellmunt, H. A. Burris, D. P. Petrylak, S. L. Teng, X. Shen, Z. Boyd, P. S. Hegde, D. S. Chen, N. J. Vogelzang, MPDL3280A (anti-PD-L1) treatment leads to clinical activity in metastatic bladder cancer. *Nature* **515**, 558-562 (2014).
127. R. S. Herbst, J. C. Soria, M. Kowanetz, G. D. Fine, O. Hamid, M. S. Gordon, J. A. Sosman, D. F. McDermott, J. D. Powderly, S. N. Gettinger, H. E. Kohrt, L. Horn, D. P. Lawrence, S. Rost, M. Leabman, Y. Xiao, A. Mokatrini, H. Koeppen, P. S. Hegde, I. Mellman, D. S. Chen, F. S. Hodi, Predictive correlates of response to the anti-PD-L1 antibody MPDL3280A in cancer patients. *Nature* **515**, 563-567 (2014).
128. R. J. Johnston, L. Comps-Agrar, J. Hackney, X. Yu, M. Huseni, Y. Yang, S. Park, V. Javinal, H. Chiu, B. Irving, D. L. Eaton, J. L. Grogan, The immunoreceptor TIGIT regulates antitumor and antiviral CD8(+) T cell effector function. *Cancer Cell* **26**, 923-937 (2014).

129. J. M. Chauvin, O. Pagliano, J. Fourcade, Z. Sun, H. Wang, C. Sander, J. M. Kirkwood, T. H. Chen, M. Maurer, A. J. Korman, H. M. Zarour, TIGIT and PD-1 impair tumor antigen-specific CD8(+) T cells in melanoma patients. *J Clin Invest* **125**, 2046-2058 (2015).
130. H. Sumimoto, F. Imabayashi, T. Iwata, Y. Kawakami, The BRAF–MAPK signaling pathway is essential for cancer-immune evasion in human melanoma cells. *The Journal of experimental medicine* **203**, 1651-1656 (2006).
131. W. Hugo, J. M. Zaretsky, L. Sun, C. Song, B. H. Moreno, S. Hu-Lieskovan, B. Berent-Maoz, J. Pang, B. Chmielowski, G. Cherry, E. Seja, S. Lomeli, X. Kong, M. C. Kelley, J. A. Sosman, D. B. Johnson, A. Ribas, R. S. Lo, Genomic and Transcriptomic Features of Response to Anti-PD-1 Therapy in Metastatic Melanoma. *Cell* **165**, 35-44 (2016).
132. J. M. Taube, R. A. Anders, G. D. Young, H. Xu, R. Sharma, T. L. McMiller, S. Chen, A. P. Klein, D. M. Pardoll, S. L. Topalian, Colocalization of inflammatory response with B7-h1 expression in human melanocytic lesions supports an adaptive resistance mechanism of immune escape. *Science translational medicine* **4**, 127ra137-127ra137 (2012).
133. J. M. Taube, G. D. Young, T. L. McMiller, S. Chen, J. T. Salas, T. S. Pritchard, H. Xu, A. K. Meeker, J. Fan, C. Cheadle, A. E. Berger, D. M. Pardoll, S. L. Topalian, Differential Expression of Immune-Regulatory Genes Associated with PD-L1 Display in Melanoma: Implications for PD-1 Pathway Blockade. *Clin Cancer Res* **21**, 3969-3976 (2015).

134. M. D. Ayers, M. Nebozhyn, H. A. Hirsch, R. Cristescu, E. E. Murphy, S. P. Kang, S. W. Ebbinghaus, T. K. McClanahan, A. Loboda, J. K. Lunceford, Assessment of gene expression in peripheral blood from patients with advanced melanoma using RNA-Seq before and after treatment with anti-PD-1 therapy with pembrolizumab (MK-3475). *Cancer Research* **75**, 1307-1307 (2015).
135. A. J. Minn, E. J. Wherry, Combination Cancer Therapies with Immune Checkpoint Blockade: Convergence on Interferon Signaling. *Cell* **165**, 272-275 (2016).
136. H. Matsushita, M. D. Vesely, D. C. Koboldt, C. G. Rickert, R. Uppaluri, V. J. Magrini, C. D. Arthur, J. M. White, Y. S. Chen, L. K. Shea, J. Hundal, M. C. Wendl, R. Demeter, T. Wylie, J. P. Allison, M. J. Smyth, L. J. Old, E. R. Mardis, R. D. Schreiber, Cancer exome analysis reveals a T-cell-dependent mechanism of cancer immunoediting. *Nature* **482**, 400-404 (2012).
137. M. DuPage, C. Mazumdar, L. M. Schmidt, A. F. Cheung, T. Jacks, Expression of tumour-specific antigens underlies cancer immunoediting. *Nature* **482**, 405-409 (2012).
138. A. Sivan, L. Corrales, N. Hubert, J. B. Williams, K. Aquino-Michaels, Z. M. Earley, F. W. Benyamin, Y. M. Lei, B. Jabri, M.-L. Alegre, Commensal Bifidobacterium promotes antitumor immunity and facilitates anti-PD-L1 efficacy. *Science* **350**, 1084-1089 (2015).
139. C. H. Chang, J. Qiu, D. O'Sullivan, M. D. Buck, T. Noguchi, J. D. Curtis, Q. Chen, M. Gindin, M. M. Gubin, G. J. van der Windt, E. Tonc, R. D. Schreiber, E. J. Pearce,



- E. L. Pearce, Metabolic Competition in the Tumor Microenvironment Is a Driver of Cancer Progression. *Cell* **162**, 1229-1241 (2015).
140. P. C. Ho, J. D. Bihuniak, A. N. Macintyre, M. Staron, X. Liu, R. Amezcua, Y. C. Tsui, G. Cui, G. Micevic, J. C. Perales, S. H. Kleinstein, E. D. Abel, K. L. Insogna, S. Feske, J. W. Locasale, M. W. Bosenberg, J. C. Rathmell, S. M. Kaech, Phosphoenolpyruvate Is a Metabolic Checkpoint of Anti-tumor T Cell Responses. *Cell* **162**, 1217-1228 (2015).
141. W. Yang, Y. Bai, Y. Xiong, J. Zhang, S. Chen, X. Zheng, X. Meng, L. Li, J. Wang, C. Xu, C. Yan, L. Wang, C. C. Chang, T. Y. Chang, T. Zhang, P. Zhou, B. L. Song, W. Liu, S. C. Sun, X. Liu, B. L. Li, C. Xu, Potentiating the antitumour response of CD8(+) T cells by modulating cholesterol metabolism. *Nature* **531**, 651-655 (2016).
142. E. Hodis, I. R. Watson, G. V. Kryukov, S. T. Arold, M. Imielinski, J. P. Theurillat, E. Nickerson, D. Auclair, L. Li, C. Place, D. Dicara, A. H. Ramos, M. S. Lawrence, K. Cibulskis, A. Sivachenko, D. Voet, G. Saksena, N. Stransky, R. C. Onofrio, W. Winckler, K. Ardlie, N. Wagle, J. Wargo, K. Chong, D. L. Morton, K. Stemke-Hale, G. Chen, M. Noble, M. Meyerson, J. E. Ladbury, M. A. Davies, J. E. Gershenwald, S. N. Wagner, D. S. Hoon, D. Schadendorf, E. S. Lander, S. B. Gabriel, G. Getz, L. A. Garraway, L. Chin, A landscape of driver mutations in melanoma. *Cell* **150**, 251-263 (2012).
143. D. H. Kaplan, V. Shankaran, A. S. Dighe, E. Stockert, M. Aguet, L. J. Old, R. D. Schreiber, Demonstration of an interferon  $\gamma$ -dependent tumor surveillance

- system in immunocompetent mice. *Proceedings of the National Academy of Sciences* **95**, 7556-7561 (1998).
144. G. P. Dunn, K. C. Sheehan, L. J. Old, R. D. Schreiber, IFN unresponsiveness in LNCaP cells due to the lack of JAK1 gene expression. *Cancer research* **65**, 3447-3453 (2005).
145. E. Wang, A. Worschech, F. M. Marincola, The immunologic constant of rejection. *Trends Immunol* **29**, 256-262 (2008).
146. J. Galon, H. K. Angell, D. Bedognetti, F. M. Marincola, The continuum of cancer immunosurveillance: prognostic, predictive, and mechanistic signatures. *Immunity* **39**, 11-26 (2013).
147. L. N. Kwong, L. Chin, Chromosome 10, frequently lost in human melanoma, encodes multiple tumor-suppressive functions. *Cancer research* **74**, 1814-1821 (2014).
148. B. C. Bastian, P. E. LeBoit, H. Hamm, E.-B. Bröcker, D. Pinkel, Chromosomal gains and losses in primary cutaneous melanomas detected by comparative genomic hybridization. *Cancer research* **58**, 2170-2175 (1998).
149. J. Bauer, B. C. Bastian, Distinguishing melanocytic nevi from melanoma by DNA copy number changes: comparative genomic hybridization as a research and diagnostic tool. *Dermatologic therapy* **19**, 40-49 (2006).
150. A. H. Shain, I. Yeh, I. Kovalyshyn, A. Sriharan, E. Talevich, A. Gagnon, R. Dummer, J. North, L. Pincus, B. Ruben, W. Rickaby, C. D'Arrigo, A. Robson, B. C. Bastian, The Genetic Evolution of Melanoma from Precursor Lesions. *N Engl J Med* **373**, 1926-1936 (2015).

151. A. H. Shain, B. C. Bastian, From melanocytes to melanomas. *Nat Rev Cancer* **16**, 345-358 (2016).
152. M. Schmittnaegel, N. Rigamonti, E. Kadioglu, A. Cassará, C. W. Rmili, A. Kiialainen, Y. Kienast, H.-J. Mueller, C.-H. Ooi, D. Laoui, Dual angiopoietin-2 and VEGFA inhibition elicits antitumor immunity that is enhanced by PD-1 checkpoint blockade. *Science translational medicine* **9**, eaak9670 (2017).
153. E. Allen, A. Jabouille, L. B. Rivera, I. Lodewijckx, R. Missiaen, V. Steri, K. Feyen, J. Tawney, D. Hanahan, I. P. Michael, Combined antiangiogenic and anti-PD-L1 therapy stimulates tumor immunity through HEV formation. *Science translational medicine* **9**, eaak9679 (2017).
154. K. Garber, Promising Early Results for Immunotherapy–Antiangiogenesis Combination. *JNCI: Journal of the National Cancer Institute* **106**, (2014).
155. T. Davoli, H. Uno, E. C. Wooten, S. J. Elledge, Tumor aneuploidy correlates with markers of immune evasion and with reduced response to immunotherapy. *Science* **355**, eaaf8399 (2017).
156. K. W. Mouw, M. S. Goldberg, P. A. Konstantinopoulos, A. D. D'Andrea, DNA Damage and Repair Biomarkers of Immunotherapy Response. *Cancer Discovery* **7**, 675-693 (2017).
157. R. Vilain, H. Kakavand, A. Menzies, J. Madore, J. Wilmott, R. Dobney, V. Jakrot, A. Cooper, B. Kong, S. Lo, 3305 PD1 inhibition-induced changes in melanoma and its associated immune infiltrate. *European Journal of Cancer* **51**, S666 (2015).

158. A. Gros, M. R. Parkhurst, E. Tran, A. Pasetto, P. F. Robbins, S. Ilyas, T. D. Prickett, J. J. Gartner, J. S. Crystal, I. M. Roberts, Prospective identification of neoantigen-specific lymphocytes in the peripheral blood of melanoma patients. *Nature medicine* **22**, 433-438 (2016).

## **VITA**

Whijae Roh was born in the city of Anyang in South Korea, on September 2, 1984, the son of Gab Kyun Roh and Joung Soon Bae. After completing his work at Hansung Science High School, Seoul in 2002, he entered Korea Advanced Institute of Science and Technology (KAIST) in Daejeon, South Korea. He received the degree of Bachelor of Science with a major in Bio and Brain Engineering from KAIST in August 2006. In a graduate school at the University of Michigan, he received the degree of Master of Science in Biomedical Engineering in April 2008 and the degree of Master of Science in Biostatistics in April 2010. In next three years, he worked as an assistant research scientist in the Bioneer corporation and the Genomic Medicine Institute at Seoul National University College of Medicine. In August of 2013, he entered The University of Texas MD Anderson Cancer Center UTHealth Graduate School of Biomedical Sciences.

Permanent address:

105 Dong 302 Ho, Bangae Art e-Pyunhan Sesang Apt.

101 Hyoryungro 2-gil, Seocho-gu,

Seoul, South Korea